Masterthesis

Investigating surface pre-treatment and diamond nanoseed deposition on glass by ultrasonic spraycoating and inkjet printing for industrial applications

PROMOTOR :
Prof. dr. ir. Wim DEFERME

BEGELEIDER :
ing. Pieter VERDING

Ewoud Jeunen, Seppe Thomas
Scriptie ingediend tot het behalen van de graad van master in de industriële wetenschappen: elektromechanica

▶▶ UHASSELT   KU LEUVEN

▶▶ UHASSELT   KU LEUVEN

2021•2022
Faculteit Industriële Ingenieurswetenschappen
master in de industriële wetenschappen: elektromechanica

Masterthesis
Investigating surface pre-treatment and diamond nanoseed deposition on glass by ultrasonic spraycoating and inkjet printing for industrial applications

PROMOTOR :
Prof. dr. ir. Wim DEFERME

BEGELEIDER :
ing. Pieter VERDING

Ewoud Jeunen, Seppe Thomas
Scriptie ingediend tot het behalen van de graad van master in de industriële wetenschappen: elektromechanica

►► UHASSELT   KU LEUVEN

Foreword

To successfully complete our master's degree in electromechanical engineering at KU Leuven and Hasselt University's faculty of engineering technology, we chose to conduct a research on diamond coatings at the research institute imo-imomec in Diepenbeek. The research question involved visualizing the evolution of various pre-treatment methods for glass substrates as well as optimising parameters for ultrasonic spraycoating and inkjet applications. The plotted evolutions will aid researchers in better understanding the degradation of these pre-treatment methods and further optimizing optical diamond coatings. The results of inkjet printing patterns with diamond nanoparticle seeds are promising and will play a significant role in heat management in microchips. We are pleased to present these methods and findings in this master's thesis.

We gained invaluable experience working with the FME group and on the ULTRAHARD project over the last four months, which we will take with us into our future careers.

Together with our internal promotor, drs. ing. Pieter Verding, we worked around this research question. Pieter helped us a lot with the principles of the used techniques as well as his assistance in the search for optimal coatings. Prof. dr. ir. Wim Deferme, our main promotor, assisted us in processing our results and writing this thesis with his extensive knowledge and experience. In addition to Wim and Pieter, project engineer Dieter Reenaers assisted us in getting started with the inkjet printer and diagnosing and resolving printer issues. As a result, we would like to express our heartfelt gratitude to these gentlemen for always guiding us with their knowledge and insights. Furthermore, we would like to thank all of the imo-imomec researchers who assisted us with our research.

Jeunen Ewoud
Thomas Seppe
February 2022

Table of contents

List of tables

List of figures

Glossary

Abbreviation	Meaning
AFM	Atomic force microscopy
CA	Contact angle
CF_4-Plasma	Carbon tetrafluoride plasma
CF	Centrifuge
CH_4	Methane
CIJ	Continuous inkjet
Co	Cobalt
CO_2	Carbon dioxide
Cr	Chromium
CVD	Chemical vapour deposition
DOD	Drop on demand
EG	Ethylene glycol
EM	Electron microscope
ETH	Ethanol
Fe	Iron
H_2	Hydrogen
H_2O	Water
IPA	Isopropyl alcohol
LA MW PE CVD	Linear antenna microwave plasma-enhanced chemical vapour deposition
Mn	Manganese
Ni	Nickel
O_2-Plasma	Oxygen plasma
OM	Optical microscope
Ra	Average roughness
Rq	Root mean square roughness
Rt	Peak-to-peak value
Rz	Difference between five highest and five lowest points
SDND	Diamond nanoparticle seeds
SEM	Scanning electron microscope
SFA	Surface free energy
SFT	Surface tension
SPM	Scanning probe microscopy
STM	Scanning tunnelling microscopy
Ta	Tantalum
Ti	Titanium
USSC	Ultrasonic spraycoater
$UV\text{-}O_3$	UV-Ozone
W	Tungsten
Wa	Waviness
Zr	Zirconium

Abstract

This research investigates two different deposition methods to apply diamond coatings. One method is inkjet printing, which deposits diamond seeds very precisely in a fine pattern mainly to improve the thermal conductivity in electronics, and the other is ultrasonic spraycoating, which creates a cloud of small droplets to coat larger surfaces like solar cells for scratch-resistant applications. Each method requires different surface conditions of the substrate: inkjet printing requires a relatively low surface free energy, while ultrasonic spraycoating requires a high surface free energy. This thesis compares a chemical to a physical pre-treatment process, respectively UV-O_3, and plasma. Moreover, this thesis aims to determine the ideal time-interval between pre-treatment and application process. The goal is to visualise the day-to-day evolution in a graph.

For this design of experiments, three sets of samples were prepared for each pre-treatment method. Of these sets, one of each was used to measure the contact angle every 24 hours during 21 days to determine the surface free energy of the surface. The other sets were used to print a pattern and spray a uniform coating with diamond nanoseeds.

As a result, this master's thesis clearly shows that depositing uniform coatings with an ultrasonic spraycoater requires a period of one to five days with a UV-O_3 treatment, whereas printing fine patterns with an inkjet printer requires at least ten days with an O_2-plasma treatment.

Abstract in Dutch

In dit onderzoek worden twee verschillende depositiemethoden onderzocht om diamantcoatings aan te brengen. De ene methode is inktjet printen, waarbij diamantzaden zeer nauwkeurig in een fijn patroon worden afgezet, voornamelijk om de thermische geleidbaarheid in elektronica te verbeteren, en de andere methode is ultrasoon spraycoaten, waarbij een wolk van kleine druppeltjes wordt gecreëerd om grotere oppervlakken zoals zonnecellen te coaten voor krasbestendige toepassingen. Elke methode vereist verschillende oppervlaktevoorwaarden van het substraat: inktjet printen vereist een relatief lage surface free energy van het oppervlak, terwijl ultrasoon spuiten een hoge surface free energy van het oppervlak vereist. Deze thesis vergelijkt een chemisch met een fysisch voorbehandelingsproces, respectievelijk UV-O_3, en O_2-plasma. Bovendien beoogt deze thesis het ideale tijdsinterval tussen voorbehandeling en applicatieproces te bepalen. Het doel is om de dagelijkse evolutie te visualiseren in een grafiek.

Voor deze opzet van experimenten werden zes sets van samples geprepareerd: drie sets voor UV-O_3 en drie sets voor O_2-plasma. Van deze sets werd er één gebruikt om de contacthoek elke 24 uur te meten gedurende 21 dagen om de surface free energy van het oppervlak te bepalen. De andere sets werden gebruikt om een patroon af te drukken en een uniforme coating met diamant nanoseeds te coaten.

Het resultaat van deze masterproef brengt perfect in kaart dat voor het afzetten van uniforme coatings met de ultrasone spuitcoater een periode van één tot vijf dagen ideaal is met een UV-O_3 oppervlaktebehandeling, terwijl voor het afdrukken van fijne patronen met inktjet een periode van minstens tien dagen nodig is met een O_2-plasma behandeling.

1   Introduction

1.1   Context

Diamond coatings are already used for applications in the industry. The tool life of diamond coated mills is much longer than uncoated mills. But diamond coatings can also be applied on different kind of surfaces for even more applications. In practice, there is a need for a scratch-resistant optical coating to protect glass for different applications. Imo-imomec is a research institute from Hasselt University that participates on a project about optical diamond coatings. This project about diamond coatings is named ULTRAHARD. Multiple companies (23 in total such as Oerlikon Balzers, Sirris, Barco, Berliner Glas, Blösch) are participating in this international project. The intention of this project is to create an optical, scratch-resistant diamond coating on glass substrates. These substrates can be used in different applications such as protective glass for solar cells, beamer lenses, and expensive watches to protect against scratches or reduce reflection. Diamond is a perfect solution for these coatings because diamond is transparent , wear-resistant, and is the hardest natural material known to man. And therefore is an ideal solution to protect these solar cells or watches. The contribution of this master's thesis is to analyse the pre-treatment processes that a glass substrate can undergo to efficiently and optimal deposit the diamond nanoparticles before the growth of the diamond coating.

The glass substrate needs to pass through different steps before the coating. The first step cleans the glass by going through an ultrasonic bath. The second step is a surface pre-treatment that changes the wetting properties of the surface. The contact angle indicates the spreading of a droplet that falls on the surface.

In the third step, diamond nanoparticles are applied to the glass substrate. The diamond is delivered as diamond nanoparticle seeds (5-15 nm) in a aqueous colloid. These seeds are applied to the glass by using an ultrasonic spray coater or an industrial inkjet printer. The diamond seeds remain on the surface after the aqueous solution evaporates.

In the fourth step, the diamond seeds are grown. This growth process happens in a linear antenna microwave plasma-enhanced chemical vapor deposition reactor (LA MW PE CVD). The diamond seeds grow around 45 nm/h in the reactor to a fully covering diamond layer. After the growing step, the coating can be checked for imperfections using an optical microscope and a scanning electron microscope (SEM). It can also be tested for durability by sandblasting or scratching the surface of the glass substrate. A schematic overview of this process can be seen in the Figure 1 .
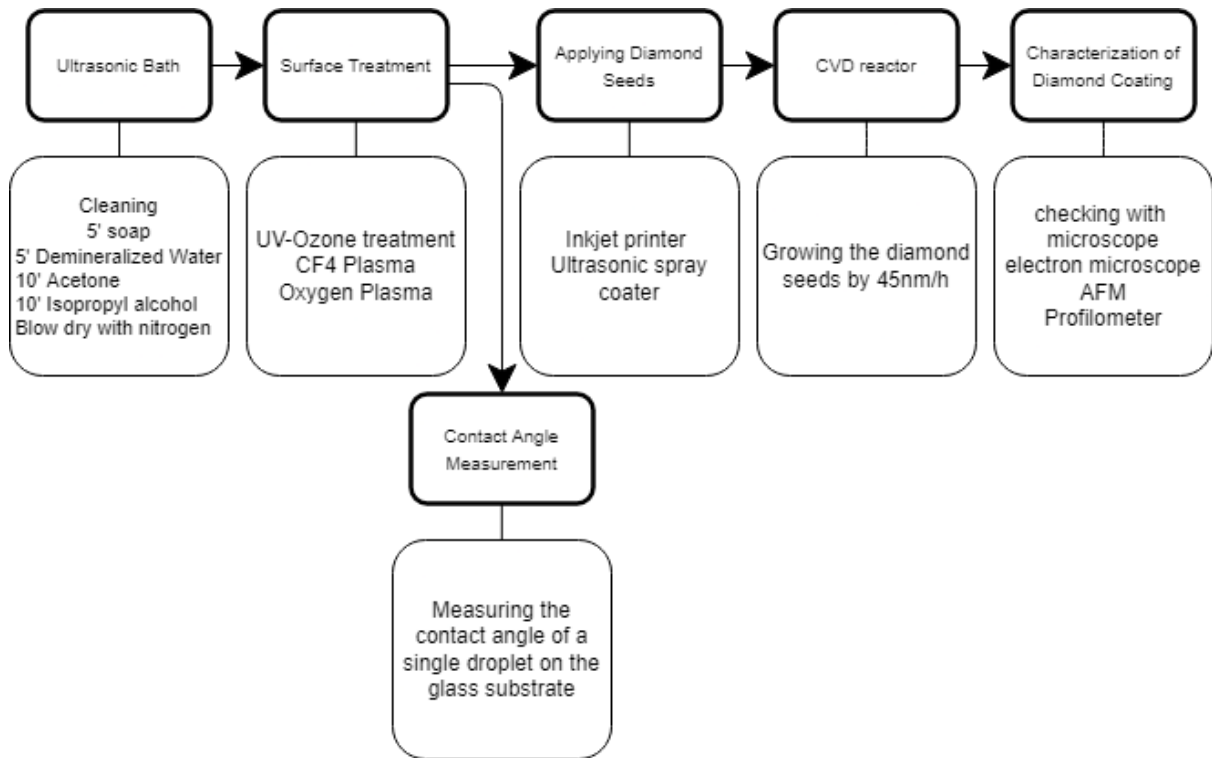
Figure 1: Pre-treatment and coating process to apply diamond nanoparticles seeds and form a uniform coating.

1.2   Research question

The industry standard to apply a uniform coating of the diamond nanoparticles is spincoating. This is a suitable method for applying a near perfect coating, but a limitation of spincoating is that the maximum sample size is restricted to six inches in diameter. Another way of applying the nanoparticle seeds is the usage of an ultrasonic spraycoater (USSC). Theoretically, the sample size is unlimited when using an ultrasonic spray coater. 3D objects like beamer lenses can also be spray coated by using a different type of nozzle.

The difference between spin coating and ultrasonic spray coating is that spin coating gives a perfect coverage. Problems like coffee rings, pinholes or delamination occur more frequently when using an ultrasonic spraycoater.

A third way of applying diamond nanoparticle seeds is inkjetting them . The inkjet printer can print patterns or areas. Low surface energy is desired when printing patterns or fine lines. This low surface energy means that a different pre-treatment is needed for the inkjet printer. The problem with these pre-treatment methods is that they deteriorate over time. This degradation relates to the surface energy and thus also to the spreading of the ink on the surface.

Different surface properties are preferred when applying diamond nanoparticle seeds with an ultrasonic spraycoater or inkjet printer. With the surface conditions optimised for each depositing technique, the possible occurring defects and problems can be minimised.

1.3 Objectives

The main objective is to determine an ideal pre-treatment, ideal period between the pre-treatment and the coating application for different kinds of substrates and ways of applying the coating . The time period may vary for an USSC or inkjet application. This objective can be considered solved if there is an exact method and timetable of every type of substrate and the different ways of applying the coating. These objectives can be split up into two distinct categories: functional and technical.

The functional objectives are:
-       having a scratch-resistant coating where the haze is limited to 5% by using the sand trickling test according to DIN 52348-1985.

The technical objectives are:
-       surface roughness of less than 20 nm for layers between 100 and 600 nm thick,
-       no pinholes in layers with a thickness of more than 100 nm,
-       the waviness of less than 20 nm for layers between 100 and 600 nm.

The wishes of the industrial partners in the ULTRAHARD projects are:
-       no visible defects with the SEM and optical microscope.

1.4 Method

Every substrate needs to be cleaned to ensure the excellent adhesion of diamond seeds to the glass substrate. An ultrasonic bath is ideal for this purpose because it is easy and quick to use. The samples are treated with different solvents to make sure it is clean.

To determine the degradation of the different surface pre-treatments over time, six sets of samples will be prepared. Three sets will be treated with a UV-ozone cleaning process while the other three undergo a O_2-plasma treatment. One set of each pre-treatment will be checked with a contact angle meter. Figure 2 shows how the contact angle can be determined. The contact angle of a droplet increases after time because the surface treatment degrades [1]. After this step, a graph can be created with the contact angle as function of time .
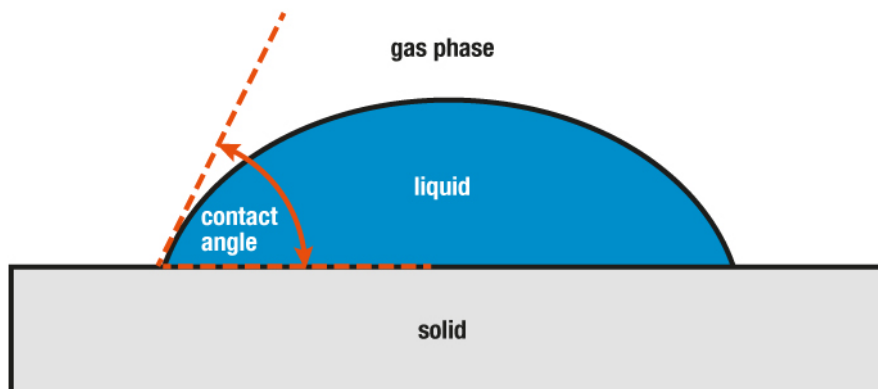
Figure 2: Contact angle of a droplet visualised [2].

The other sets will be coated with diamond seeds by using the ultrasonic spray coater or the inkjet printer. After this step, the seeds are grown into a full coating by using the CVD reactor.

When these grown samples are checked by a microscope, electron microscope, or a profilometer for roughness, the effect of the degradation of the surface pre-treatment, i.e. the decrease of the surface energy can be monitored. For the inkjet printer, it is preferred to have a low surface energy to create a high resolution of the pattern. It is preferable for the ultrasonic spraycoater to have a sample with high surface energy to ensure good coverage of the diamond seeds.

When all the samples are inspected, a new graph can be created. And an ideal time can be defined between pre-treatment and applying the diamond seeds. By defining this time, it is possible to eliminate as many defects as possible.

2 Literature research

The following chapters of this thesis discuss the techniques and materials used. Firstly, this thesis discusses diamond as a material, the applications and possible substrates. After this, it will review the principle of wettability and the possible problems in a coating. After this, the literature research discusses the materials and methods used to treat the glass's surface, deposit the nanoparticles, and grow diamond on a glass substrate. This master thesis uses the ultrasonic spray coater and the inkjet printer to apply the nano-diamonds to the substrate. After the depositing step, the diamond growth happens in a chemical vapour deposition (CVD) reactor. The concept of the CVD system is introduced, but a detailed description falls outside the scope of this thesis. This literature research also shows how to characterize the coatings both morphological and mechanical.

2.1 General introduction in diamond coatings

2.1.1 Diamond as a material

Natural diamonds [3] are created deep below the earth's surface and requires high temperatures and pressures to form. Diamond crystals are carbon atoms that are tetrahedrally bonded with sp3 hybrid bonds. The structure is a body-centric cubic, like shown in Figure 3.
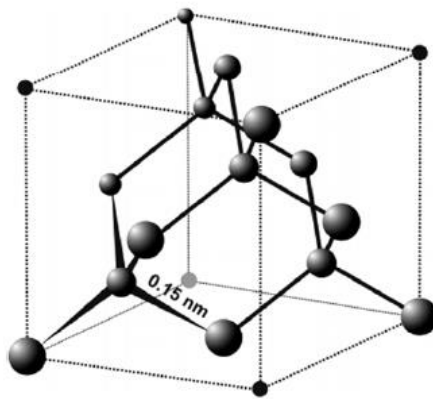
Figure 3: Body-centric cubic structure of diamond [4].

It is possible to create synthetical diamonds with multiple techniques. General Electric Company was the first to create synthetic diamonds in 1954 using high pressure and high temperature. Chemical vapour deposition is also a way to create diamonds. This is discussed in 2.2.4. It is also possible to create diamonds using a shockwave. Shock waves are of a short duration, so the diamonds created are only a few nanometres thick [3].

Natural diamond has many impurities that are present in the diamond lattice. Researchers identified these objects and their effect on the optical, thermal and mechanical properties of diamond. The major impurity is nitrogen but notable amounts of oxygen and hydrogen are also present.

The absorption of infrared, ultraviolet and visible light has led to a classification. Most diamonds are type I and their absorption edge is around 330 nm. while type II has the absorption edge around 220nm. This is due to the nitrogen that is present in the diamond. The table below shows the percentage of nitrogen per type of diamond.

Table 1: Diamond types and nitrogen content [3].

Type	Characteristics	Nitrogen abundance
Ia	Around 98% natural	N up to 0,3%
Ib	About 0.1% of natural	N in single substitutional sites
IIa	about 2%	Very low N level
IIb		Extremely low nitrogen level

The thermal conductivity of diamond is very high and is a major factor in its performance in many applications such as machining, grinding and polishing which creates high temperatures. The thermal conductivity of diamond is 2000 W/mK at room temperature [5] and is around 5 times higher than copper (386 W/mK) [6].

The optical properties of diamond are excellent. This makes diamond ideal for detector applications. Type II diamonds are transparent in the range from 220 nm to 2.5 µm. Type I is transparent from 330 nm to 2.5 µm. Colourless diamonds are the rarest and most valuable, however it is possible to have coloured diamonds. The most common colours are yellow and brown but other colours can also occur like orange, pink, green, blue, red and black. This colour is due to the absorption bands in the visible region. The yellow colour for example increases as the nitrogen percentage increases. The diamond appears green at nitrogen contents of around 300 - 400 ppm.

The chemical reactivity of diamond is also very good because the material is inert to most forms of chemicals and cannot be affected by acids except the acids that act as oxidizing agents at high temperatures. The chemical reactivity [3] of diamond is also very good because the material is inert to most forms of chemicals and cannot be affected by acids except the acids that act as oxidizing agents at high temperatures. Diamond can react with oxygen but only above 900 K. Diamond can react with two different groups of metals at high temperatures. One group includes W, Ta, Ti and Zr, these can react chemically to form their respective carbides. The other group includes Fe, Co, Mn, Ni and Cr. These metals are true solvents of carbon in their molten states.

The high strength of the carbon bond in diamond is the source of the excellent wear and mechanical properties. Diamond is known to be the most rigid material on any measurable scale, which makes the dislocation of the atoms very difficult. Table 2 shows the hardness properties of diamond [7].

Table 2: Hardness properties of diamond [7].

Property	Value (GPa)
Knoop hardness (500 g load)	[001] Surface = 56 – 102 [111] Surface = 88
Vickers hardness	Polycristalline = 85 -100 Single cristal = 70 – 100

The high thermal conductivity and low friction properties combined with these high strength properties are ideal in cutting applications, optical coating applications or as a heat conductor in sensors. These applications will be discussed in section 2.1.1.2.

2.1.1.1   Diamond seeds

The diamond seeds [8] used in this thesis are from Plasmachem. The Single-Digit NanoDiamonds (SDND) have a particle size of 5-15nm. The delivery of the diamond seeds happens in a demineralised water solution with 50 mg/ml diamonds. This solution is diluted in more demineralised water for use in the ultrasonic spraycoater or mixed with other solvents for the inkjet printer.

A dilution in demineralised water is a possibility to apply the diamond seeds. The boiling point of water is 100°C. The specific heat (Cp) of water is 4.187 kJ/kg K [9]. This means that water needs a lot of energy to heat up and makes it more difficult to evaporate, leading to more extended drying times. Water has a high surface tension, and this high surface tension is the cause of higher contact angles, making the uniform coverage of the coating more difficult. The influence of the surface tension will be discussed in section 2.1.4. The advantage of water is that it is safe to use and forms no hazard to the operator. The risk of coffee rings is greater because the diamond nanoparticle seeds have more time to settle due to the capillary flow. This phenomenon will be discussed later. A possible solution is to raise the temperature of the substrate or to move to a different solvent.

Normally, acetone would be a suitable solvent for the formulation because of the low boiling temperature (56.05°C). The specific heat (Cp) of acetone is 2.14 kJ/kg K [10], this means that the acetone evaporates quickly on the surface of the substrate, and the effect of coffee rings is minimal. A disadvantage of the use of acetone is that it is hazardous when inhaled. The disadvantage of using the Plasmachem nanoseeds in acetone is that the seeds settle and collect on the bottom of the solution due to the modification of the seeds. This makes acetone as a solution unusable.

2.1.1.2   Applications of a diamond coating

CVD diamonds are already being used in multiple applications in the industry. Diamond-coated cutting tools are used to reduce machine downtime and improve part quality in automated manufacturing processes due to diamond's low friction and thermal conductivity properties [11].

Figure 4: Diamond coated cutting tools [12].

Diamond's high thermal conductivity can help with thermal management in electronic devices. The packing and power density in integrated circuits increase faster than the cooling efficiency of the substrate material. So the heat spreading material must have a high thermal conductivity while also maintaining a thermal expansion rate that is compatible with the substrate. The mismatch between silicon and gallium arsenide or soldering joints which are now being used creates thermal stresses in the device and can fail. Aluminium and copper have generally been used for heat spreading purposes, but these have a significant mismatch with silicon. Therefore it can be helpful to use diamond as reinforcement embedded in a thermal package substrate [13].
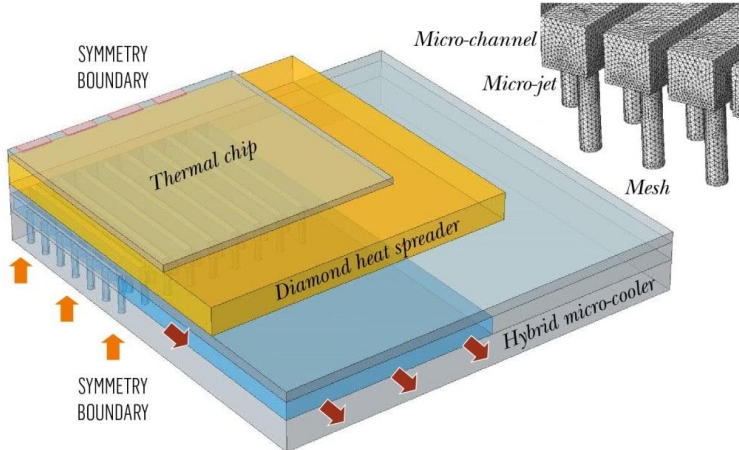
Figure 5: Diamond used for cooling applications in electronic devices [14]*.*

The optical properties of diamond make it attractive to use as a thin film coating for multiple applications. The optical transparency in the broad wavelength range, chemical stability and hardness makes it possible to protect optical fibres against mechanical or chemical damage. Due to the high refractive index, thin films can also be used to enhance the sensing properties of optical fibre devices [15].

Diamond thin films can also be used on solar cells as an anti-reflection and protective coating due to the mechanical hardness, low friction coefficient and high refractive index. This anti-reflective coating increases the efficiency of the solar cells.

Diamond thin films can also be used on mobile phones. Modern mobile phones have sapphire glass, which scores a nine on the Mohs scale. Where diamond scores a ten. The high thermal conductivity will reflect heat away from the phone's display, resulting in cooler-running phones [16].
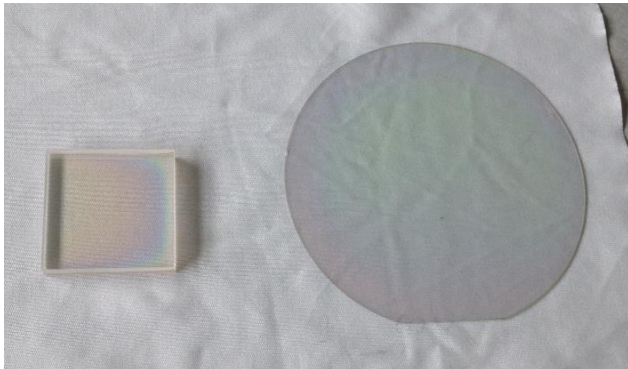
Figure 6: Diamond coated glass on the left vs sapphire glass on the right [14].

2.1.2 Substrates

Three types of glass are used in this project. These are:
- borosilicate glass (Corning eagle 2000),
- fused silica (Neyco),
- float glass (AGC).

The different types of glass substrates are listed above, with the manufacturer between brackets after the name. Each type has different mechanical properties, which means they will behave differently when coated and grown up in the reactor. This different reaction is an extra challenge and can lead to a distinct set of ideal parameters for each substrate.

2.1.2.1 Important parameters

Each glass has its mechanical properties. This ensures that not all glass substrates will react the same on the treatment. The reaction can be linked to different sets of parameters. Therefore it is vital to know the relevant parameters for the research. The relevant parameters for the research are:
- expansion coefficient,
- hardness,
- roughness,
- chemical composition,
- melting point.

In Table 3 below, those parameters are given for each of the materials.

Table 3 : Mechanical properties of glass substrates.

	Borosilicate	Fused silica	Float glass
Expansion coefficient	$31.8*10^{-7}/°C$ (0°C-300°C)	$5.5*10^{-7}/K$ (20°C-320°C)	$9*10^{-6}/K$ (20°-300°)
Hardness	Vickers: 642	Vickers: 700	Vickers: 458
Roughness Ra (nm)	<0.5 to <1.0	1,44	2.496
Chemical Composition	62.7 wt% SiO_2, 26.9 wt% B_2O_3, 6.6 wt% Na_2O, 3.5 wt% Al_2O_3	99.93 wt% SiO_2, 0.029 wt% Al_2O_3, 0.010 wt% CaO, 0.001 wt% Fe_2O_3, 0.025wt% SO_3, 0.005 wt% Others	72.5 wt% SiO_2, 13.7 wt% Na_2O, 9.12 wt% CaO, 4.14 wt% MgO, 0.247 wt% SO_3, 0.13 wt% Al_2O_3, 0.103 wt% Fe_2O_3, 0.04 wt% K_2O, 0.01 wt% TiO_2
Softening point	958°C	1683°C	600°C

With these parameters, the first main difference is the softening point. The softening point of fused silica is substantively higher than that of borosilicate glass or float glass, the one with the lowest softening point. These temperatures are essential for when the samples are grown in the reactor. The higher the softening point, the higher the allowed temperature for the reactor is.

The hardness of fused silica and float glass is comparable, while the borosilicate is slightly softer than the first two. The expansion coefficient is essential when the samples are grown because of the heat in the reactor. When the substrate heats up, it will expand with its given expansion coefficient with the lower the value, the less it will expand, and so will the applied diamonds. If these two values differ too much, it will cause stress in the layer and, in extreme cases, even delamination. With the thermal linear expansion coefficient of the diamond being $1,0\times10$-6 K^{-1} [17], most of the glass substrates are in the same range as the diamond.

There is also a big difference in the different elements found in the glass, with fused silica being the purest, almost entirely made out of SiO2 and borosilicate having the minor share of SiO2. In contrast, float glass has the highest amount of other elements in it.

2.1.3   Possible problems in coatings

The coating and growing of samples is a complex process with many parameters which can go wrong. Therefore several problems can be encountered while trying to find the ideal way of manufacturing samples. Some come from the coating process, while others emerge when the samples are grown in the reactor. The following paragraphs are the problems listed, which were encountered the most during the testing. Some of these problems are related to the seeding techniques used.

2.1.3.1   Delamination

Delamination in coatings can occur due to multiple reasons. The properties of the coating or substrate are dependent. But also, the distribution of stress is essential. The surface of the substrate is not perfectly smooth or large, which can cause these residual stresses. Other causes of the residual stresses result from the manufacturing process, which can be the growth mechanism, mismatches in thermal expansion of the coating and the substrate or cooling techniques.

The interface stress is linearly proportional to the thickness of the coating. Thin coatings are less sensitive to delamination. The coating can fall off during the cooling phase when the thickness is above a critical level.

The surface of a substrate cannot be perfectly smooth or flat. Edges, corners or holes are always present on a substrate. These "imperfections" are also the cause of residual stresses. Figure 7 shows the shear and tensile stresses on different kinds of "imperfections" [18].
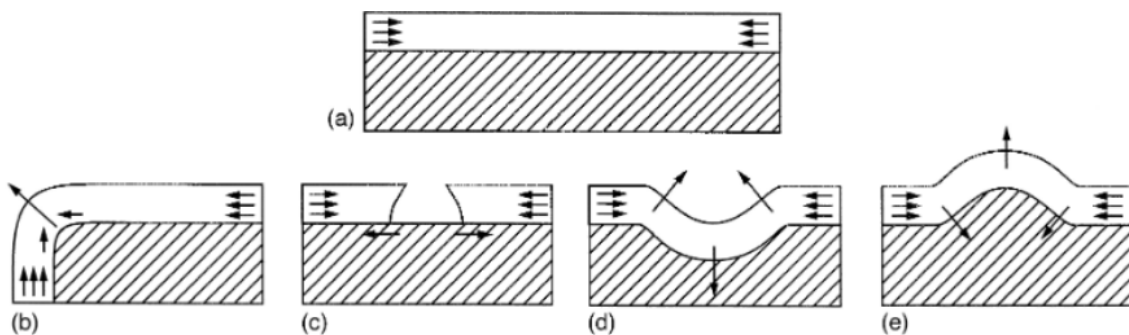
Figure 7: Residual stress visualised on a perfectly flat and smooth substrate (a). Tensile and shear stresses are shown on a corner (b), pore (c), grove (d) and edge (e) [18].

2.1.3.2 Coffee rings and the Marangoni effect

Coffee rings is one of the most common problems encountered during spray coating or printing. A coffee ring is not preferred because this increases the surface roughness, and there is a significant chance of non-uniform coverage. The coffee ring effect appears due to the capillary flow when a droplet evaporates at the edges. This solvent that is lost at the edges needs to be replenished by a solvent from the centre. This solvent contains solute, and these particles are deposited at the edges. When the solvent evaporates, the solute stays and stains, which causes the coffee ring effect. The effect of coffee rings can be minimised and needs to be, but this can never be eliminated. One of the principles which counteract coffee rings is Marangoni flows. When the droplets start to cool, a temperature gradient is introduced, which leads to a surface-tension gradient at the free surface of the droplet. It is this surface-tension gradient that induces the Marangoni flow. This flow carries particles from the surface to the centre, where they dive down and are absorbed by the centre onto the sample, or they go to the edge where the cycle starts again [18].
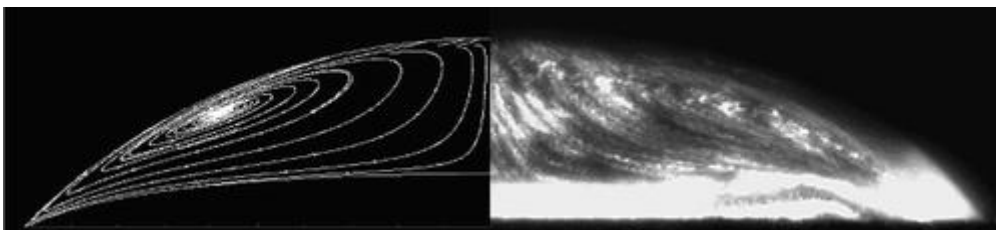
Figure 8: Marangoni flows visualised in a droplet [20].

2.1.3.3 Pinholes

Another problem is pinholes. They appear when the samples are not homogeneously coated, so when they are grown, they don't cover the entire surface, and small holes, pinholes, will appear. The thicker the layer, the lesser chances are of having pinholes. Because when the diamond seeds grow they grow in every direction, so when growing thick layers, 500 nm for example, every gap between diamonds less than one micrometre will be closed. An example of pinholes is shown in Figure 9.
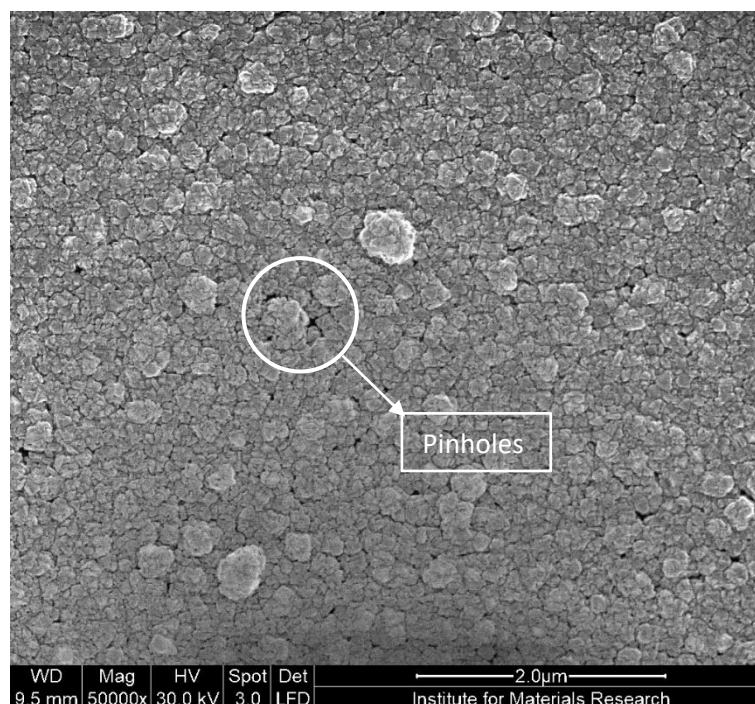
Figure 9: Black dots are pinholes on a seeded substrate where the grey particles are diamond nanoparticle seeds.

2.1.4　Wettability and surface free energy

To overcome the earlier mentioned problems, the surface free energy of the substrates can be altered. This will influence the wettability of the substrate.

2.1.4.1　Wettability

Wettability [21] can be described as the preference of a solid to be in contact with fluid rather then with another based on interfacial and the balance of surface forces. The wettability of a surface can be determined by the balance of three forces: attractive van der Waals forces, electrostatic double-layer forces that can be attractive or repulsive and steric forces. Since it is impossible to determine the value of each of these forces individually, it is necessary to find a method to determine the wettability of a surface. These techniques include contact angles, spontaneous or forced imbibition, capillary pressure and NMR response in cores. In this research, only the contact angle measurement will be used.

2.1.4.2　Surface free energy

Surface free energy (SFE) [21] has a significant influence on the wettability of solids by liquids. Therefore, it is an essential parameter for optimising coating processes and any other type of solid-liquid contact.

The term surface free energy is sometimes switched with surface tension (SFT). These two are interchangeable but as it relates to solid surfaces, usually surface free energy is used. The unit of SFE is mJ/m² (millijoule per square meter) as the energy per area, the unit of SFT is mN/m (millinewton per meter) but is also sometimes used for SFE. The symbol is σ (small sigma). In some cases, γ (small gamma) is used, but this is rarer.

The word free does not mean that the surface has no energy. The term relates to the amount of energy converted into mechanical work as opposed to internal energy, where the heat-related entropy is also included.

Systems aim for a state of free energy that is as low as possible. Liquids do this in a way that they minimise their surface area for the given volume due to the SFT. Ideally, this is a perfect sphere. Solids cannot change their surface area by deforming, but they can interact with a liquid to reduce free energy. The surface can be wetted. This shows that the SFE of a solid is closely related to its wettability.

2.1.4.2.1　Influencing the surface energy

For the coating of objects, good wettability and an equally high SFE is desired. But if the goal is to protect objects from water, it is beneficial to reduce the wettability. If the goal is to coat the surface entirely, it is of prime interest to increase the SFE. The most popular ways are plasma, flame and corona treatment. There are also some chemical methods with oxidizing agents. An essential step for these methods to work is the removal of low-energy contaminations by fats or oils. If this is done correctly, the surface will have a higher SFE. If low wetting, thus low SFE, is required, it is usually achieved by coating low-energy substances.

2.1.4.3   Contact angle

Wettability is measured by contact angle (CA) θ (small theta). The CA value is obtained by dropping a droplet on the substrate and optically measuring the angle between the contour of the droplet and the plane of the surface. This plane is called the baseline. The CA can be calculated using Young's equation, which states that the results come from a force equilibrium of three energy components that long for a state of minimal surface or interface:

- The SFE of the solid, σ_s
- The SFT of the liquid, σ_l
- The interfacial tension (IFT) between solids and liquids, σ_{ls}

The relation between these components can be described in Young's equation below:

$$\sigma_s = \sigma_{sl} + \sigma_l \times \cos \theta$$

In Figure 10 below the visual representation of Young's formula can be seen during a CA measurement.
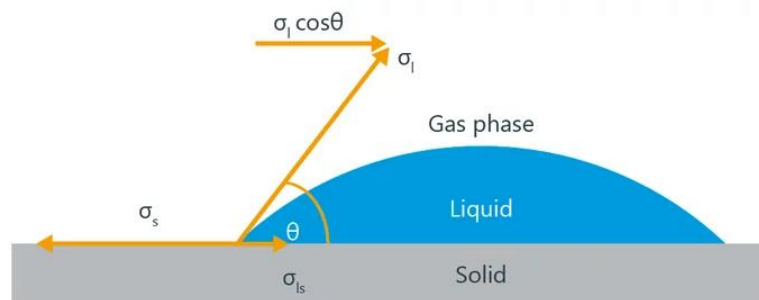
Figure 10: Young's force equilibrium during solid wetting[21].

2.1.4.4   Desired angles

There are several different pre-treatments available for each desired result. When choosing the suitable pre-treatment, the question is: what behaviour must be induced? The glass needs to be hydrofoil for the ultrasonic spraycoater to provoke a good spreading of the droplets. When there is a need to print patterns with the inkjet, it is beneficial to have a more hydrophobic character. It is not because there are different needs for the coatings that they have to have a different pre-treatment. It can be solved by increasing the time between treatment and applying the coating because the effectiveness of the pre-treatment deteriorates with time [1].

2.1.4.5   Practically measuring the contact angle

The contact angle measurement in this research is performed using the dataphysics contact angle system OCA contact angle meter. The software for visualizing and characterizing the measurement is SCA20.

2.1.4.5.1   Method

The substrates can be divided into four quadrants. The goal is to get a representative average of each substrate. Therefore a droplet, and thus a measurement, will be dispersed on each quadrant of the substrate. The droplet has a volume of 0,5 µL and is dispersed with a speed of 0,10 µL/s, the liquid is deionised water.

The method used for these measurements proceeds as follows. The droplet is dispersed on the substrate, which is positioned on a platform. A bright light backlights the droplet, and the camera positioned in front of the stage captures the scene. This scene is visible on the program on the computer. These two lines are positioned in the droplet as seen in Figure 11 below. With these lines, the contact angle of that particular scene can be determined. This value is only correct for that instance because the droplet flows out a bit over time. For this reason, a video of the process is captured, the CA value can thus be monitored over time.
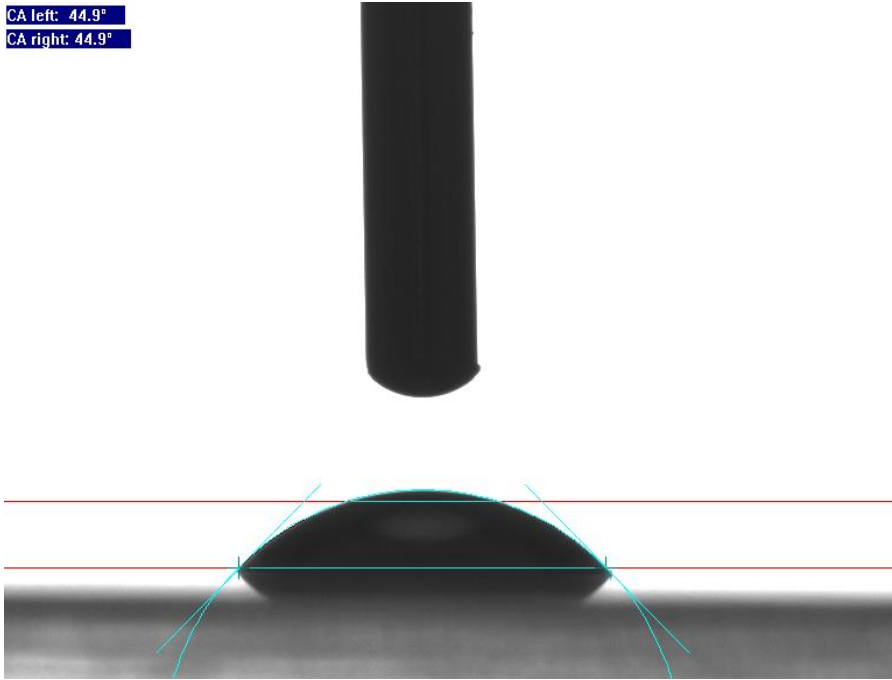
Figure 11: Contact angle measurement on the SCA20 software.

2.1.4.5.2   Calculating the contact angle

The graph created with all the CA data can be exported to excel. Here the non-linear part is removed and a linear regression is performed on the last 40 points. With the function rule of this trend line, the actual CA can be determined. An example can be found in Figure 12.
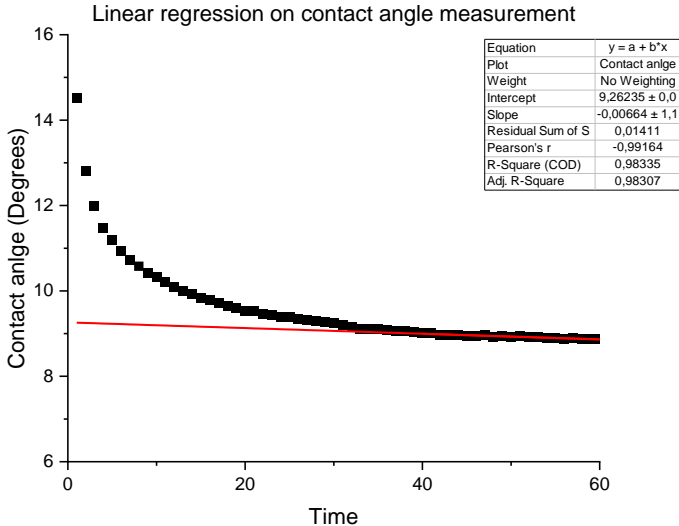
Figure 12: Performing linear regression on a contact angle measurement.

2.2 Material and methods

2.2.1 Cleaning the substrates

To prevent the incorporation of unwanted species (dust…) in the final layers, that could hinder the transparency or adhesion of the diamond coatings, first, the substrates are thoroughly cleaned in several steps. The first step is to clean it with an ultrasonic cleaner in different solutions for a specific time. An ultrasonic cleaner works on ultrasonic frequencies. This frequency causes micro-vibrations which vibrates the samples and shakes the contamination of the surface. The ultrasonic cleaner available in the lab is a VWR USC-T ultrasonic cleaner and operates at 45 kHz [22] to get the samples as clean as possible. First, the pieces are submerged in a soapy water mixture for five minutes, then for five minutes in demineralised water, then for ten minutes in acetone. The last fluid is isopropanol alcohol, in which the samples are also immersed for 10 minutes. After each cleaning fluid, the pieces are rinsed off with the next cleaning solution. When the cleaning is finished, the pieces are dried using pressurised nitrogen.

2.2.2 Surface treatment of samples

It is needed to apply a surface treatment to the substrate before applying the diamond nanoparticle seeds. Each treatment has a different effect on the contact angle of the droplets on the glass. The preferred treatment is chosen depending on the application of the glass and the deposition technique.

2.2.2.1 UV ozone

The cleaning process of UV-O_3 [23] is an effective way of removing organic contaminants. An important step is to remove any inorganic contaminants with pure water or any other solvents which is discussed in a previous paragraph. The principle of UV-O_3 cleaning is as follows. The organic contaminants are converted into volatile materials (e.g. water, nitrogen) by the decomposition of the UV light and the oxidation of the ozone. The emitted light of the mercury vapour lamps has a wavelength of 184.9 nm and 253.7 nm. The atmospheric oxygen will absorb the ultraviolet light with a wavelength of 184.9 nm to form O_3 with the following reaction:

$$O_2 \rightarrow O + O$$
$$O_2 + O \rightarrow O_3$$
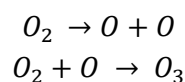
After this reaction, the ozone absorbs ultraviolet light with a wavelength of 253.7 nm to decompose the O_3. This ozone forms oxygen with a strong oxidizing ability. The organic compounds can be removed from the surface by irradiating them with energy stronger than the bonding energy. These contaminants formed by photolysis react with oxygen to form molecules like CO_2 and H_2O and are removed from the surface. This cleaning method is ideal as a surface treatment for applying a coating on glass or metals. Contaminants that are removable by UV-O_3 are, for example: cutting oils, vacuum-pump oils, soldering fluxes, human sebum, contaminants adsorbed during long-term air exposure or carbon films that form during vacuum evaporation. A schematic figure can be seen Figure 13 below. The wettability of the substrate depends on several factors like lamp intensity, ozone concentration, humidity, substrate temperature, exposure time and nature of the substrate.

Low Pressure Mercury Lamp

UV light
185nm&254nm

H_2O

CO_2

In-Ga-Zn-O GEL
Sub.

185nm
$O_2 \Rightarrow O+O$
$O+O_2 \Rightarrow O_3$

254nm
$O_3 \Rightarrow O_2+O^*$
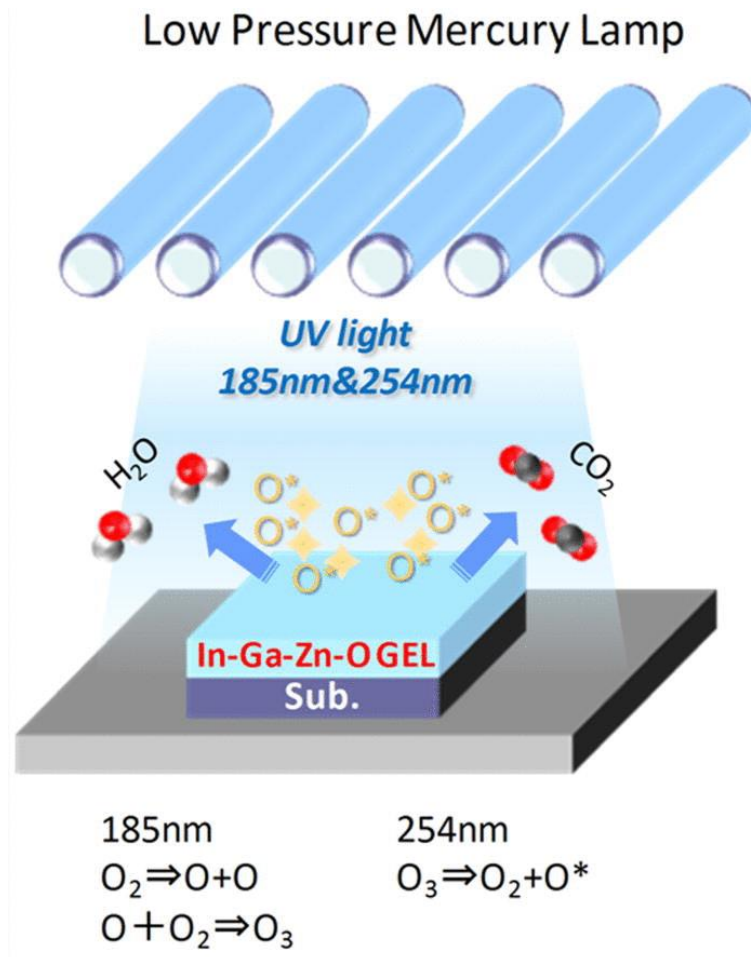
Figure 13: Principle of UV-O_3 surface treatment [24].

The advantages of UV-Ozone cleaning are [25]:
- it has low charging damage on substrates,
- it is a dry process.

The disadvantages are [26]:
- inorganic contaminants cannot be removed,
- staining and discoloration can occur,
- parts must be precleaned,
- safety precautions are necessary.

It is crucial to make sure that there is no leakage while the cleaning process is in progress. Ultraviolet light is dangerous and can cause skin burns or eye disorders. The ozone that forms in progress is toxic. Therefore it is recommended to ventilate the radiation room before opening the cover of the machine.

2.2.2.2 Plasma surface treatment

Plasma surface treatment [27] is a treatment that changes the surface energy of a material to improve the adhesion/bonding characteristics. This surface treatment process can be used on many materials such as plastic polymers, paper, glass or metals.

Plasma is the fourth state of matter. It exists out of ions and electrons. When additional energy is added to the gas state, it becomes ionised and reaches the plasma state. The plasma surface treatment used in this research is performed in a vacuum chamber. The plasma comes into contact with the substrate and transfers the additional energy to the surface to allow subsequent reactions like shown in Figure 14. These adapted properties of the surface are ideal for printing or adhesive bonding. The surface tension also changes when changing these properties of the surface. This surface tension impacts the wettability of the surface and thus the spreading of a droplet. Using oxygen as a gas during the plasma treatment improves the wettability of the surface. This wettability will probably be beneficial when coating an area. Using CF_4 as gas will decrease the wettability of the surface. The fluoride in the gas causes poor wettability. This will be needed when printing a pattern or fine lines.
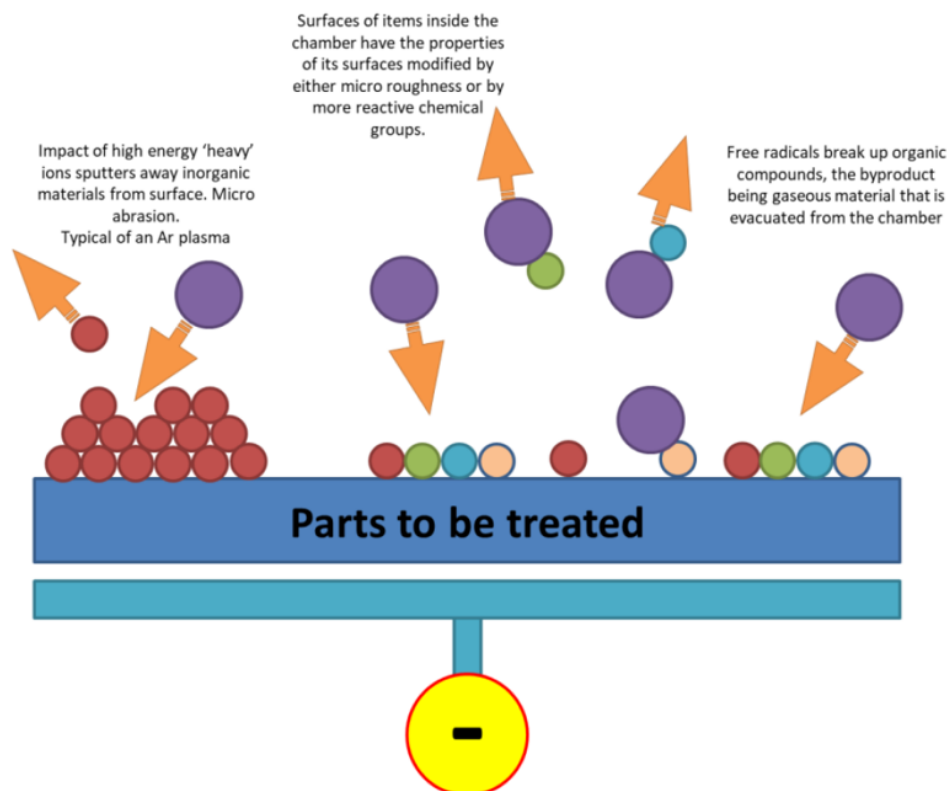
Figure 14: Principle of Plasma surface treatment [28].

The advantage of plasma surface treatment is that it is a low-temperature treatment with a short treatment time (+- 1 min). The amount and size of samples are limited to the size of the plasma ball. It is only limited to the surface of pieces, and the plasma penetration is relatively deep compared to UV-O_3 [29].

2.2.2.3 Corona Discharge

A corona discharge [30] occurs when the air around a conductor gets ionised. The plasma has a typical purple glow and adapts the adhesion of a surface. Corona discharge causes surface activation by bombarding it with plasma ions. These plasma ions improve the adhesion capabilities. Other applications of corona discharge are to sanitise pool water, remove pesticides and chemical agents from the air, or reduce drag on flat surfaces.

The purple glow is a side effect that occurs when the positive ions recombine with electrons, forming neutral atoms. These atoms release a photon of light when they reform. These released photons ionise more atoms to keep the process of corona discharge going.

There are two forms of corona discharge: *positive* and *negative*. The polarity of the electrode determines this. Positive corona discharge has a lower free electron density, but these are more concentrated and contain more energy. On the other hand, negative charges are bigger than positive ones. This is because the electron density is smaller and more spread out.

Corona discharge is used as a surface treatment to improve the wettability and adhesion of the surface without affecting the properties. It also improves the surface tension effectively so that the surface becomes more adhesive to inks and coatings. A disadvantage of the corona treatment is that it will be degraded over time unless a coating or ink is applied.

2.2.2.4 Comparison of the different surface pre-treatments

Table 4: Comparison of pre-treatment techniques.

	UV-O_3	O_2-plasma	CF_4-plasma	Corona discharge
Duration	15-120 min	1-3 minutes	1-3 minutes	1 minute
Wettability	Increases	Increases	Decreases	Increases
Advantage	Removes organic contaminants Low cost Dry process	Cleans substrate	Cleans substrate	Improves wettability without changing properties
Disadvantage	Inorganic contaminants remain Staining and discoloration Precleaning parts	Needs vacuum Etches surface Degrades rapidly	Needs vacuum Etches surface Degrades rapidly	Not consistent

2.2.3 Applying the diamond nanoparticle seeds

There are various ways to apply diamond seeds to a surface to create a coating. This thesis will discuss only two applications of applying the diamond nanoparticle seeds. Other ways of applying these seeds are spincoating or dipcoating.

The industry standard to apply coatings is by using a spincoater. The advantage of spincoating is that the result is a thin, uniform coating. The disadvantage of this technique is that the substrate size is limited. The spin coating process is commonly used for microelectronics manufacturing, like photo resistant coatings. A ultrasonic spray coater will be used to overcome the disadvantage of the small substrate size in a spin coater.

Another technique to apply diamond nanoparticle seeds is to use dipcoating. Dipcoating or immersion coating is when the substrate is submerged into a solution. A disadvantage of this technique is that two sides of the substrate are coated and that the amount of coating solution is much more significant than the other processes [31].

2.2.3.1 Ultrasonic spray coater

One of two ways the samples will be coated in this research is with the ultrasonic spray coater, abbreviated to USSC. The USSC is normally used for uniform coating and not for the printing of patterns. Specific patterns with the proper nozzle, for example, the accumist, can be printed without as much detail as with the inkjet printer. Therefore in this thesis, the USSC will primarily be used for the complete coating of substrates.

2.2.3.1.1 Principle of ultrasonic spraycoating

Spray coating [32] uses tiny droplets of coating material diluted in a liquid to deposit this on a substrate. The nozzle is fitted with piezo electrics that vibrate at an ultrasonic frequency. This ultrasonic vibration atomises the droplets. Many process parameters need to be controlled to ensure a uniform coating. The coating material concentration in the solution, the solvent used to spray the coating material, the number of spray passes, the nozzle speed, flowrate of the solution, distance to the substrate, temperature of the substrate, shroud pressure, vibration power. An ultrasonic spraycoater exists out of a syringe pump that supplies the solvent without any significant pressure. A ultrasound generator that vibrates the nozzles to create the standing waves and a heated bed to adjust the substrate temperature. The nozzle is usually mounted on a 3 axle system that is programmable in the XYZ direction. A schematic overview can be seen in Figure 15.
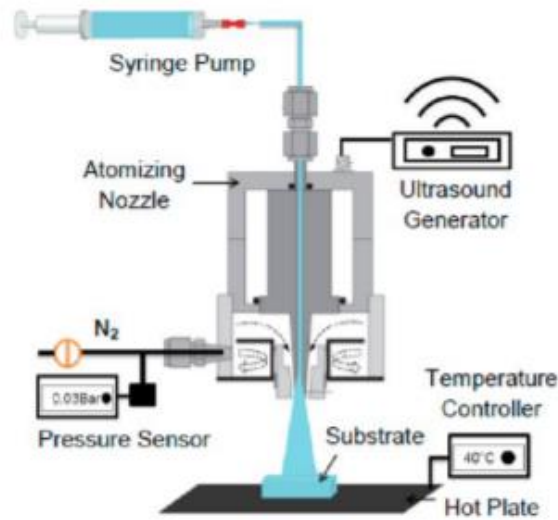
Figure 15: Working principle of ultrasonic spraycoating [32].

2.2.3.1.2 Nozzle type

The USSC can be equipped with different types of nozzles to spray different kinds of materials. An impact nozzle is used in this thesis to apply the diamond seeds to the substrate's surface. A schematic overview can be seen in Figure 16. Electrical energy is converted into mechanical energy by piezo crystals. This mechanical energy is then transferred to the solvent to create the standing waves on the nozzle [33]. The nozzle vibrates at a natural frequency of 120 kHz. The ideal droplet size can be optimised by adjusting the vibration power of the nozzle. The impact nozzle uses nitrogen as a shroud gas to push the droplets down to the surface.
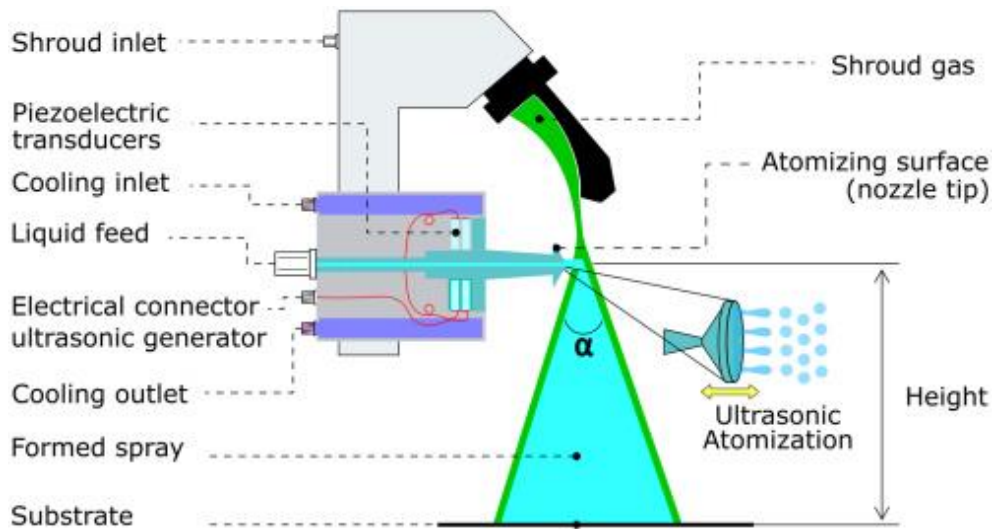
Figure 16: Schematic structure of impact nozzle [34].

2.2.3.2 Inkjet printer

Inkjet printing [35] is an easy, cheap and reliable method for printing. Almost all office/household printers are inkjet printers. This technology has been around since 1950. The inkjet printer uses droplets that are placed very precisely to form a pattern or figure. This precision requires a combination of multiple skills like chemistry, engineering and fluid dynamics.

Apart from printing ink, ink-jetting technology can also be used in an industrial setting to apply coatings, functional materials or even microstructures. The costs, reduction of waste and faster prototyping are benefits of this technology.

Industrial inkjet printers are classified into two big groups. The continuous (CIJ) or drop on demand (DOD) principle (see Figure 17 below). The continuous principle ejects drops continuously from the cartridge. These droplets are then ejected onto the substrate or are collected and re-used. This principle is commonly used for coding and marking purposes. The advantage of CIJ printing is its ability to use volatile solvents. This advantage allows the ink to dry quickly and helps adhesion on multiple substrates. The disadvantage is that it has a lower resolution and uses more ink.

Drop on demand printing is a technique where the drops are ejected from the cartridge when needed by a pressure pulse. The printer in this master's thesis uses a piezoelectric crystal to eject the drops. An electric signal creates a distortion. This distortion then creates a pressure pulse that ejects the droplet. Piezoelectric printing is the most advanced printing technique. It is a nozzle-based technique that is sensitive to clogging. The cartridge exists of a reservoir that connects to a narrow tube. This thin tube is called the restrictor. The advantage of DOD is the excellent resolution, good reliability and the use of multiple fluids. The main disadvantage is the cartridge. This cartridge is expensive, and a new cartridge will be needed for every different ink/fluid.
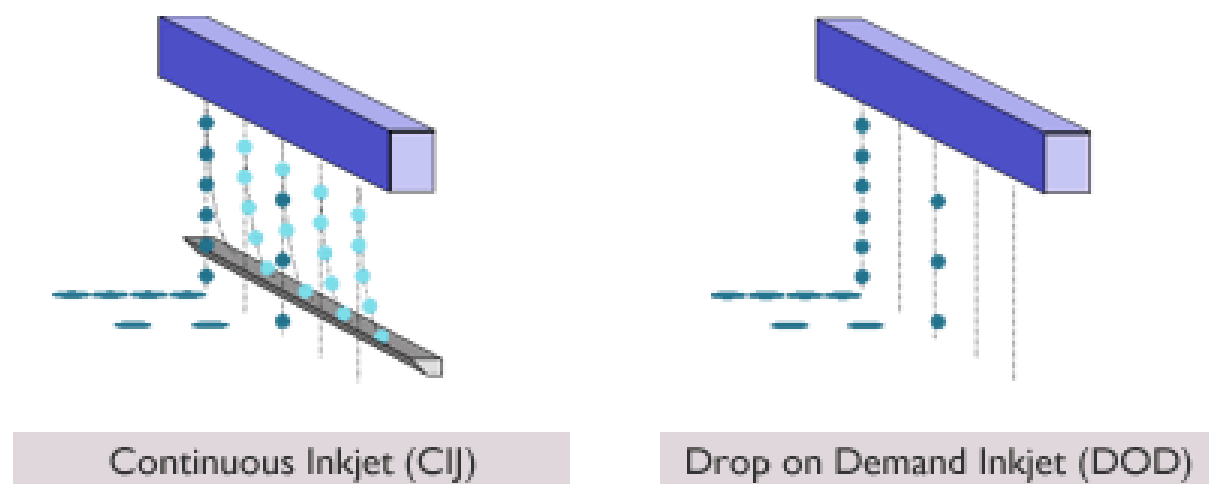
Figure 17: Continuous vs Drop on Demand printing.

The printer in the lab is a Fujifilm Dimatix materials printer [36]. The printer is designed to deposit fluidic materials on a substrate the size of an A4. The substrates are held in place by a heated vacuum table. The 16 nozzles of the cartridge are placed 254 µm apart. The drop spacing of the cartridge is adjustable by turning the cartridge on the printer. A built-in drop-watch camera allows the characterisation of the droplets ejected from the cartridge.

Figure 18: Fujifilm dimatix inkjet printer [36].

Inkjet printing is a solution to print different materials for multiple applications because of its low cost, few steps and low material loss. For example, it is used in digital textile printing because of its efficiency. Organic light emitting diodes (OLED) and other display pixels can be printed for computers, automobiles, TV, or mobile phones. Inkjet printing can also create wearable and flexible devices . These devices then can be mounted on the human skin like in the figure below or on fabric [37].
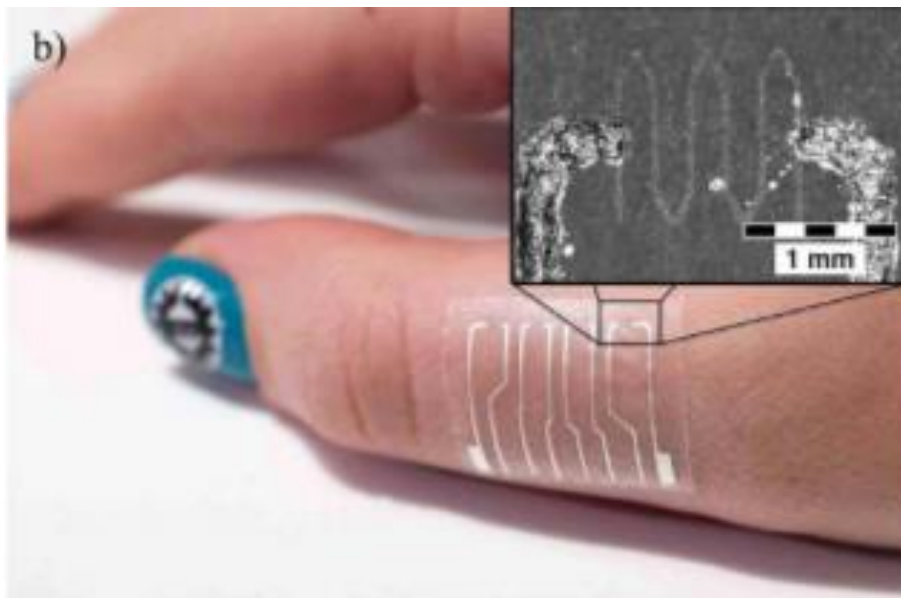
Figure 19: Printable sensor on human skin [38].

2.2.4 Diamond growth

Chemical vapour deposition (CVD) [4] is a technique that involves the deposition of carbon atoms on a solid substrate. The substrate can already be diamond or can be a non-diamond substrate. CVD differs from the High-Pressure High-Temperature (HPHT) method, which General Electric introduced in 1955. Growing diamonds in a CVD reactor is a complex process where diamond is synthesised from pure methane at a pressure of 13-40 Pa. The growth rate can be more than 10 µm/h by using enhanced methods and altering the flow of carbon as well as the stage temperature [39].

Scientists introduced enhanced methods to dissociate carbon-containing compounds by thermal or plasma processes. The growth rate in these enhanced CVD reactors depends on the transport of the reactant species to the substrate. Diamond growth is already possible from 100°C by altering the parameters of the CVD system. This low temperature makes it possible to grow diamonds on substrates with a low softening point. The expansion rate of the substrate is also less because of the low temperature. The low expansion rate reduces the stress in the substrate and coating [40].

The system used at IMO-IMOMEC is a linear antenna microwave plasma-enhanced chemical vapour deposition (LA MW PE CVD) system. Plasma-assisted systems use carbon-containing gasses mixed with a low concentration of hydrogen. The CVD system at IMO-IMOMEC uses a mixture of CO_2, H_2 and CH_4. The neutral radicals determine the growth process. The neutral molecules of CH_4 gas do not participate due to the high Gibbs free energy of CH_4 gas [41].

The microwave plasma-enhanced CVD shown in the picture below is commonly used as a growth method because of its many advantages, such as avoiding contamination on the coating due to electrode erosion. The plasma density produced by microwaves is also higher, and the growth rate can easily be increased by increasing the microwave power. A third advantage is that the plasma has a spherical shape in the middle of the reactor. This shape is easy to handle, keeps the reactor walls clean, and avoids carbon deposition. A disadvantage of the ball-shaped plasma is that the diamond quality can differ between the centre and the edge of the plasma ball, and that it is difficult for 3D objects.
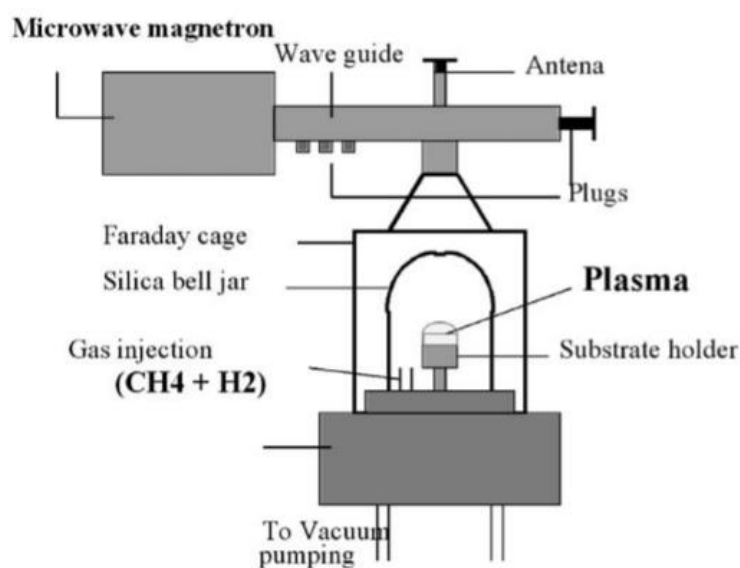
Figure 20: Microwave plasma-enhanced CVD process [42].

2.2.4.1 Principle of CVD growth

Growing diamonds in a CVD system is a complex process where the conditions need to be metastable. The gas phase, surface, chemical processes are complex, making the distinction between diamond, graphite or amorphous carbon difficult. Also, the effects of gas-phase chemistry, complex heat transport, nucleation, surface chemistry, and diffusion are difficult to understand.

Several factors have an impact on the quality of the diamond.
- Gas dissociation before the deposition is essential to achieve the desired growth rate.
- Hydrogen is required for efficient growth.
- The quality of the diamond increases if oxygen is added in the process.

For more info on chemical vapour deposition and diamond growth, it is possible to consult these links [5], [7], [39], [40].

2.2.5 Characterisation of the coating

The substrates need to be examined and characterised after the growth step. An optical microscope and scanning electron microscope can characterise the coating for any defects. The thickness and the roughness of the layer can be examined by a profilometer or atomic force microscopy.

2.2.5.1 Morphological characterisation

2.2.5.1.1 Optical microscope

An optical microscope [43]–[45] uses multiple convex lenses to enlarge small objects. Using different lenses can enlarge objects up to 300x that are not visible to the human eye. The magnification of a microscope is, however, not the biggest issue.

It is almost impossible to make a perfect image of a natural object because of the large range of wavelengths of visible light. Any point becomes a diffraction spot due to the unavoidable diffraction of the light passing through the lens. This is called spatial resolution. A so-called blur is created when two of these diffraction spots are too close together. Objects smaller than 0.2 µm cannot be seen using an optical microscope. A possible solution to this is to reduce the optical wavelength or use an electron microscope. Electron beams have a shorter wavelength than photons, so the resolution becomes better by using an electron beam.

Figure 21: Carl zeiss microscope [46].

There are several ways to enhance the contrast in an optical microscope. Brightfield and darkfield are the two most common.

Brightfield microscopy is suitable for observing the natural colours of the sample. A bright background illuminates the object. This generates dark parts of the sample.

Darkfield microscopy shows the sample on a dark background. The sample appears bright and reflects the light from the object into the lenses. A disadvantage is that darkfield microscopy is sensitive to dust.

2.2.5.1.2 Electron microscope

An electron microscope (EM) [47] has the same principle as an optical microscope. The main difference is that an electron microscope uses a beam of electrons to point at the object.

All EM's are based on the same principle:
-   a piece of tungsten is heated and forms a stream of high voltage electrons. This stream is then accelerated in a vacuum to the object. An electron beam in a vacuum act as radiation with a very short wavelength;
-   this accelerated stream is restricted and focused using different electromagnetic lenses into a thinner beam;
-   in the irradiated sample appear interactions, which affect the beam;
-   these interactions are then detected and formed into an image.

EM's could be separated into two major types. The transmission electron microscope (TEM) and scanning electron microscope (SEM). Only the SEM shown in the picture below is used in this research and will therefore only be clarified.
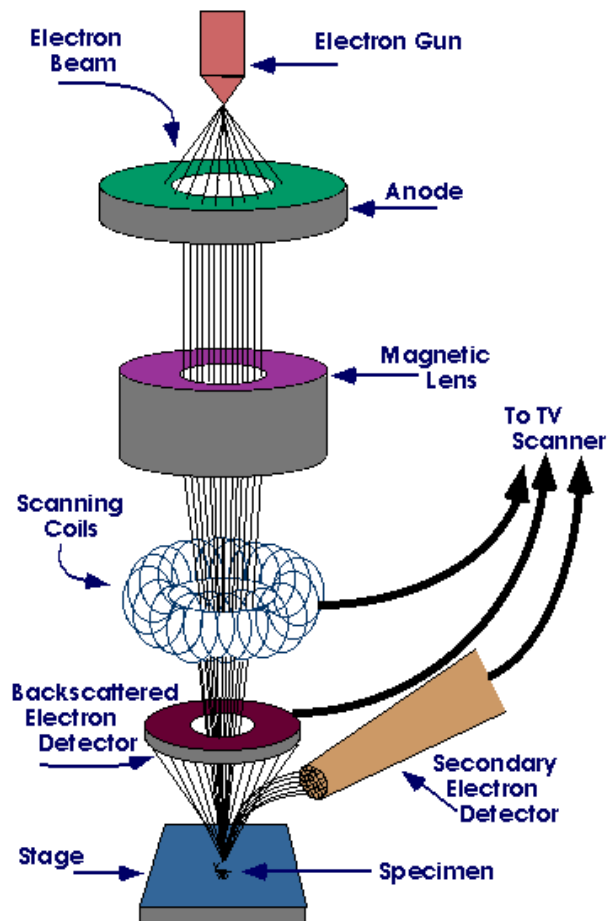
Figure 22: Working principle of a SEM.

The scanning electron microscope [48] has multiple advantages over an optical microscope. It has a significant depth of field, which allows for more of a specimen to be can be in focus. The short wavelength of electrons has a much higher resolution so smaller objects can be observed.

The electrons in an SEM are focussed into a fine point that scans over a specimen. These electrons react with the surface of the sample to create a topological image like shown in Figure 23. Secondary electrons and X-rays are backscattered from the object when it is struck with the electron beam. A detector captures these emitted electrons from the sample to produce the magnified image that is sent to the monitor.

An SEM microscope produces its electrons mainly from a tungsten filament. This is common because the electron source is cheap, reliable, and suitable for low magnification imaging.

| WD | Mag | HV | Spot | Det | 2.0μm |
| 9.5 mm | 50000x | 30.0 kV | 3.0 | LFD | Institute for Materials Research |
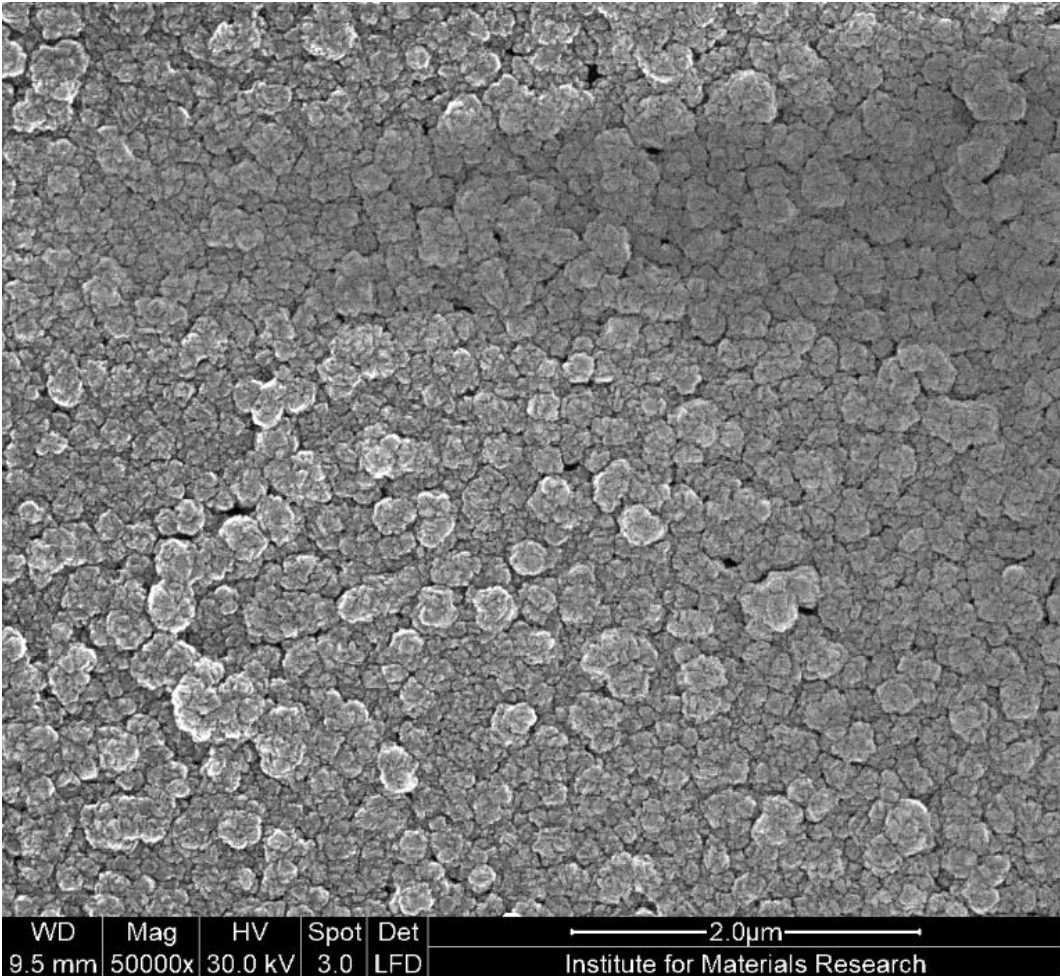
Figure 23: Diamond coating magnified with a SEM microscope.

2.2.5.1.3 Atomic Force Microscopy

Scanning Probe Microscopy (SPM) [49] is a technique that uses physical probes that scan the sample to create surface images. SPM is divided into two groups. Scanning Tunnelling Microscopy (STM) and Atomic Force Microscopy (AFM). STM is based on electrical current and has an excellent ability to measure with atomic resolution but can only be used on conductive and semi-conductive surfaces. In contrast, AFM can be used on insulating surfaces.

Atomic Force Microscopy creates a 3D profile of the object by measuring the force of a probe and the object's surface. The AFM consists of multiple components, as shown in the picture below. The probe, cantilever, scanner, laser, data processor and a photodetector.
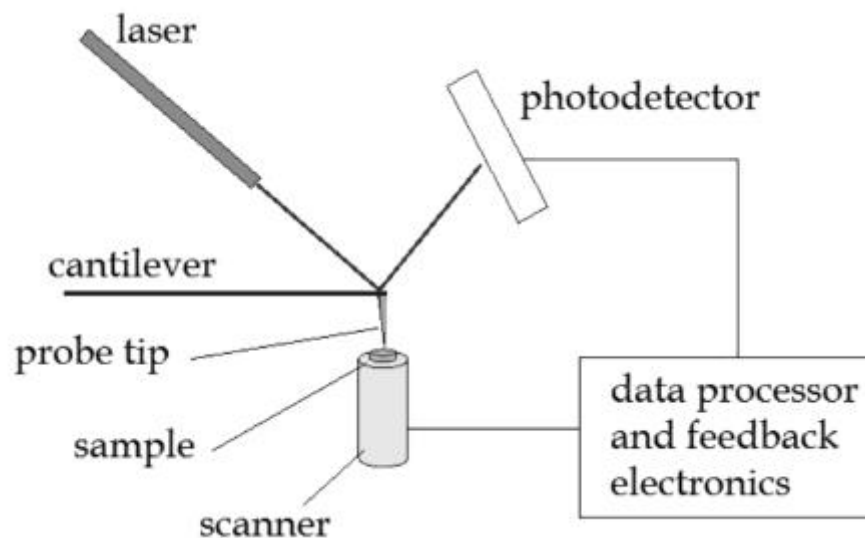
Figure 24: Principle of Atomic Force Microscopy [49].

The probe, which has a less than 10 nm radius, is mounted on a flexible cantilever that acts like a spring and touches the surface lightly. Hooke's law can describe this force:

$$F = -k \times x$$

Where F is force, k is spring constant and x is deflection.

A laser diode reflects on the cantilever and into a photodiode. This reflection changes as the cantilever bends. This bending is indicative of the interaction force of the probe's tip. The data processor acts as electronic feedback to keep the deflection of the cantilever constant throughout the scanning process.

The AFM can be used in three different modes. In contact mode the probe-surface distance is limited to 0.5 nm, and the contact force is kept constant. This is a fast scanning mode for rough samples.

Tapping mode [50] limits the contact by vibrating the cantilever near its resonance frequency. The attractive and repulsive interactions will reduce the sinusoidal motion of the tip as it comes near the surface. The feedback loop will keep the amplitude constant. This method tracks the sample line by line.

In non-contact mode where the probe oscillates above the sample. The surface is measured using the feedback loop to track the changes in amplitude when attractive forces pull on the probe's tip. The downside is that it generates a low-resolution image, and contaminants can interfere while measuring.

AFM can also be used for applications other than topographical measurements. It can use a contact or tapping mode variation to measure electrical, magnetic and thermal properties in multiple fields to characterise polymers, semiconductors, thin films and coatings, cells and many others.
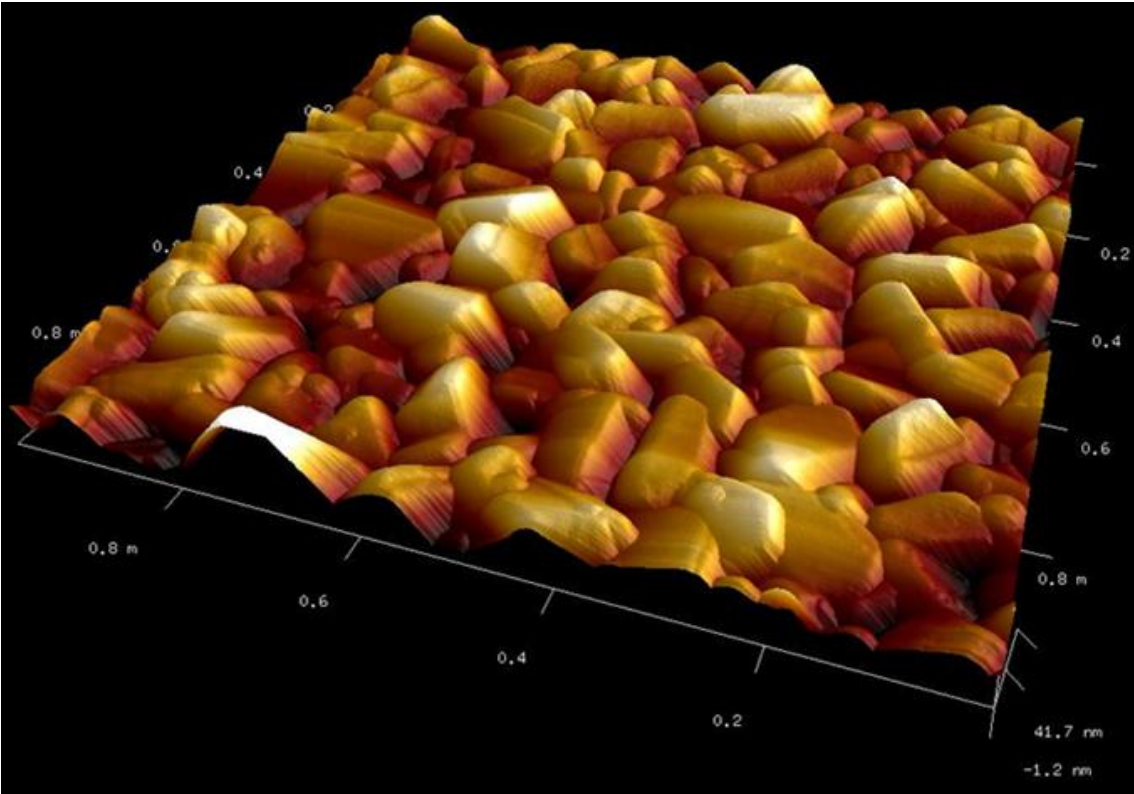
Figure 25: AFM measurement of a diamond seeded substrate.

2.2.5.1.4   Profilometer

One of the instruments that help characterise the diamond layer after the growing stage is the Dektak. The roughness is an essential parameter of the diamond layer, same with the waviness.

The principle of the Dektak is that a stylus with a diameter of 2 µm drags across the surface. This stylus follows the hills and valleys of the coating over a set distance and time according to the ISO4288: '96 standard. The slower the time, the more precise the measurement is.

A problem with the measurements is that they are not 100% accurate because the stylus has a diameter of 2 µm. Therefore it skips over the small indentations, which contributes to the overall roughness of the sample. If it is desired to know the exact roughness, Atomic Force Microscopy can be used, but the profilometer gives an adequate value to make an approximation.

With the samples sprayed with the inkjet printer, it is possible to measure the layer thickness if they are not fully coated. This is achieved by dragging the stylus from an uncoated part onto the coated part. With the software, it is then possible to calculate the height difference between these two areas.

2.2.5.1.5   Results

The results that are acquired by using the profilometer are roughness's and waviness. It is possible to get a lot of values, but the most relevant for this research are; Ra, Rq, Rz and Wa. The meaning of these is given below.

Ra Is the average roughness over a surface. It takes into account all the valleys and peaks. The way it can be calculated is shown below [51].

$$R_a = \frac{1}{l_m} \int_0^{l_m} |y| \, dx$$
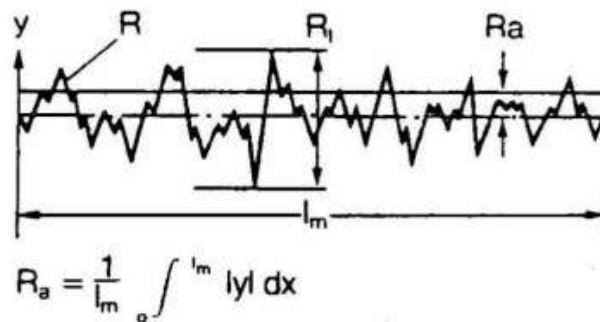
Figure 26: Visual representation of Ra[52].

Rq stands for root mean square. This indicates the root mean square value over the measured line [53].

$$Rq, Pq, Wq = \sqrt{\frac{1}{lr} \int_0^{lr} Z^2(x) dx}$$

Root means square height (for a roughness profile)
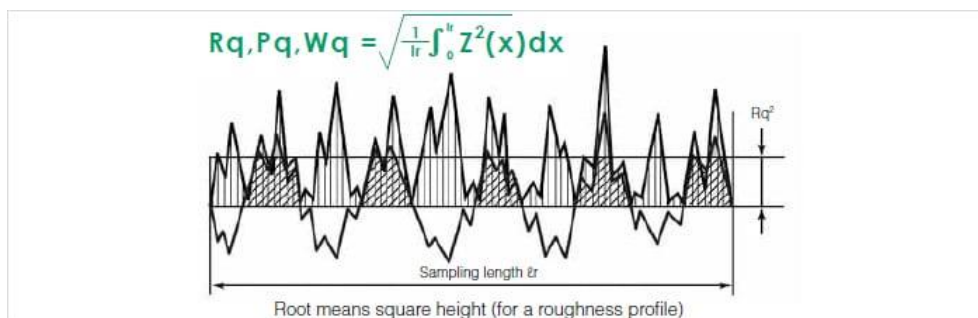
Figure 27: Visual representation of Rq[53].

48

Rz calculates the difference between the mean of the five highest peaks and the five lowest valleys [54].
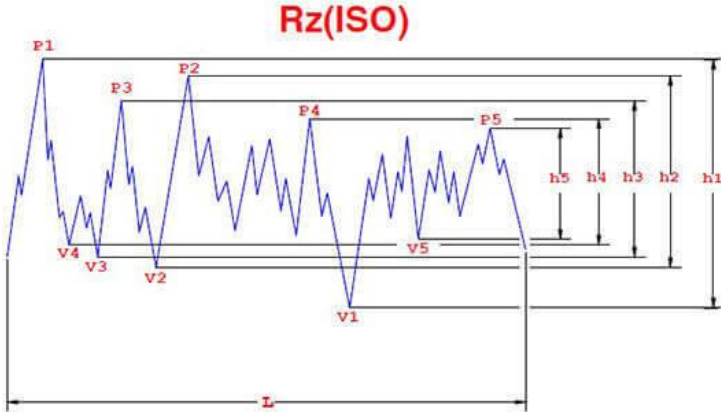
*Figure 28: Visual representation of Rz[54].^*

Wa is similar to Ra in that it uses the arithmetic mean [55]. But whereas Ra calculates the roughness value, Wa calculates the waviness of the surface that is measured. As shown in Figure 29, waviness is independent of roughness. Also, waviness is usually measured over a longer distance to get an accurate picture of the sample's profile.
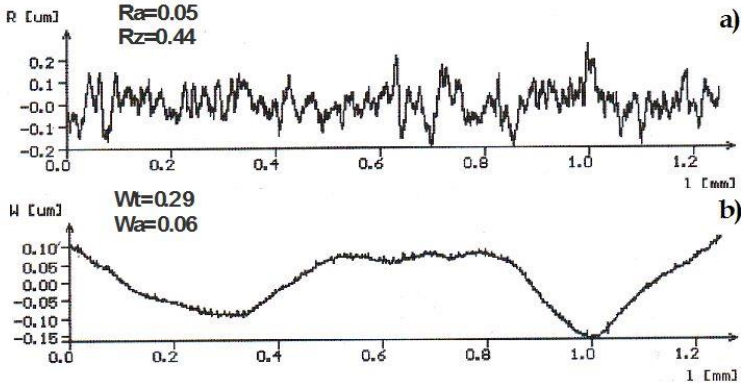
Figure 29: Visual representation of Wa[56].

2.2.5.2   Mechanical characterisation

2.2.5.2.1   Sand trickling test

The sand trickling test tests resistance to coating abrasion due to particle impact. This feature is critical for the quality of the coating because the effectiveness over time can be measured here. For this test (according to DIN 523458, 1985), 3 kg of sand with fixed grain size is dropped perpendicularly from a height of 1.5m over a rotating sample [57]. Afterwards, the damage can de be determined by comparing the haze before and after.
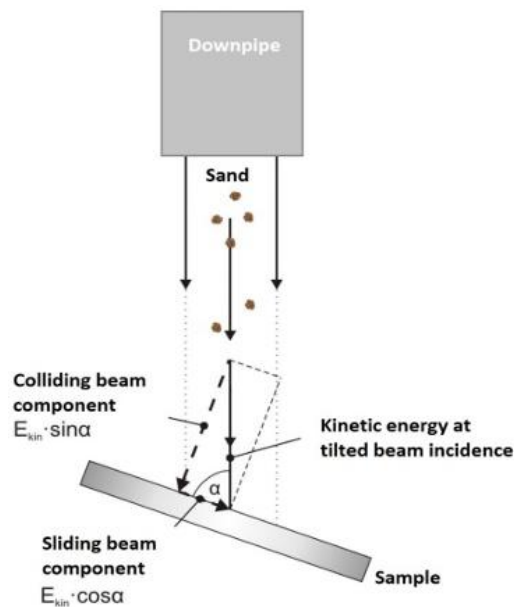
Figure 30: Sand trickling test [58].

2.2.5.2.2   Scotch tape test

A test to examine the adhesion of the layer to the substrate is the scotch tape test [59]. In this test, a thin pressure-sensitive tape is applied, and several cuts are made in it. There are two methods, method A which is more suited for on-site use, while method B is more appropriate for laboratory use. Method B cannot be used with coatings thicker than 125µm. The methods are discussed more in detail down below.

Method A:
Before applying the tape, an X-cut is made on the film. Then after the tape is applied and torn off, the adhesion can be scored on a scale from 0 to 5.

Method B:
Method B is comparable with A as in that there are also cuts made and tape applied. The difference lies in the pattern of the cuts and the assessment of the results. The cut type is in a lattice pattern, and the effect is evaluated by comparison with descriptions and illustrations.

The scotch tape test is a challenging test to do in the same manner every time. Therefore in this research, the test will not be used to assess the quality of the coating. Another reason for this is the size of the samples. It is not possible to meet the test's requirements, i.e. the length of the cuts.
A simplified version of this test can be conducted to test the adhesion of the coating to the sample quickly, but this test was designed for paint layers or other coatings but nothing as hard as a diamond coating. Therefore results may not be what is expected or desired.

3 Results

This section discusses the results of this thesis. Firstly, a good set of parameters for each deposition technique is needed. The following two sections will discuss the achieved parameter set and why these are chosen. After this, the next chapter will discuss the setup of the surface pre-treatment experiment and the achieved results. A surface pre-treatment method is needed to influence the surface conditions of the substrate. These improved surface conditions can help achieve better results when spray-coating or inkjet printing diamond nanoparticle seeds on them.

3.1 Optimizing the inkjet printing process

The inkjet printer is one of two deposition techniques used in this research. The following paragraphs will explain the main parts of inkjet printing. The first part is the ink composition. This is detrimental to the success of the prints. The next part is parameters. Here the optimizing and testing of the different parameters will be explained. The next part will explain the procedure of printing. And lastly, a conclusion will be drawn.

3.1.1 Determining the ink composition

A crucial part of the success of inkjet printing depends on the ink composition. The two essential parts of inkjet ink are surface tension and viscosity. Therefore the optimising of this ink took quite a few steps. In Table 5 below are all the used ink compositions listed. The ideal ink was not found because this falls out of the scope of this thesis, but the final ink gave good enough and repeatable results for the research.

The first iteration of ink was a combination of 10% demineralised water and 90% ethylene glycol with a concentration of 3 g/l SDND. This ink was very stable with almost no clogging of the nozzles. It can be concluded that it has suitable viscosity and surface tension, but the evaporations capacity was not as desired. For this reason, the mixture was altered, but the solvents stayed the same, to three different inks, namely:

- 80% Ethylene glycol and 20% demineralised water
- 70% Ethylene glycol and 30% demineralised water
- 60% Ethylene glycol and 40% demineralised water

These gave better results, but still not as desired because of the slow evaporation that caused flow behaviour. Therefore ethanol was mixed with the new ink to help the evaporation. The problem with a three fluid mixture is that the surface tension is complicated to determine. So, the first ink was mixed with only the surface tension of ethanol and ethylene glycol combined. 58.2% ethylene glycol 35.9% ethanol 5.8% demineralised water 3 g/l. The goal here was to minimise the effect of the water and almost only end up with a mixture of ethylene glycol and ethanol. The problem here was that the printing was not stable enough and that the nozzles kept clogging.

The probable cause of this problem is that the mixture's viscosity is not right, although the surface tension falls in the ideal window (25-35 mN/m) [60]. To overcome this problem, the ethylene glycol concentration was increased to 70%, and the ethanol concentration was lowered to 24%. This did solve the clogging issue but brought back the same evaporation problem.

To decrease the viscosity and increase the evaporation rate, the water concentration was raised, and the ethylene glycol one was set back to its original value. This ink composition gave good results but did cause frequent clogging of the nozzles.

Part of this problem is due to the clusters of diamond nanoparticle seeds in the ink. For the subsequent optimisation, the ink was put in a centrifuge for 5 hours with a simulated force of 10000 g. This appeared to be too much because the ink came out of the centrifuge clear with all the seeds settled in the bottom. Therefore, the time in the centrifuge was decreased to 30 minutes at 5000 g. This ink is not perfect, but it is sufficient for this research.

Table 5: Different ink composition.

Iteration	Ink (3g/l)	Centrifuge
1)	90% Ethylene glycol 10% demineralised water	/
2)	80% Ethylene glycol 20% demineralised water	/
3)	70% Ethylene glycol 30% demineralised water	/
4)	60% Ethylene glycol 40% demineralised water	/
5)	55% Ethylene glycol 25% ethanol 20% demineralised water	/
6)	58.2% Ethylene glycol 35.9% ethanol 5.8% demineralised water	/
7)	55% Ethylene glycol 25% ethanol 20% demineralised water	5 hours 10000g
8)	55% Ethylene glycol 25% ethanol 20% demineralised water	30 minutes 9000g
9)	55% Ethylene glycol 25% ethanol 20% demineralised water	30 minutes 9000g

3.1.2   Optimizing the inkjet parameters

Because it was one of the first times diamond was printed using an inkjet printer, most parameters needed to be optimised. There was a starting point from previous tests using the inkjet printer, but a lot of finetuning was necessary.

These parameters were determined on Corning Eagle 2000 glass substrates that were cleaned with 5' of soap water, 5' of demineralised water, 10' of acetone and 10' of isopropyl alcohol. The remaining organic contaminants were removed by treating the samples with 30 minutes of UV-Ozone.

3.1.2.1   Hotplate temperature

The first investigated parameter was the hotplate temperature. This plate is the surface on which the substrates lays on. To aid with the evaporation of the ink, the hotplate has a higher temperature.
The highest this setting could go is 60°C. Tests were performed at 40°C, but a wet spot was still visible after printing. Therefore the preferred setting for this master's thesis is 60°C. The samples during these tests were printed with the settings shown in Table 6, with the hotplate temperature being varied.

Table 6: Hotplate parameters.

Parameter	Setting
Number of nozzles	1
Dropspacing	20 µm
Print speed	1 kHz
Number of layers	1
Cartridge voltage	23,50V

3.1.2.2   Dropspacing

Another critical parameter is drop spacing. This setting determines the space between each drop. This is important because if the drop spacing is too small, the droplets will flow into each other too much, and they will cling together. If the drop spacing is too big, the drops will be solitary, and there will not be even coverage. The settings of these printed samples during the test were as seen in Table 7, with the dropspacing being varied during the tests.

Table 7: Dropspacing parameters.

Parameter	Setting
Hotplate Temperature	60 °C
Number of nozzles	1
Print speed	1 kHz
Number of layers	1
Cartridge voltage	23,50V

The range from 5 to 50 µm with steps of 5 µm was tested. In the image below, on the left is 5 µm, in the middle 20 µm and on the right is 50 µm. On the pictures below, it is visible that 5 µm results in heavy flow behaviour while at 50 µm, the individual drops are distinctly visible. This uneven coverage is not desired, and on the 20 µm drop spacing, the surface is considerably better covered.
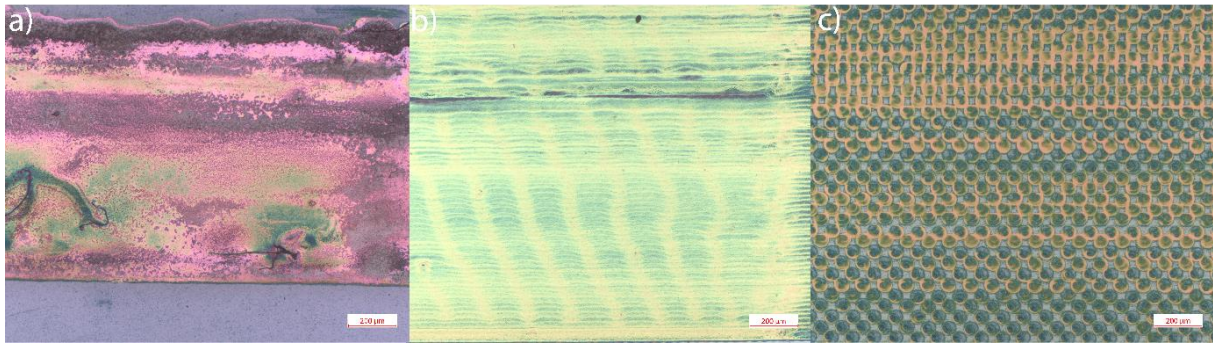
Figure 31: Comparison of the drop spacing. 5 µm (a), 20 µm (b), 50 µm (c).

Because it is visible that 20 µm gives the most homogenous coverage of the top three, below are 15 µm, 20 µm and 25 µm shown. 15 µm has good coverage but still shows some flow behaviour at the top. 25 µm gave pretty bad results with a lot of clumping of drops, the expected results of 25 µm are that the drops would be spaced farther apart. However, the image shows a lot of flow behaviour and inconsistent coverage, so it appears that something went wrong during the printing process. Due to the lack of time, it was impossible to print another sample after the results were examined. Out of these three, the conclusion remains that 20 µm is the best result and, consequently, the preferred choice.
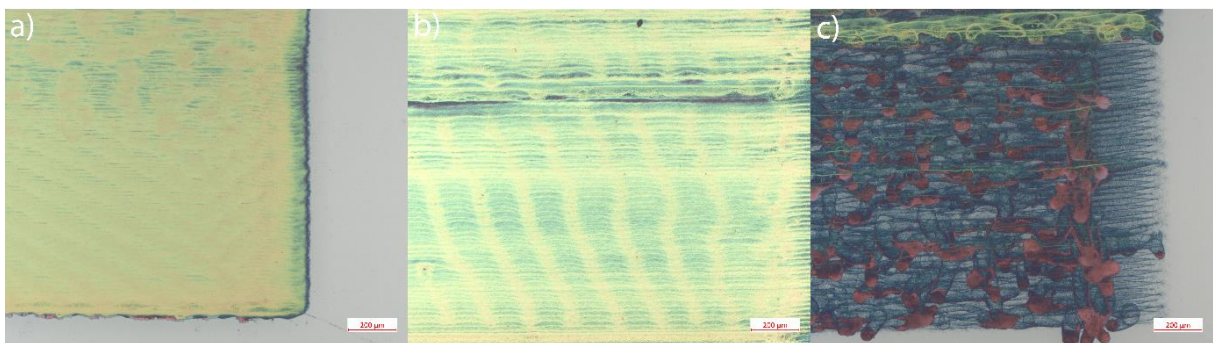
Figure 32: Comparison of drop spacing. 15 µm (a), 20 µm (b), 25 µm (c).

The roughness of the different drop spacing shows a linear upward trend as seen in Figure 33, except for one outlier. This trend can be explained since the spacing between the droplets gets bigger and bigger, so it is not homogenously covered at one point. The needle of the Dektak then moves from the unseeded glass to the diamond layer giving a significant height difference and eventually a higher Ra value.

Optically, the substrate with 15 µm drop spacing shows a better result with minimal or no flow behaviour. The average surface roughness is similar to 20 µm drop spacing. However, the printing time increases with the 15 µm drop spacing. Therefore, the decision was made to use the 20 µm drop spacing.
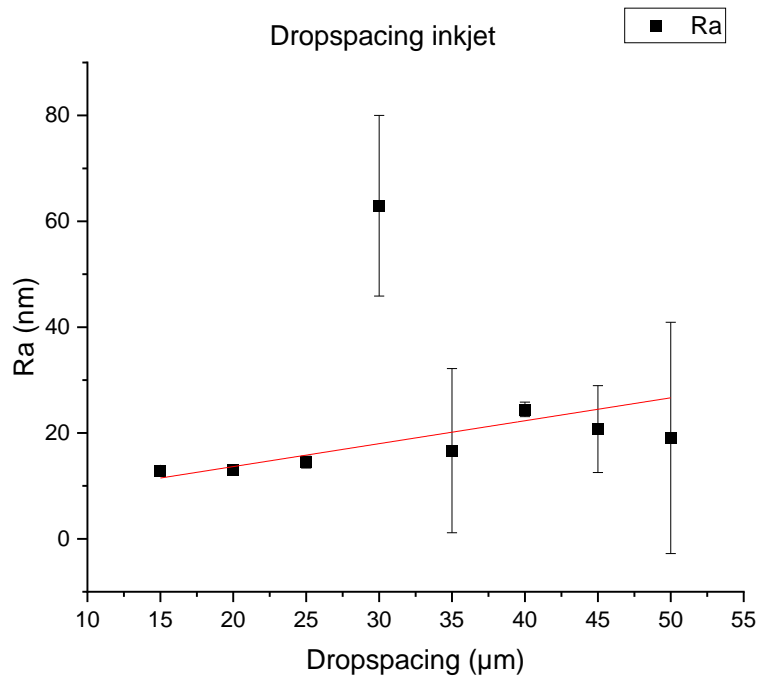
Figure 33: R_a roughness of inkjet samples with different dropspacing.

The waviness value of the different drop spacing samples shows a similar trend to the Ra ones, but there is a lot more variance in the measured values as seen in Figure 34 below. Some of this variance can be assigned to where the waviness is measured, such as between the drops or on the drops.
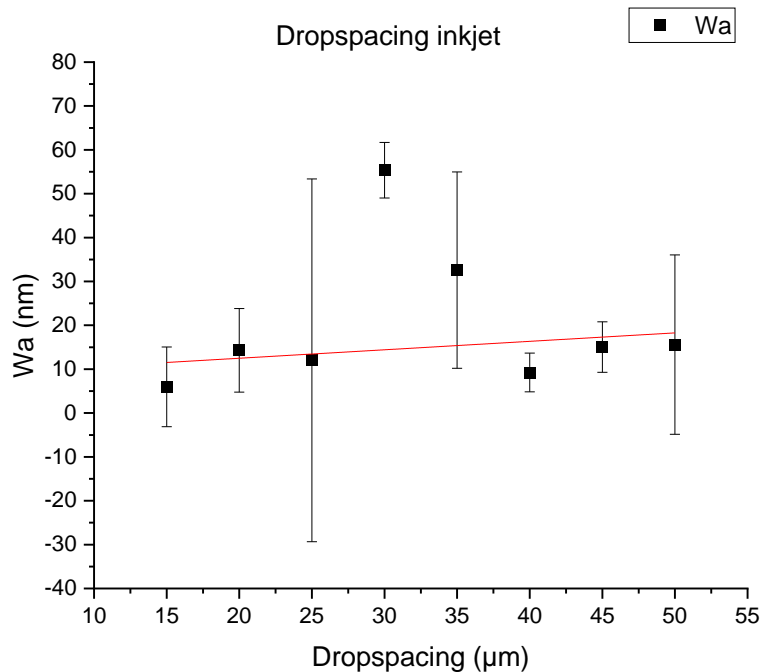
Figure 34: W_a waviness of inkjet samples with different dropspacing.

These data points of 30 and 35 µm drop spacing are considered outliers because the expectations are not in line with the results, and there is no indication as to why these drop spacings would give such a spike in the roughness and waviness.

3.1.2.3 Number of nozzles

Each cartridge has 16 nozzles that can be used to print. Samples were printed using 1, 2, 3, 4, 5, 6 and 7 nozzles. These samples were printed with the parameters shown in Table 8, with the variable parameter being the number of nozzles.

Table 8: Number of nozzles parameters.

Parameter	Setting
Hotplate Temperature	60 °C
Dropspacing	20 µm
Print speed	1 kHz
Number of layers	1
Cartridge voltage	23,50V

The sample printed with one nozzle is visible in Figure 35 a). One nozzle gives a decent result with not a lot of flow behaviour. The sample printed with two nozzles shows more flow behaviour with not good coverage. This is shown in Figure 35 b). The more nozzles were used, the worse the results got with a lot of flow behaviour and uneven coverage of the samples. This is visible in Figure 35 c) and d) below. The extra liquid deposited on the sample increases the drying time and increases the likelihood of droplets clumping together.
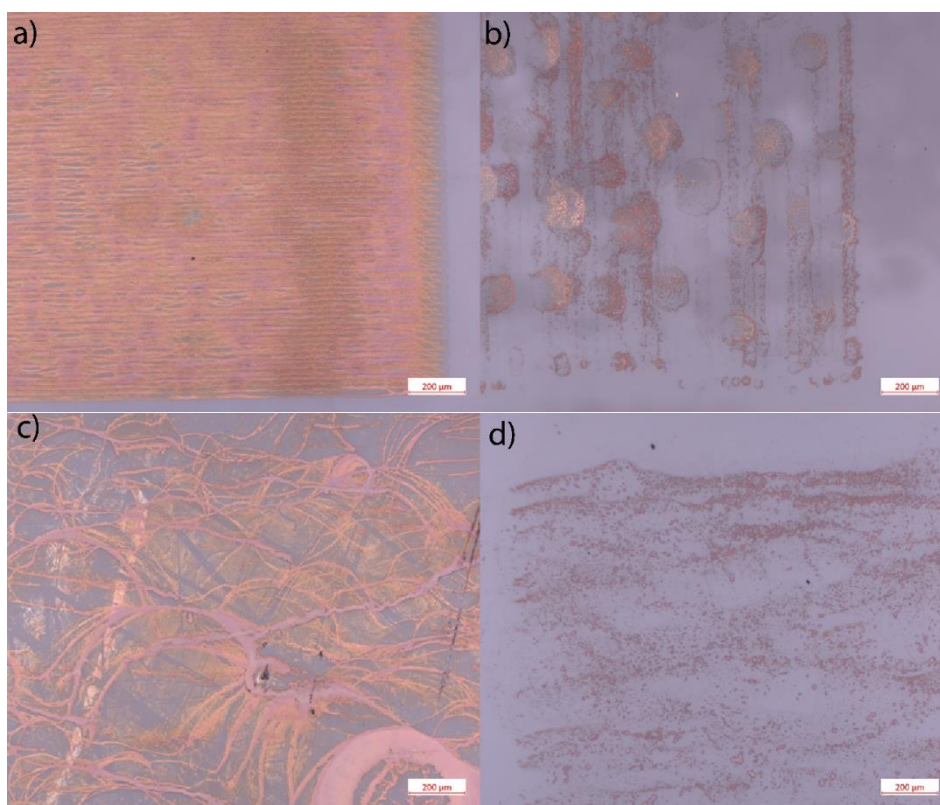
Figure 35: Comparison of different amount of nozzles used. one nozzle (a), two nozzles (b), three nozzles (c) and four nozzles (d).

Because the results got worse, the more nozzles were used, the decision was made to use one nozzle in the rest of the testing. The number of which nozzle was used varied because of the clogging, but the amount used stayed the same, namely one. Therefore, the number of the nozzle will not be mentioned because it is irrelevant. Only the number of nozzles will be mentioned. So from now on, one.

3.1.2.4   Print speed

After the drop spacing was fixed, the following parameter was the print speed. The speed is expressed in kilohertz (kHz). If the drops are deposited too quickly, the previous drop is not evaporated and can flow into the prior one. This results in heavy flow behaviour.

The different tested speeds are 1 kHz, 2 kHz, 5 kHz, 10 kHz. The lowest the printer can go is the 1 kHz, giving the best results when printing, as visible below. The parameters used to print these samples are listed below in Table 9, with the speed being varied during these tests.

Table 9: Print speed parameters.

Parameter	Setting
Hotplate Temperature	60 °C
Dropspacing	20 µm
Number of nozzles	1
Number of layers	1
Cartridge voltage	23,50V

The Figure 36 below clearly shows that the higher the printing speed, the more severe flow behaviour occurs. To ensure that this problem is reduced to a minimum, it was decided to set the print speed to the lowest setting, namely 1 kHz. The problem with this setting is although it is the best one, it also takes the longest to print.
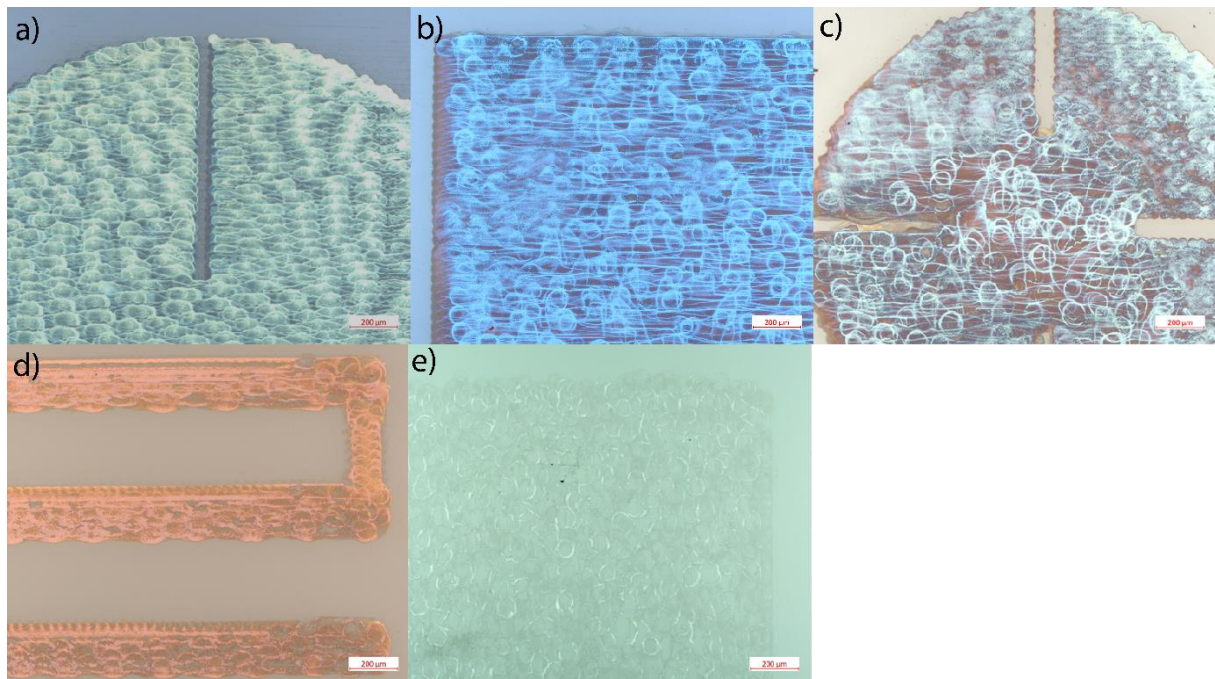
Figure 36: Comparison of different printing frequency's. 1 kHz (a), 1,5 kHz (b), 2 kHz (c), 5 kHz (d) and 10 kHz (e).

3.1.2.5   Number of layers

Another requirement was that there should be as complete coverage of the substrate as possible. After reviewing the test with one layer with an SEM microscope, as seen in Figure 37 below, it was apparent that one layer was not sufficient for the even coverage. The parameters used to print these samples are listed below in Table 10, with the number of layers being varied during these tests.

Table 10: Number of layers parameters.

Parameter	Setting
Hotplate Temperature	60 °C
Dropspacing	20 µm
Print speed	1 kHz
Number of nozzles	1
Cartridge voltage	23,50V
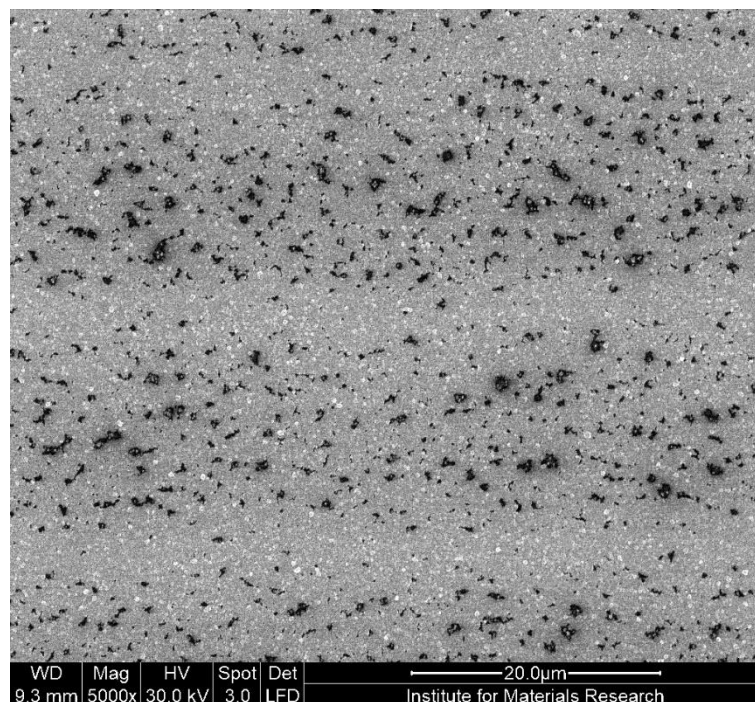
Figure 37: SEM image 1 layer. The black spots are regions not covered with diamond nanoparticle seeds. The grey regions are diamond nanoparticle seeds.

To get better coverage, samples with two layers and a 10 µm shift between those were printed. The shift is half the drop spacing to print in between the drops to get better coverage. On the SEM image Figure 38 below, it is evident that there are lesser gaps but still not ideal.
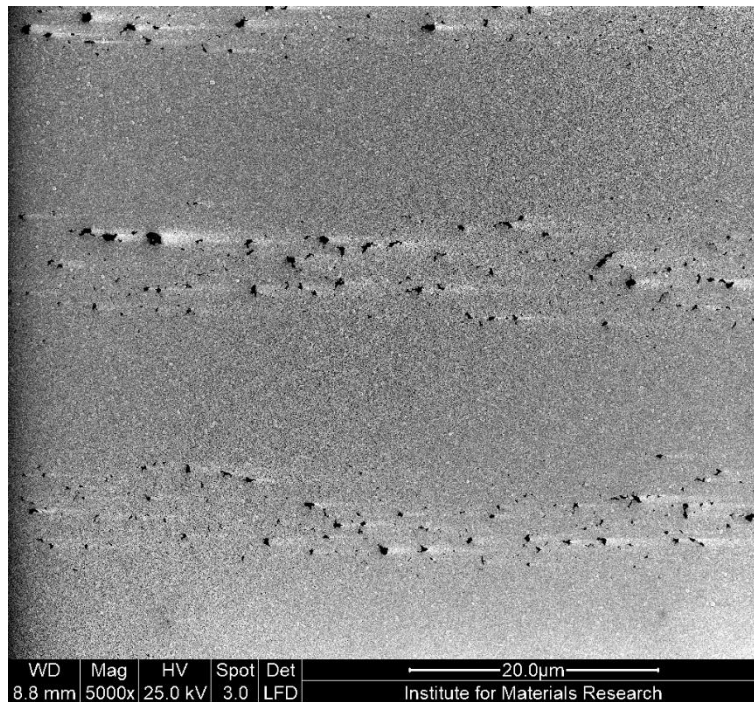
Figure 38: SEM image of 2 layers with more uniform coverage.

The test with three layers was a bit more complicated because the shift was not as straightforward as with the two layers, and printing two layers on top of each other did not give good results. But the results with three layers are better as the coverage is homogeneous. As seen in Figure 39 below, the surface looks entirely covered.
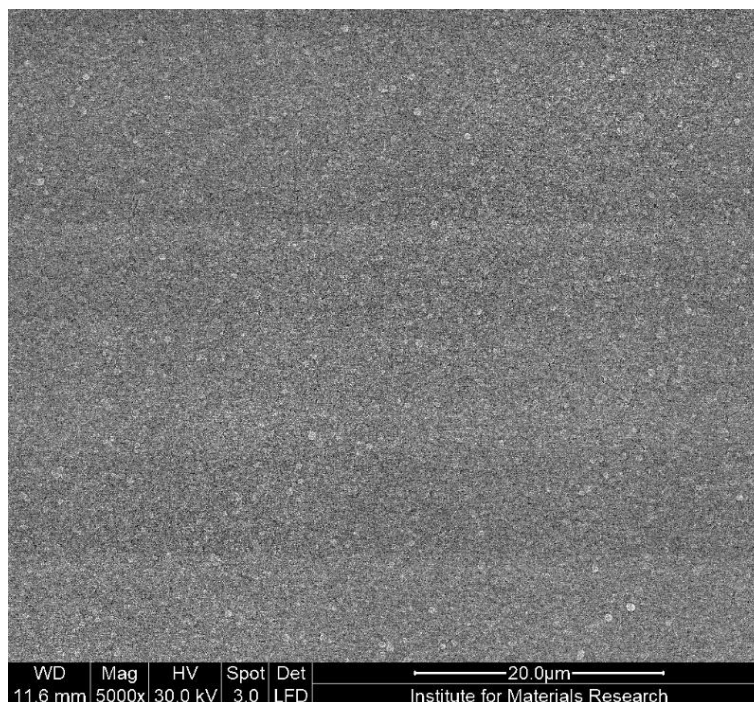
Figure 39: SEM image of 3 layers with an almost uniform coverage.

Although the results with three layers were better, the decision was made to continue with two layers. Because printing with three layers took too much time and the shift was not so successful, for patterns, it is also better to print with two layers for the definition of the image.

3.1.2.6   Cartridge voltage

The cartridge voltage controls the voltage of the piezo crystal of the nozzles. The different cartridge voltages used are 15.50 V, 18.00 V, 19.00 V, 23.50 V, 25.00 V, 30.00 V, 34.00 V. After these tests, it became apparent that the nozzles were less prone to clogging with higher cartridge voltages. Therefore it was decided to continue the printing of the samples with 34.00 V. The parameters used to print these samples are listed below in, with the cartridge voltage being varied during these tests.

Table 11: Cartridge voltage parameters.

Parameter	Setting
Hotplate Temperature	60 °C
Dropspacing	20 µm
Print speed	1 kHz
Number of nozzles	1
Number of layers	2

3.1.3 Inkjet printing procedure

A procedure was written to make sure the results were as repeatable as possible. This procedure is a combination of advice from people with previous experience on the inkjet and things learned during our earlier experiments.

1. The first step is to turn the printer on. Ensure that there is nothing on the printer plate because it will calibrate its engines and axles. The calibration starts by checking the okay box when you open the Dimatix program.

2. While the printer is heating, the desired pattern can be selected. Each pattern has its drop spacing. In this case, the head angle must be adjusted accordingly, in this case, 4,5° (Figure 40), because a drop spacing of 20 µm is used.
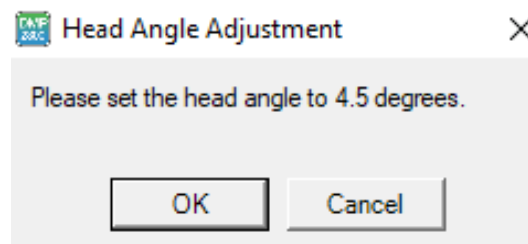
Figure 40: Head angle adjust window 20 µm.

3. After the printer is done calibrating, the hotplate needs to heat up. This will take some time, and the printer cannot be started unless the hotplate is up to temperature.

4. When it is up to temperature the substrate can be loaded. Make sure it is reasonably parallel (this can be corrected). Turn on the vacuum. After the substrate is loaded, it is advised to wait 1/2 minutes. This is because the sample will need to get up to the temperature of the hotplate, as visible in Figure 41 below. The sample will not reach the set temperature due to the thickness and insulation of the glass.
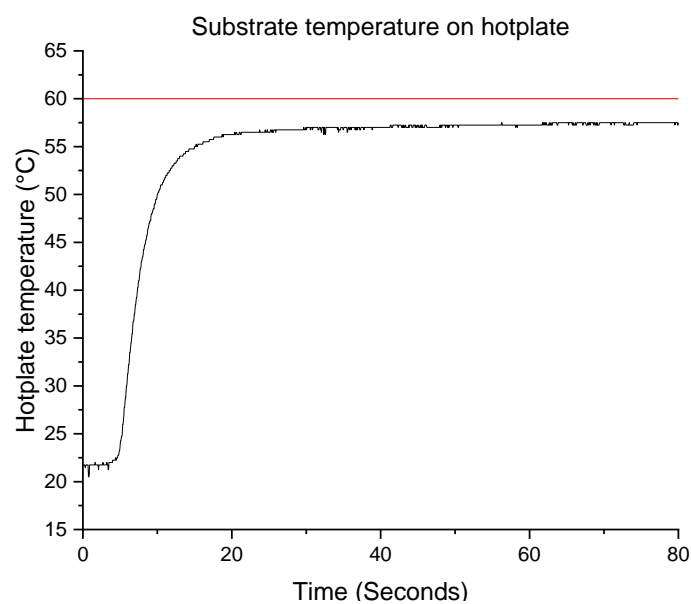
Figure 41: Warm up time substrate inkjet.

5. Use the fiducial camera to set the print origin to the desired place. Line up the cross with the corner of the sample, use the step function to go 2 mm inside in the x and y-direction. Set the reference point and print origin in the centre of the screen. Close the fiducial camera (Figure 42).
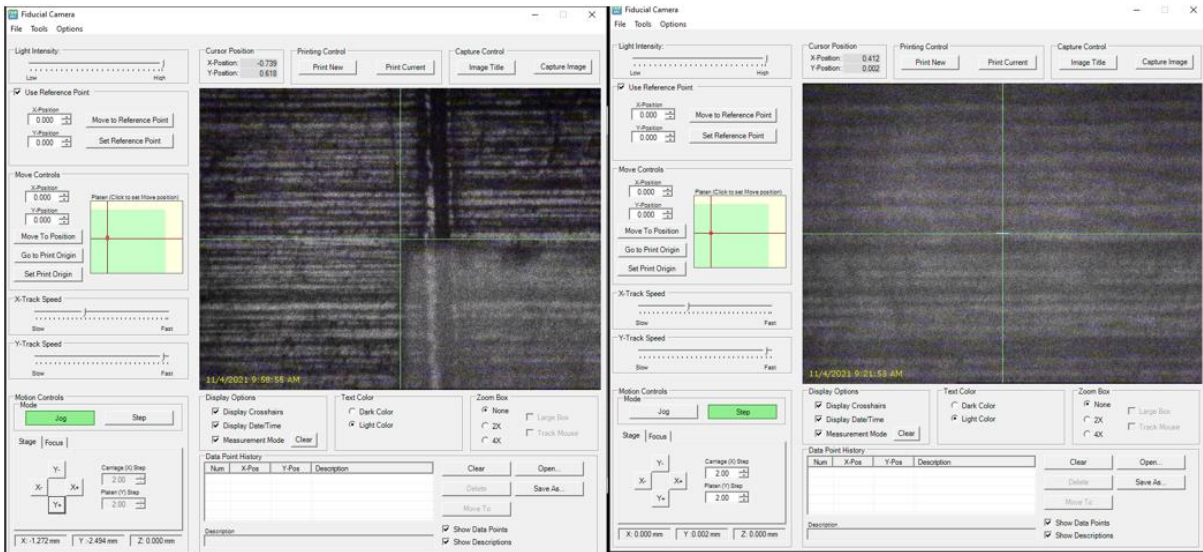
Figure 42: Fiducial camera.

6. Open drop watcher. Before the print head is stopped, the frequency toggle control needs to be slid back and forth. Then check the box of the nozzle that will be used. If it is not clogged, a straight stable drop should be visible (Figure 43). If this is okay, the print can be started.
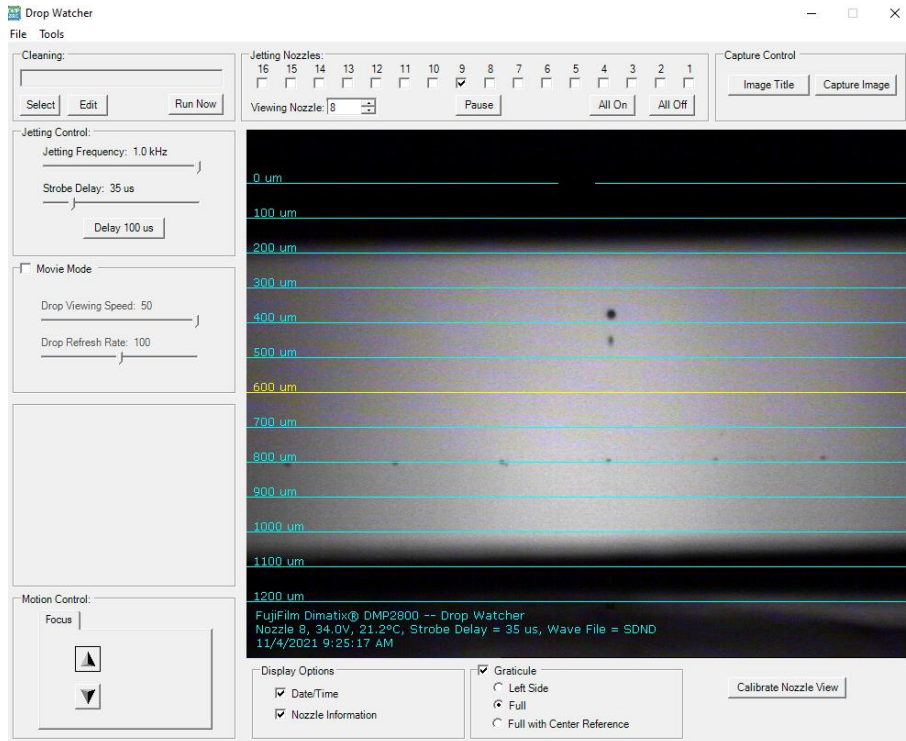
Figure 43: Drop watcher with one drop visible of one nozzle.

7. After the first layer, a layer shift will be done. Open the fiducial camera again, use the step in the y-direction the go 0,06 mm downwards, then go 0,05 mm upwards (Figure 44). This will result in a net movement of 10 µm (half of the drop spacing).
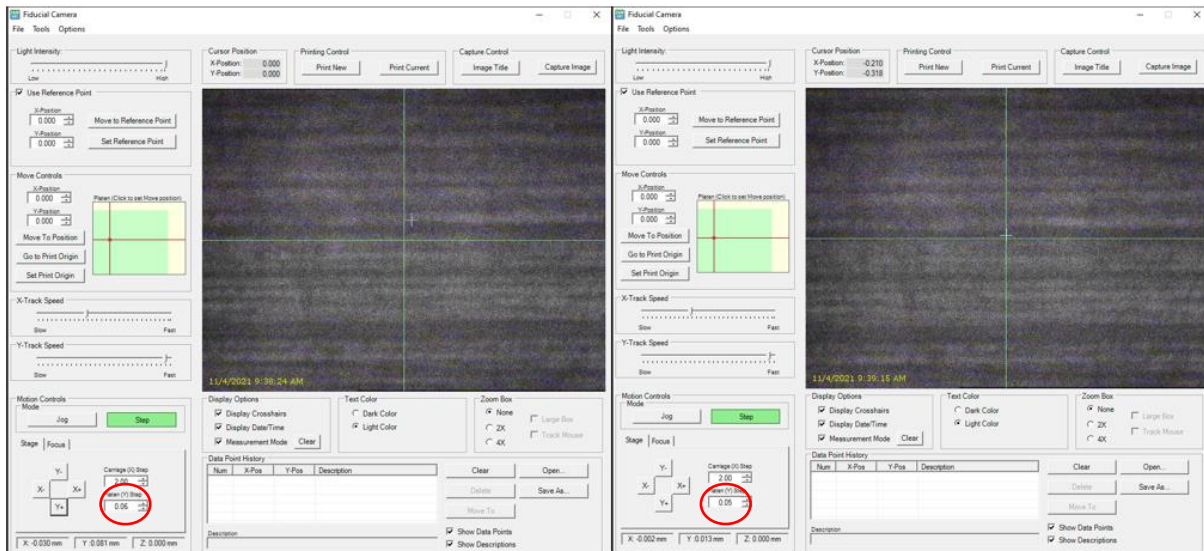
Figure 44: Fiducial camera used for the 0,10 µm step.

8. Open the drop watcher again to check if the nozzle is not clogged. If it is not, the printing of the second layer can be started. If it is, find another nozzle that jets nice and isn't clogged. Change the selected nozzle in the cartridge settings and start printing.

9. When the second layer is printed, change the pattern to the dots. The head angle will need to be changed to 51,9° because of the greater drop spacing (Figure 45). Please don't move the carriage too much because it will give an error, and the printer will need to be power cycled. After that, open drop watcher again and repeat step 8. Then print the dots.
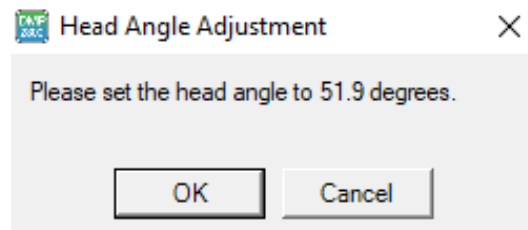
Figure 45: Head angle adjust window 200 µm.

10. When the printing is done turn of the vacuum and unload the substrate.

All the samples during the pre-treatment experiment were printed using this procedure. This procedure was designed to avoid variation in the printing process.

3.1.4   Conclusion

The first tested parameter was the hotplate temperature. It was beneficial for the ink to have a higher hotplate temperature because it aided the evaporation and significantly improved the results. Therefore it was decided to set the value to 60°C as it cannot go any higher.

The best drop spacing relates to the diameter of the drops deposited onto the surface. After tests ranging from 5 to 50 µm, with this liquid and volume of drops (1 pL), it was concluded that the best drop spacing is 20 µm. This could be confirmed both visually and with the microscope.

The number of nozzles was easily determined because it was immediately visible that the deposited liquid with more than one nozzle was too much after the initial test. Therefore the conclusion was that one nozzle gave the best result.

With the print speed, the speed with which the droplets were deposited was tested. This test made it apparent that more flow behaviour occurred with a higher deposition rate. Therefore the chosen setting is 1 kHz. It takes longer to print a sample at this speed, but it gives the best results.

The number of layers is detrimental to ensuring a close homogeneous substrate coverage. After the tests, it appeared that three layers gave the best result for even coverage, but this was not feasible because of the time it takes to print three layers. Therefore it was decided to print the samples with two layers.

The cartridge voltage was altered as the test samples were printed. As the voltage was increased, it was apparent that clogging became less frequent. Higher than 34,00 V did not seem to be effective; therefore, this was the set value.

After the tests were completed, a base set of parameters was determined. The goal of these parameters was to make sure that the achieved results were under the same circumstances. The same goes for the procedure. Listed in the table below are the used parameters and ink.

Table 12: Final parameters inkjet.

Parameter	Setting
Hotplate Temperature	60 °C
Dropspacing	20 µm
Print speed	1 kHz
Cartridge voltage	34,00V
Number of nozzles	1
Number of layers	2
Ink composition	55% EG 25% ETH 20% H_2O 3g/L 5000G 30' CF

With the optimised parameters above, it is possible to achieve good repeatable results such as shown in Figure 46. This printed substrate shows straight lines near the edge of the pattern. The flow behaviour in the centre of the surface is reduced to a minimum. The lines in the pattern that are visible are the path lines of the nozzle of the printer.
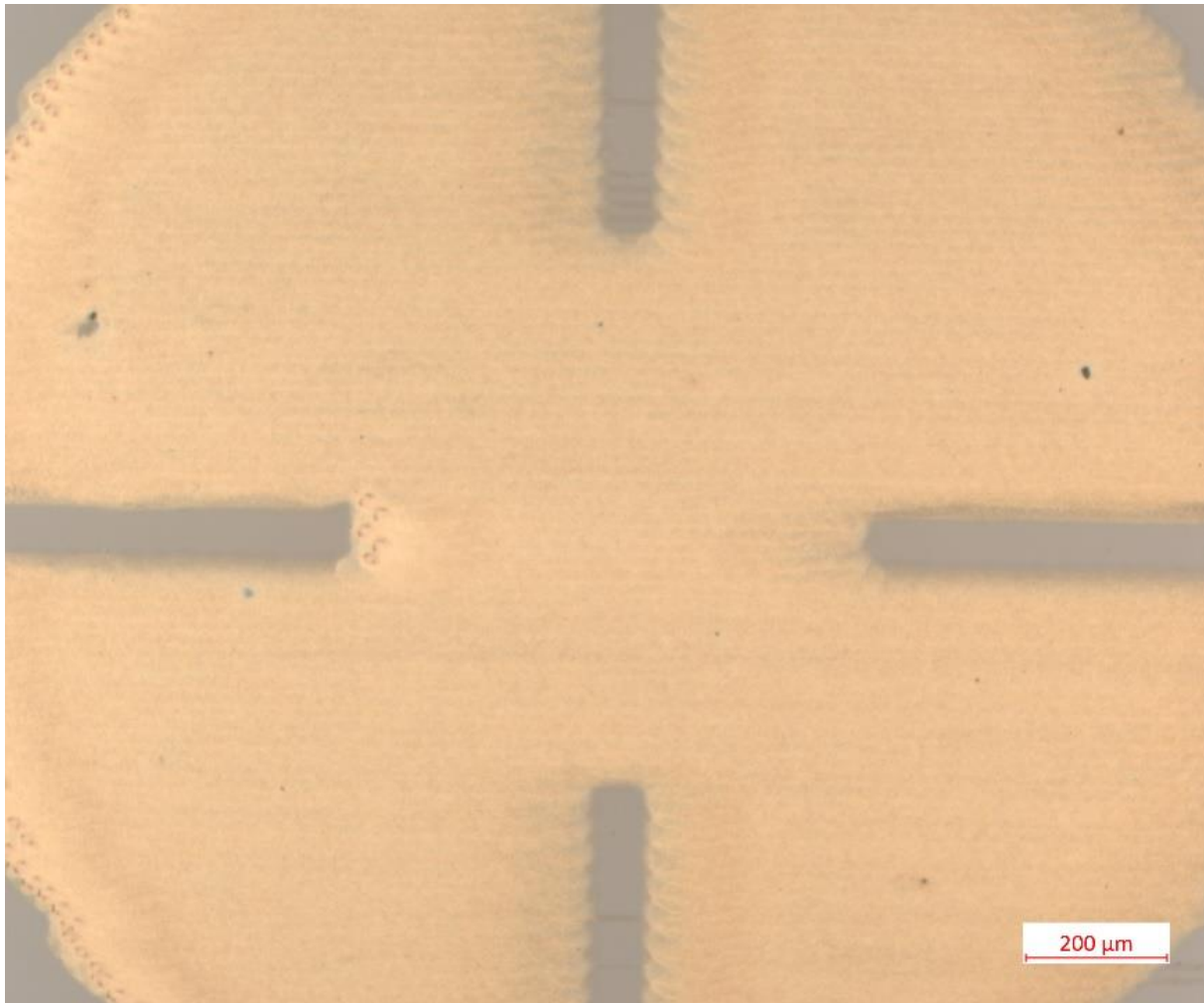
Figure 46: Printed cloverleaf pattern with achieved parameter settings.

3.2 Optimizing the ultrasonic spraycoating process

An ideal set of spray coat parameters can become a uniform coating on glass substrates. An iterative process is needed to become this perfect set of parameters. This section discusses each parameter and the ink used in the ultrasonic spray coater.

3.2.1 Previous work on ultrasonic spraycoating

A previous master's thesis [61] has already studied the influence of each parameter. Therefore the parameters of this master's thesis shown in Table 13 will be used as a starting set for further optimisation.

Table 13: Concluded parameters of previous master's thesis [61].

Parameter	Symbol	Unit
Hotplate Temperature	T	90 °C
Vibration Power	P	4 W
Flowrate	Q	0,25 ml/min
Shroud Pressure	p	1,3 PSI
Number of Layers	N/A	240
Nozzle Type	N/A	Impact nozzle
Dwell Time	t	10 seconds
Nozzle Speed	V	50 mm/s

These parameters were determined on Corning Eagle 2000 glass substrates that were cleaned with 5' of soap water, 5' of demineralised water, 10' of acetone and 10' of isopropyl alcohol. The remaining organic contaminants were removed by treating the samples with 30 minutes of UV-Ozone.

3.2.1.1   Ink composition

The previous master's thesis investigated the ink composition used to apply the diamond coating. This same ink is also currently used in the ULTRAHARD project. The ink has a concentration of 0,05 g/L diamond nanoparticle seeds dissolved in demineralised water. The droplets generated by the ultrasonic spray coater contains enough diamond nanoparticle seeds to reduce the Marangoni effect. Coffee rings will occur if the concentration is higher than 0,05 g/L. A disadvantage of this low concentration is that multiple layers are needed to ensure good coverage of diamond nanoparticle seeds. Figure 47 shows an example of a badly seeded substrates with a significant amount of coffee rings.
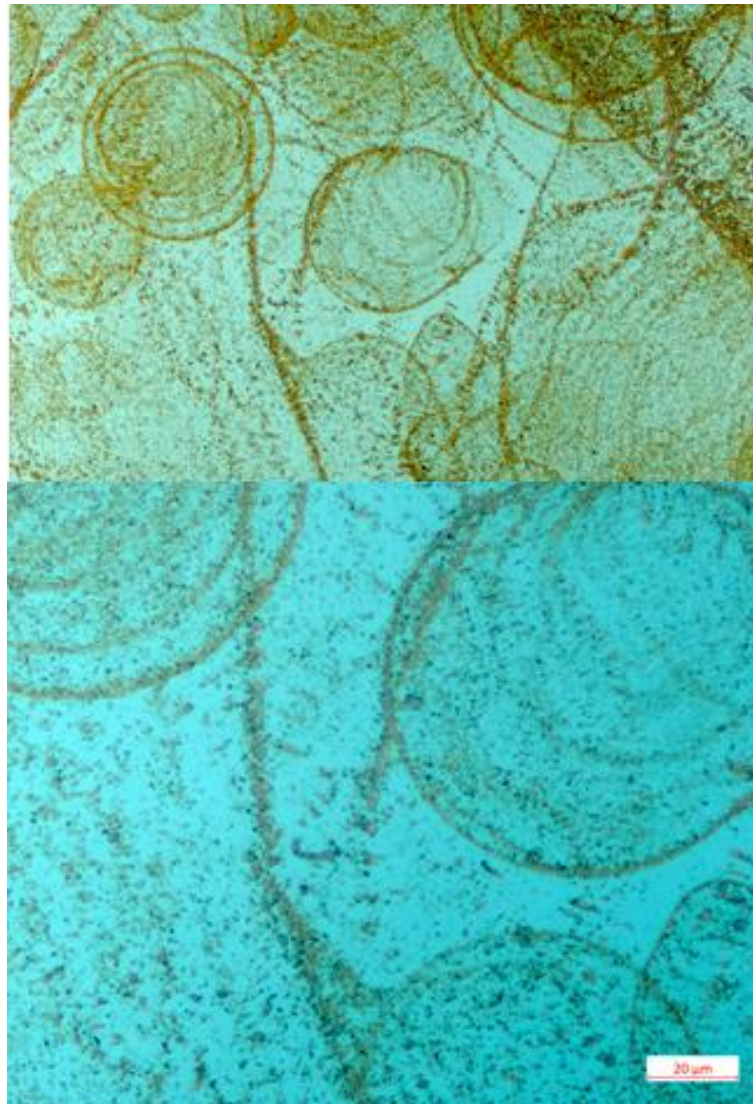
Figure 47: Seeded samples with many coffee rings.

3.2.2 Optimizing the ultrasonic spraycoating parameters

This thesis constructs a matrix to further determine the ideal parameters for the ultrasonic spray coater. Table 14 shows the matrix below. The glass substrates used for this are Corning Eagle 2000 with a thickness of 0,500 mm. After the deposition process, the substrates are morphologically and mechanically characterised to determine which setting is optimal.

Table 14: Matrix of different parameters for ultrasonic spraycoating.

Parameter	Setting
Hotplate Temperature	80;90;100 °C
Flowrate	0,25;0,30;0,35;0,40;0,45;0,50 ml/min
Amount of layers	50;80;100;120;160 layers
Dwell Time	0;3;5 seconds

3.2.2.1 Hotplate temperature

The hotplate is a heated plate where the glass substrates are placed during the spray coating process. The hotplate's temperature is adjustable and has an influence on the roughness as well as the optical properties of the diamond coating.

A lower temperature makes the evaporation of the ink solvent slower. The diamond nanoparticles have more time to settle and create coffee rings. These coffee rings can be visible with an optical microscope. A higher hotplate temperature decreases the evaporation time. The diamond nanoparticles have a limited time to settle due to this rapid evaporation time. This high temperature ensures no uniform coverage and a possible higher roughness of the coated surface.

The parameters shown in Table 15 are the other parameters for the ultrasonic spraycoater used to deposit the diamond nanoseeds.

Table 15: Other parameters for ultrasonic spraycoating.

Parameter	Setting
Flowrate	0,25 ml/min
Nozzle Speed	50 mm/s
Number of Layers	160
Vibration Power	4 W
Shroud Pressure	1,3 PSI
Dwell Time	3 seconds

After the deposition process, the samples are grown up to around 100 nm. These are then characterised morphologically by scanning electron microscope and optical microscope. The pictures below show the difference on a microscopic level. Figure 48 shows no visible difference when seen on the scanning electron microscope.
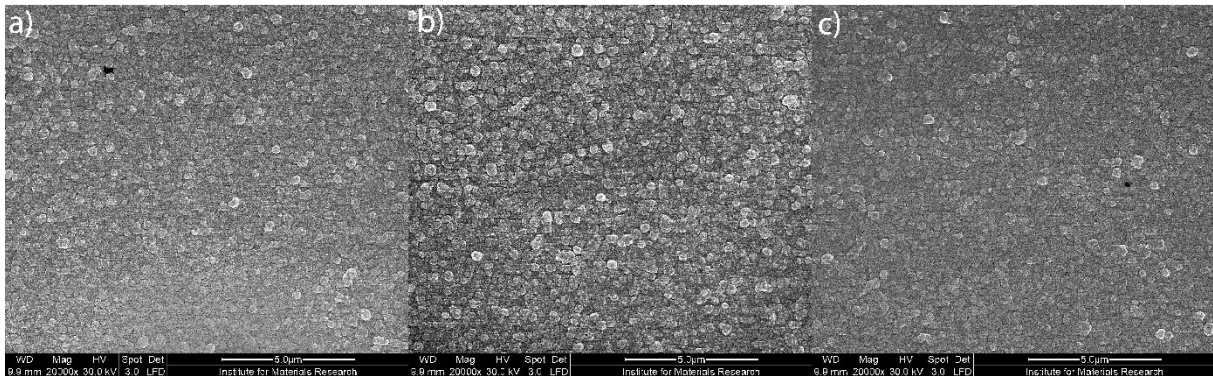
Figure 48: Differences in hotplate temperature. 80 °C (a), 90 °C (b), 100 °C (c).

When these samples are observed on a smaller scale with the optical microscope, it becomes visible that a lower hotplate temperature has more coffee rings. Figure 49 shows these coffee rings that have a dark purple ring. This darker colour shows that there are more diamond nanoparticle seeds in that location. The substrates with a higher hotplate temperature show fewer coffee rings, which is more preferred.
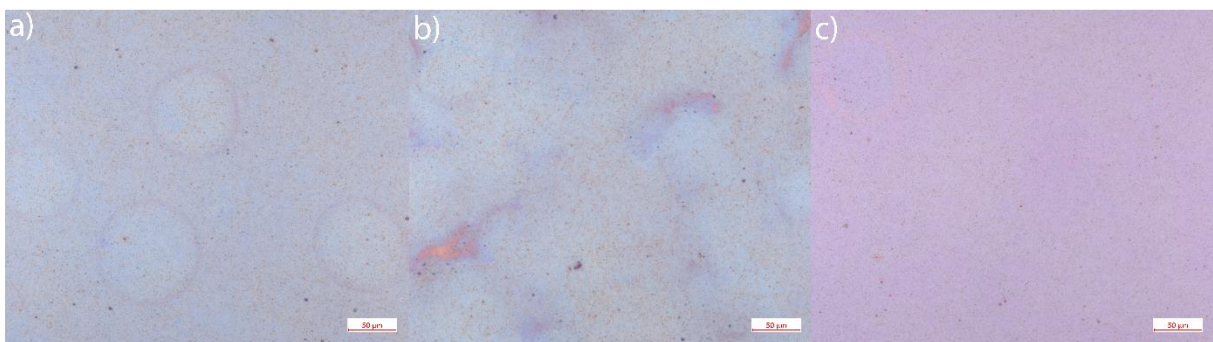
Figure 49: Differences in hotplate temperature. 80 °C (a), 90°C (b), 100°C (c).

A profilometer also characterises these samples. The graph below shows that a higher hotplate temperature results in higher average surface roughness (Ra).
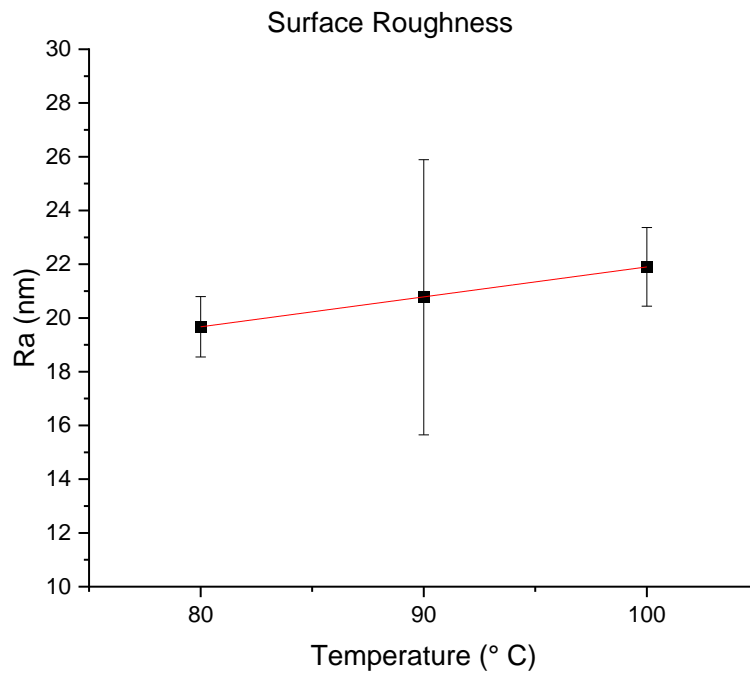
Figure 50: Surface roughness plotted in function of the hotplate temperature. An increase in hotplate temperature increases surface roughness.

A consideration has to be made between having a substrate with almost no coffee rings and a substrate with low roughness. Therefore, a hotplate temperature of 90°C is ideal for depositing diamond nanoparticle seeds. This temperature has limited coffee rings and a relatively low surface roughness.

3.2.2.2   Ink flowrate

A syringe pump provides the ink with almost no pressure to the impact nozzle. The pump speed to deliver the ink is a crucial parameter. It is possible to get a non-uniform coverage of diamond nanoparticle seeds with a low flow rate. This non-uniform coverage can be solved by increasing the number of layers. The number of layers also increases the depositing time. A flow rate that is too high is not so necessarily bad for the surface coverage, but it increases the substrate's surface roughness.

A base set of parameters is used to test out the influence of the flowrate. These parameters can be found in Table 16.

Table 16: Flowrate parameters.

Parameter	Setting
Hotplate Temperature	90 °C
Nozzle Speed	50 mm/s
Amount of Layers	160
Vibration Power	4 W
Shroud Pressure	1,3 PSI
Dwell Time	3 seconds

The influence of the flow rate was tested by increasing the flow rate in steps of 0,05 ml/min were made with a starting point of 0,20 ml/min. Figure 51 shows the influence of the flowrate. This is only visible with a scanning electron microscope.
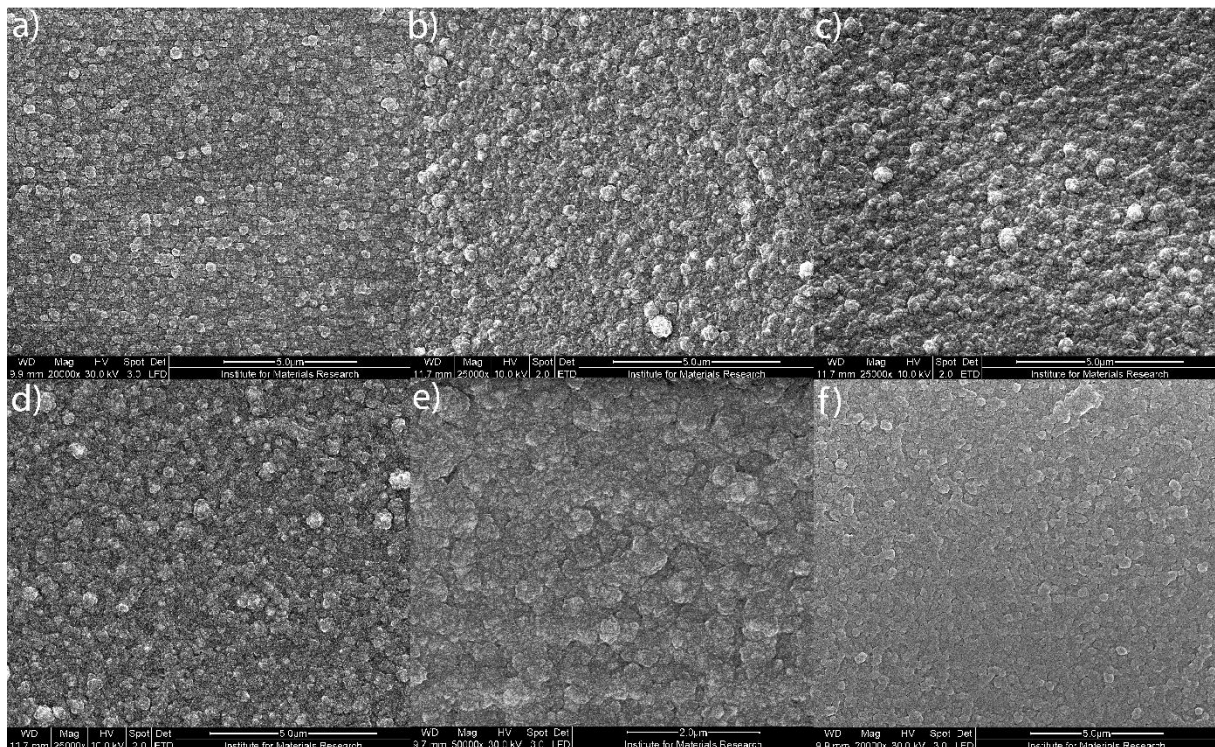
Figure 51: Influence of flow rate visible on SEM. 0,25 ml/min (a), 0,30 ml/min (b), 0,35 ml/min (c), 0,40 ml/min (d), 0,45 ml/min (e), 0,50 ml/min (f).

On Figure 51 d) it becomes visible that the diamond nanoparticles start to tangle together. This tangling is not preferred and increases the surface roughness of the substrate.

3.2.2.3 Number of layers

Ultrasonic spraycoating requires multiple layers to deposit enough seeds for uniform coverage. Other parameters like the ink flowrate and the layer thickness also influence the number of layers. A higher flowrate deposits more diamond nanoparticle seeds, therefore there are more nanoparticle seeds on the substrate, and fewer layers are needed. The influence of the layer thickness is also an important parameter. When the coating is grown inside the CVD reactor, the nanoparticle grows in every direction. So a thicker layer also influences the uniform coverage of the diamond coating. However, a higher flowrate also has a higher surface roughness.

For testing the influence of the amount of layers. A base set of parameters was chosen for the remaining settings of the ultrasonic spraycoater. These parameters can be found in Table 17.

Table 17: Parameters for number of layers.

Parameter	Setting
Hotplate Temperature	90 °C
Flowrate	0,25 ml/min
Nozzle Speed	50 mm/s
Vibration Power	4 W
Shroud Pressure	1,3 PSI
Dwell Time	3 seconds

By increasing the number of layers, the chance of getting pinholes in the coating decreases. Figure 52 shows three samples with a different number of layers. Figure 52 a) has 50 layers, b) has 80 layers and c) has 100 layers. The layer thickness of these samples is 132,8 nm.
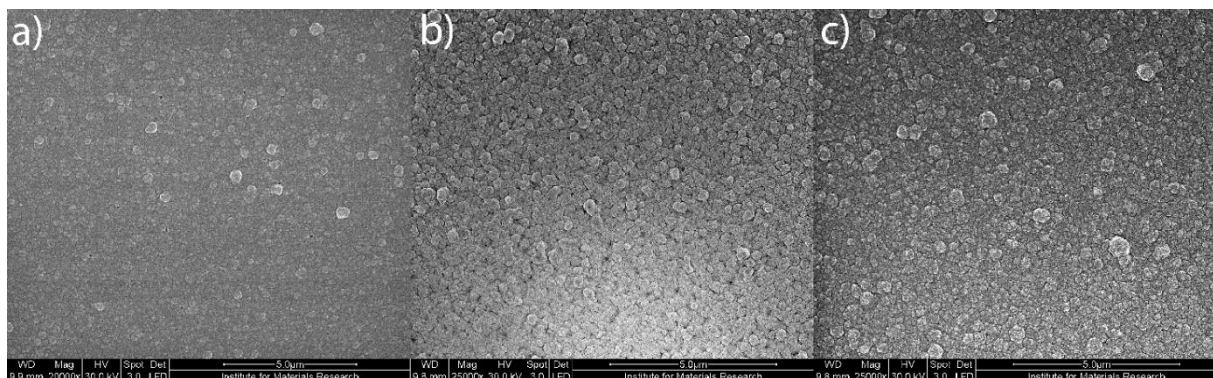
Figure 52: Number of layers seen on SEM. 50 layers (a), 80 layers (b), 100 layers (c).

The substrate with 50 layers clearly shows some form of pinholes. These pinholes are not preferred because the coating is not fully covered and increases the surface roughness. Even the substrate with 80 layers still shows some pinholes when magnified. These pinholes can be seen on Figure 53. This figure also shows each individual nanoparticle seed. The black space around these nanoseeds are places on the substrate that are not fully covered.

Figure 53: SEM picture of 80 layers with pinholes.

A profilometer was also used to characterise these substrates. The graph below shows a slight increase in surface roughness when the number of layers is increased.
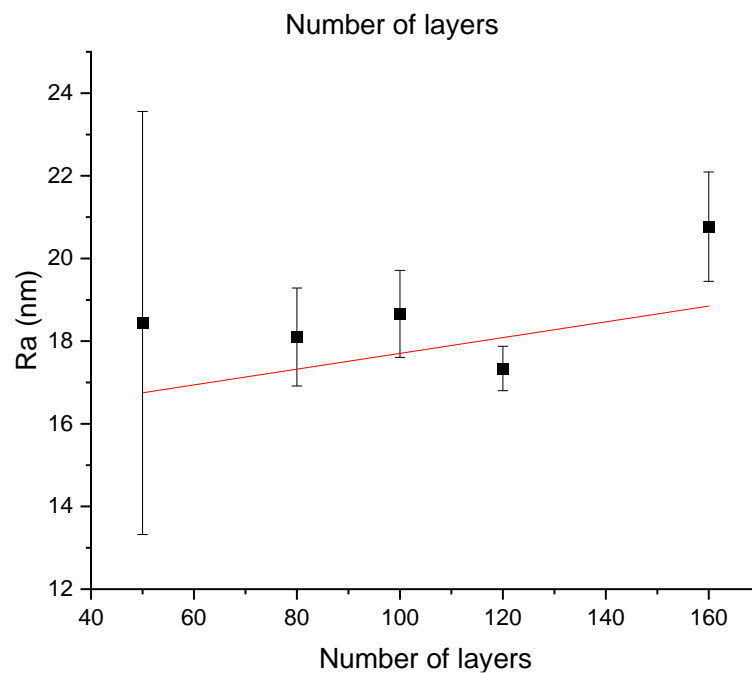
Figure 54: Influence on number of layers. 50 layers has a large variation because of a non-closing layer.

3.2.2.4 Influence of dwell time

The dwell time is when the nozzle waits before applying a new layer onto the substrate. This time is adjustable and is an essential parameter of this ultrasonic spray coater. The droplets blown onto the surface by the impact nozzle need time to evaporate before applying a new layer. Flow behaviour can occur when a new layer is applied to droplets that are not yet evaporated. This flow behaviour can increase surface roughness slightly due to the Marangoni flows in the droplets.

To test the influence of the dwell time, a set of parameters was chosen for the remaining settings of the ultrasonic spraycoater. These parameters can be found in Table 18.

Table 18: Parameters for dwell time.

Parameter	Setting
Hotplate Temperature	90 °C
Flowrate	0,25 ml/min
Nozzle Speed	50 mm/s
Number of layers	160
Vibration Power	4 W
Shroud Pressure	1,3 PSI

This coffee ring effect is visible on Figure 55, a) shows a sample where the dwell time was set at zero seconds. The solvent did not have enough time to evaporate. B) clearly shows less coffee rings but they are still present. From five seconds and onwards the effect of these coffee rings start to minimalise.
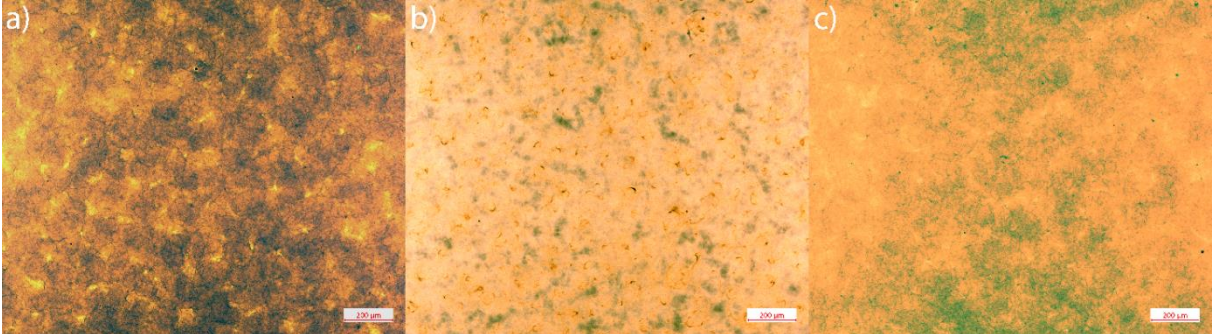
Figure 55: Difference in dwell time on optical microscope a) 0 seconds, b) 3 seconds, c) 5 seconds

The graph below confirms that a longer dwell time slightly decreases average surface roughness. The disadvantage is that the duration of the spraycoating process increases. A compromise has to be made between a good coating layer and a process that has an acceptable duration.
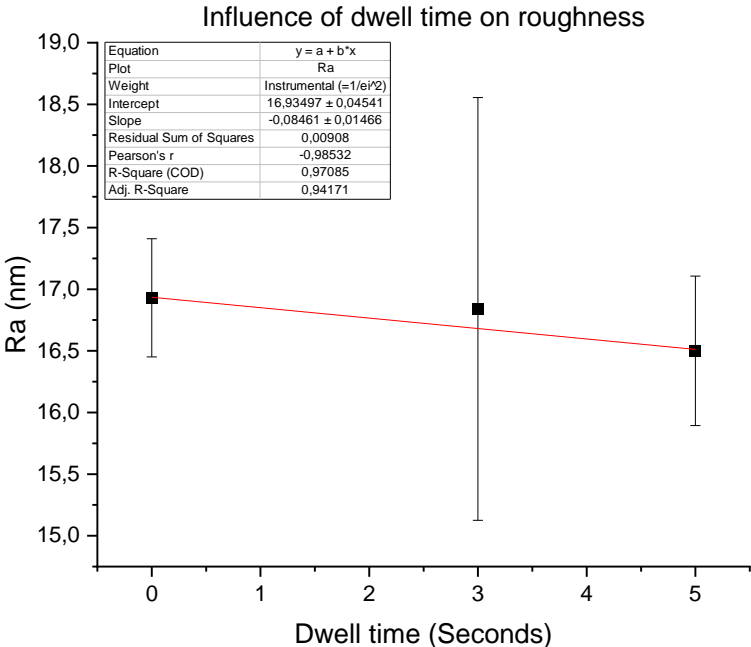
Figure 56: Influence of dwell time on roughness.

3.2.3   Ultrasonic spraycoating procedure

Multiple steps need to be followed to apply diamond nanoseeds to a glass substrate. The first step in ultrasonic spraycoating is to turn on the machine, computer and nitrogen source. In step two, the ultrasonic spray coater needs to be initiated to be ready to spray. The ink is loaded into the syringe pump and purged to remove air. The correct parameters are set in step three. All parameters except shroud pressure and hotplate temperature are set on the computer.

A fused silica glass substrate is placed on the hotplate. The temperature of the substrate is very important. The graph below shows the time a substrate needs to get up to temperature. The hotplate temperature is set at 90 °C. However, the graph shows that the substrate does not reach this temperature. This is because the fused glass has a thickness of 0,720 mm. This is relatively thick and insulates the heat. The graph also shows that the temperature converges after 20 seconds.
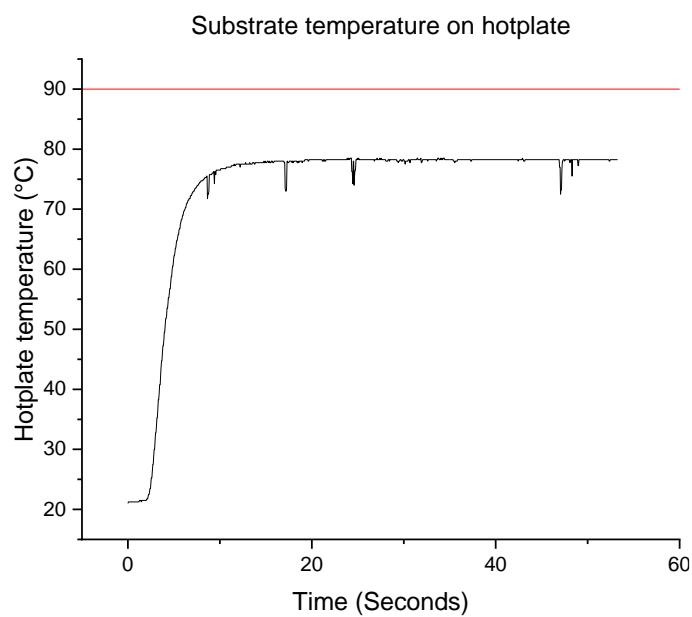
Figure 57: Warm up time of substrate on hotplate.

When the substrate has reached its temperature, the operator can start the spraycoating process.

3.2.4   Conclusion

These tests conclude that an ultrasonic spray coater can create a diamond coating with a relatively low average surface roughness of around 20 nm. The ideal hotplate temperature looks to be 90 °C. This temperature reduces coffee rings the most while maintaining a low surface roughness.

The ink flowrate is preferred to be as high as possible to get as many diamond nanoseeds as possible on the surface. However, the nanoseeds start to tangle when too many are deposited. The conclusion is that the tangling begins to form from 0,40 ml/min. An ideal setting for the flowrate is between 0,25 and 0,35 ml/min.

The conclusion from the test with the number of layers is that 80 layers are not enough. Pinholes and non-uniform coverage still occur. The surface roughness will increase as the number of layers increases. So a consideration has to be made between surface roughness and uniform coverage. A sample with 120 layers has a relatively low surface roughness while maintaining a consistent coverage with almost no pinholes.

The dwell time or time between layers also influences the result of a diamond coating. A longer dwell time seems better for the surface roughness because the solvent in each layer has time to evaporate. However, a longer dwell time increases the processing time. So a consideration has again to be made in this case. A dwell time of five seconds seems to be working well.

Each parameter of the ultrasonic spraycoater influences each other, A compromise has to be made between each parameter to get a good result. The parameters of the previous master's thesis, together with the results of these tests, are a good set of parameters to use for the following experiments. The table below shows the parameters used.

Table 19: Parameters used for following experiments.

Parameter	Setting
Hotplate Temperature	90 °C
Ink Flowrate	0,25 ml/min
Nozzle Speed	50 mm/s
Number of layers	120
Vibration Power	4 W
Shroud Pressure	1,3 psi
Dwell Time	5 seconds

With these settings, an uniform coating can be formed with a thickness of 229 nm. This cross section can be seen in Figure 58.

Figure 58: Cross section of uniform coating.

The coating that can be formed by ultrasonic spraycoating is a uniform coating that is fully closed and where the pinholes are reduced. Th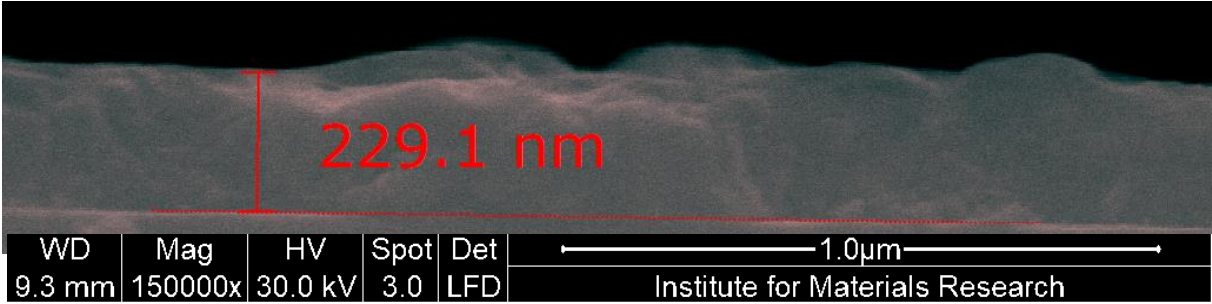e disadvantage is that a ultrasonic spraycoated sample has a higher surface roughness than a spincoated sample. A fully closed coating is shown on a SEM picture in Figure 59.
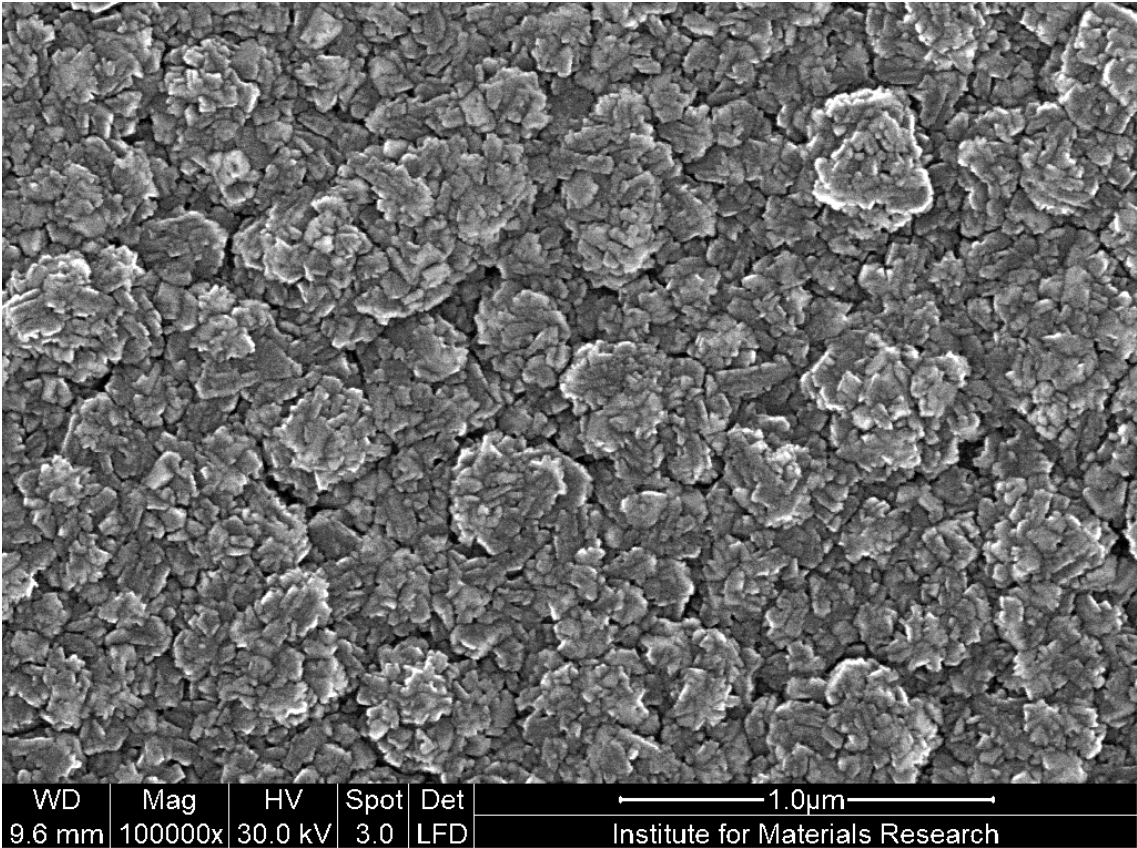
Figure 59: Fully closed coating seen on SEM.

3.3 Pre-treatment methodology

The sections that follow discuss the effect of various pre-treatment methods on fused silica glass. The goal is to determine which procedure is best suited to each depositing method and how long the pre-treatment affects the glass before diminishing over time. Following this, the best conditions for depositing diamond nanoparticle seeds can be determined, and an optimal coating can be created.

3.3.1 Methodology

A UV-O_3 and O_2-plasma treatment increase the surface free energy, and a CF_4-plasma treatment which decreases the surface free energy, will be applied on fused glass substrates with a thickness of 0,720 mm and a size of 14 x 14 mm. This surface free energy will be determined by daily measuring the contact angle of a droplet on these substrates for a specific time interval. A 21 day time interval is chosen because this is long enough to see the influence of the degradation of these pre-treatment processes. The expectation is that the surface conditions will not change after these 21 days.

Three sets of 21 samples per set will be cleaned and prepared for each of the three pre-treatment methods. One set will be used to deposit diamond nanoparticle seeds with an ultrasonic spraycoater for 21 days. The second set will be used to deposit diamond nanoparticle seeds with an inkjet printer for 21 days. The third set is reserved for a daily contact angle measurement. A schematic overview of the experiment can be seen in the figure below.
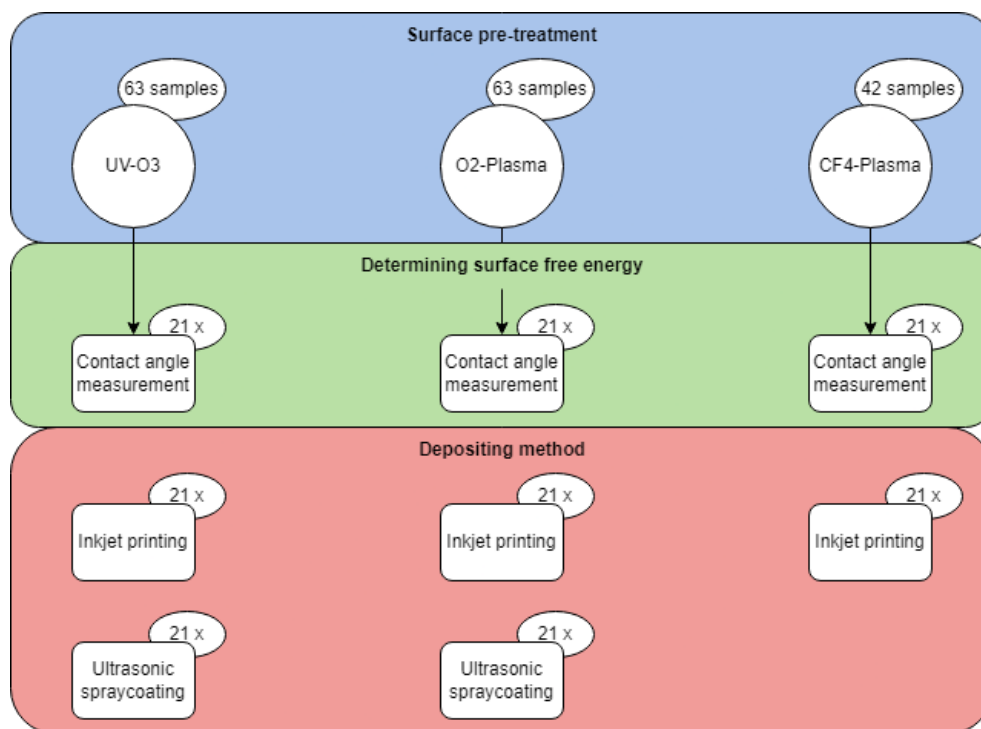
Figure 60: Schematic overview of pre-treatment experiment.

After these 21 days, a day-to-day graph of the evolution of the contact angle can be plotted. The same evolution can be analysed by characterizing the coated samples morphologically and mechanically. Afterwards, a specific time interval or contact angle can be determined to guarantee a well-coated sample.

A unique pattern was designed to test every aspect and detail of inkjet printing. This pattern can be seen in Figure 61. Two different cross figures are drawn to test small straight patterns in two different directions. A comb is designed to test different spacing distances ranging from 20 µm to 140 µm. This is also in two different printing directions. A surface is also drawn to characterise the full surface printed by the inkjet printer. And lastly, the logo of IMO-IMOMEC is placed in the design to measure the thickness of the letters.

Figure 61: Designed test pattern for inkjet printing.

Because the inkjet printer works on the Drop On Demand principle, a droplet is placed on every pattern pixel. With a drop spacing of 20 µm, the jetted drops are too close together to each other. This close spacing of the droplets will enhance the flow behaviour and, therefore, decrease the diamond coating quality.

This problem can be solved by running a checkerboard script on the bitmap figures. This script deletes two pixels out of a 2x2 matrix, creating a checkerboard pattern of the figure. The checkerboard version of the designed pattern can be seen in Figure 62.
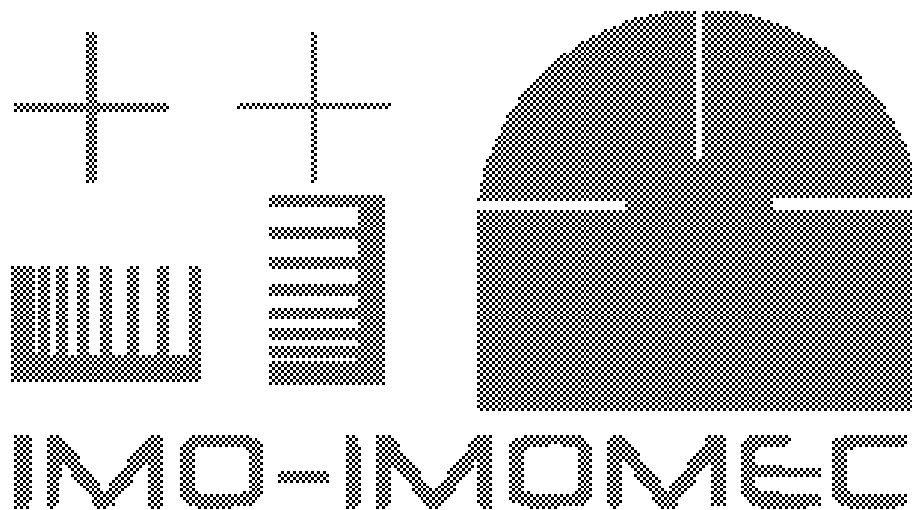
Figure 62: Checkerboard version of designed pattern.

82

3.3.2 Expectations

It is expected that ultrasonic spraycoating will require a high surface free energy or a low contact angle. This high surface free energy will aid in the surface expansion of the droplets produced by the impact nozzle. A droplet with a larger surface area will disperse more nanoparticle seeds and evaporate more quickly. As a result, a pre-treatment method that increases surface free energy will be required. Both UV-O$_3$ and O$_2$-Plasma are capable of accomplishing this. To ensure that the droplets spread sufficiently, the spraycoating process is expected to be performed almost immediately after the pre-treatment method. If the surface free energy is too low, the droplets will not spread sufficiently, and coffee rings or even a non-uniform coating are expected. Figure 63 gives a schematic overview of how the droplets spread on the surface. An unfavourable condition is a droplet with a high contact angle. On the favourable side, the droplets have a low contact angle and spread enough on the surface.
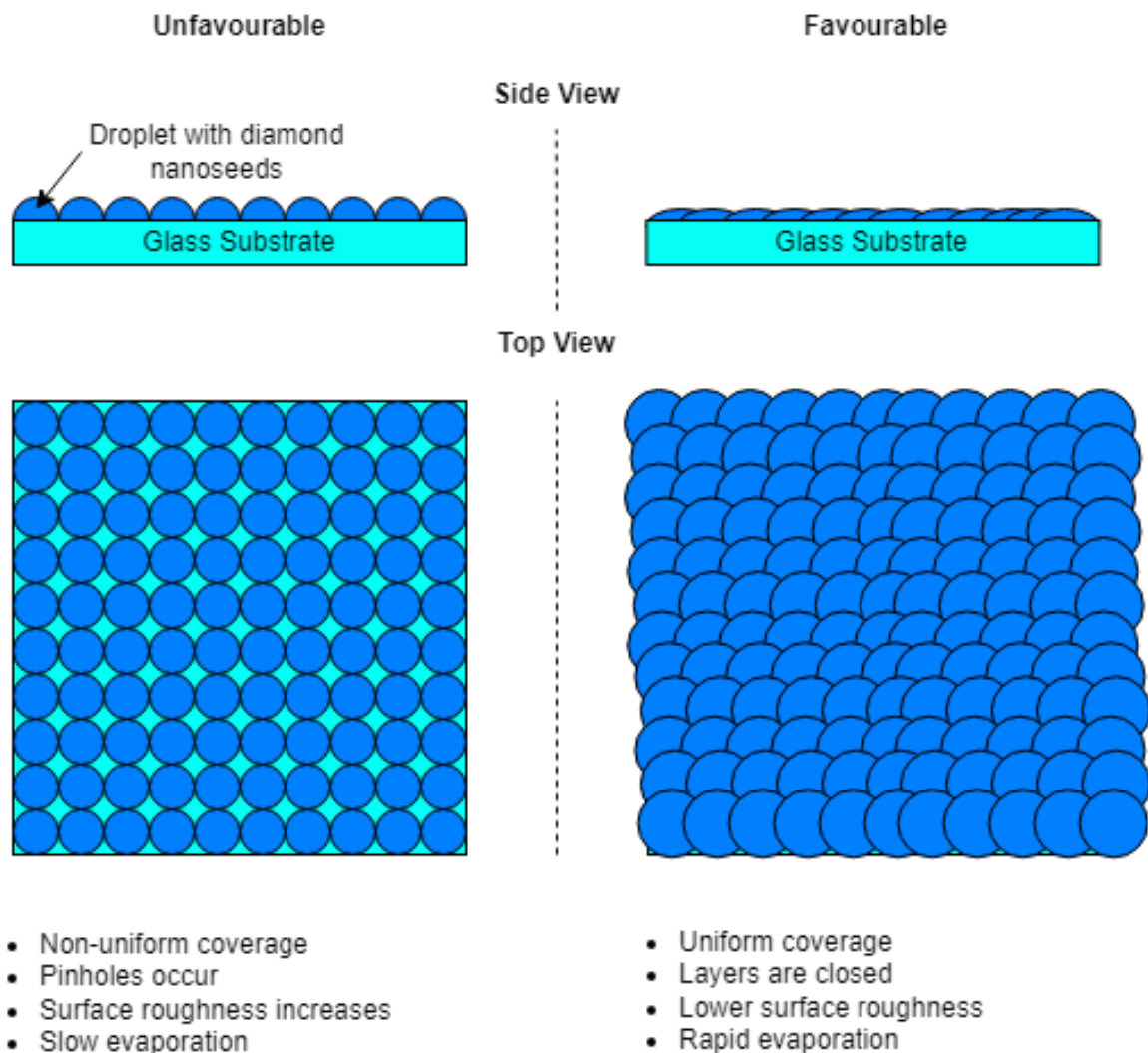
Figure 63: Unfavourable versus favourable surface conditions for ultrasonic spraycoating.

The expectation for inkjet printing is that it requires a low surface free energy or a high contact angle. A high contact angle will aid in increasing the resolution of printed patterns, and smaller patterns will be possible if the contact angle is increased. Because of the smaller surface area, the solvent will evaporate more slowly, so a longer processing time is needed and the chance of coffee rings is increased. Figure 64 shows this in a schematic overview. When the contact angle is low, the droplets will spread out and no fine patterns are possible to print. It is preferred to have the contact angle as high as possible to reach very fine prints.
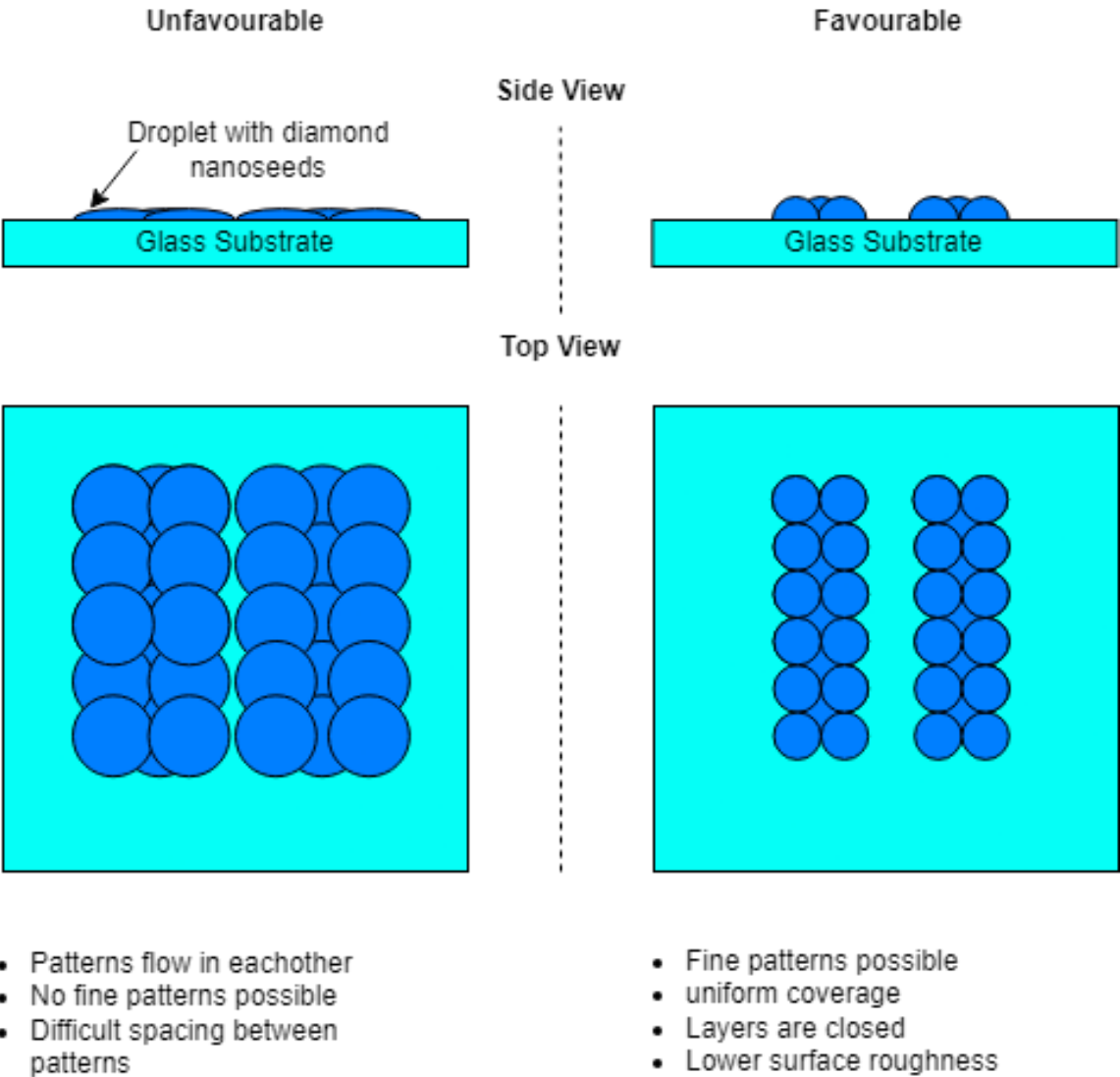
Figure 64: Unfavourable vs favourable surface conditions for inkjet printing.

3.4 Results of contact angle measurements

This section discusses the influence and evolution of the different pre-treatment processes on fused silica glass. The contact angle measurements were performed daily to plot the evolution and influence of the pre-treatment processes on uncoated fused silica glass.

3.4.1 UV-Ozone

As discussed previously in this thesis, UV-ozone is a pre-treatment process that increases the surface free energy of the substrate. In order to plot the evolution, samples had to be cleaned by the UV-O_3 process. The stage of the UV-Ozone machine is not big enough to accommodate 63 samples. Therefore, the experiment was split up into three equal parts.

3.4.1.1 Pre-treatment of 30 minutes

The duration of the UV-O_3 process is adjustable. The first experiment was performed with a duration of 30 minutes. After this, a second experiment was performed with the other time periods. The first contact angle is measured directly after the treatment process, while the others have a 24 hour time interval between them. The first graph of measured contact angles can be found in Figure 65.
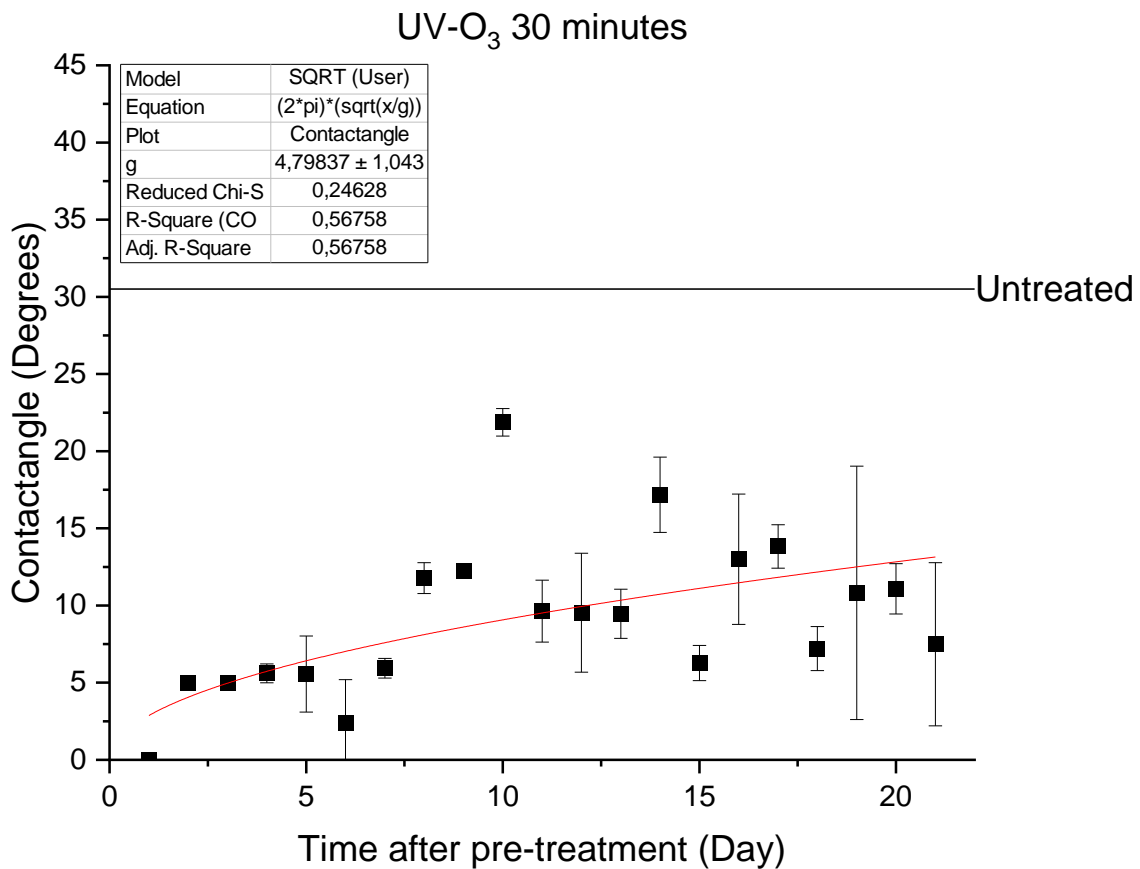
Figure 65: Contact angle values of a 30 minute UV-O₃ treatment.

The graph above shows that the contact angle stays around five degrees for 2-3 days before gradually increasing to fifteen degrees. The influence of each batch of samples is visible in this graph. The first seven samples show a linear trend. The second batch from day 8 to day 14 shows a different linear trend with a more significant standard deviation. This variation between batches is due to variation in machine settings. The stage of the UV-O$_3$ machine is adjustable and is not examined before starting this experiment. The time the samples were in an ozone environment after the treatment is also possible for the variation between the batches. The process stops after the configured time, but the operator has to remove the ozone before opening the cover.

A root function can be fitted on these data points to visualise the evolution of the surface conditions. The data points show a beginning linear trend. Moreover, after ten days, this linear trend seems to decrease. A root function looks to fit the most to this trend.

The standard deviation can also be plotted in the function of the day. Figure 66 shows this in a graph. A linear trend becomes visible when the outliers are masked. This trend indicates that the standard deviation or variation of the contact angle increases. The first three points have no variation due to the low contact angle of the droplet. This contact angle could not be measured due to the rapid flowing of the droplet. The increasing linear trend also shows that the contact angle becomes unreliable when the time after the pre-treatment increases.
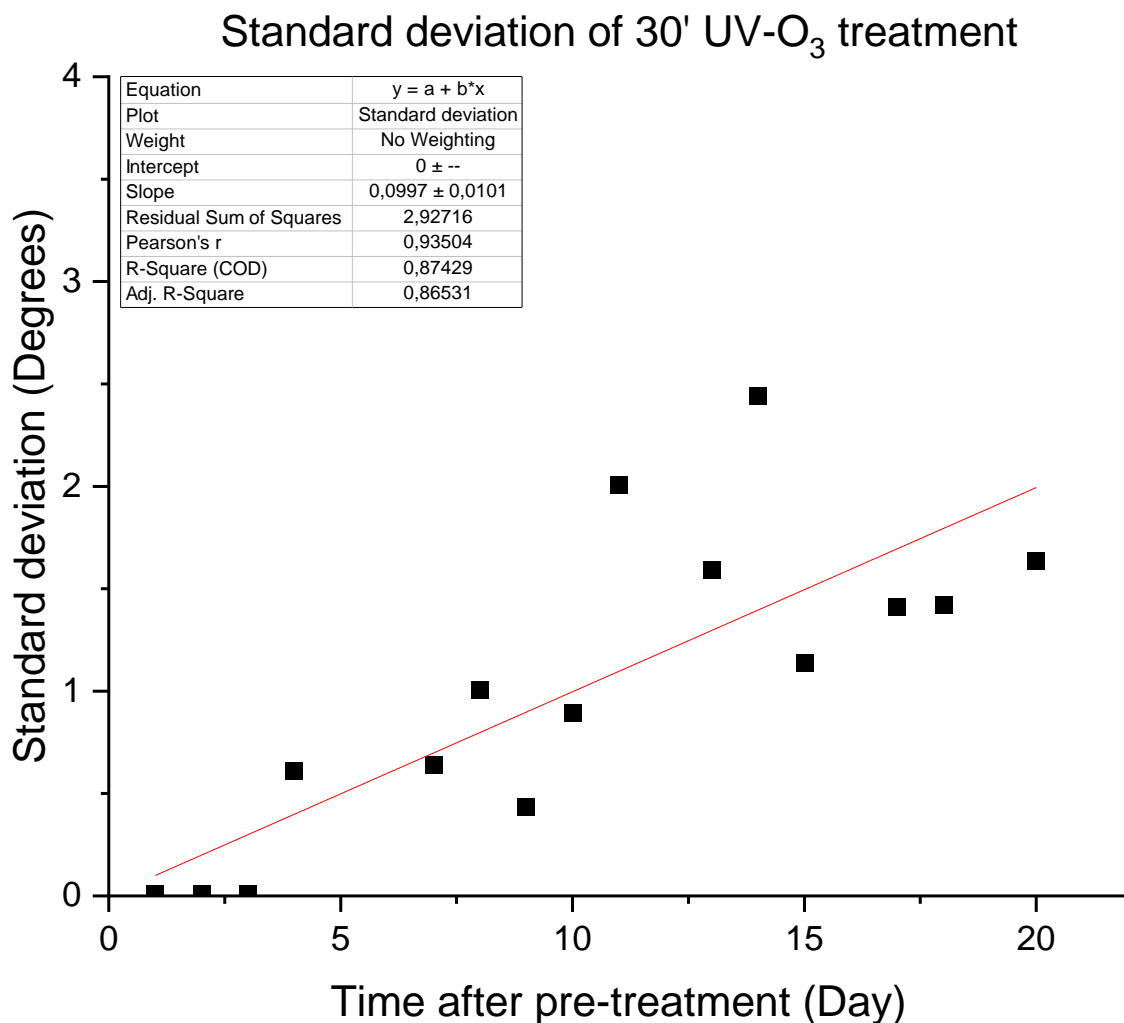
Figure 66: Standard deviation of contact angles plotted in function of day.

3.4.1.2 Pre-treatment of 15 minutes

A second UV-O$_3$ experiment was performed with other periods. The contact angles of a fifteen minute UV-O$_3$ treatment can be found in Figure 67. What stands out is that the contact angle values start to lean to an untreated value from day 15. The variation between different batches is again visible, especially between weeks two and three. A possible cause of this variation can be due to a previous cycle of the UV-O$_3$ machine. The mercury lamp needs to heat up to be efficient. Fifteen minutes does not seem to be enough to heat the lamp. The mercury lamp is already heated if a fifteen-minute cycle is done after another cycle.

The same root function is fitted on this graph. The beginning of the function shows a linear trend which converges after fifteen days.

The chemical process that needs to happen in these fifteen minutes seems not enough to give the fused silica glass good surface conditions. Therefore, the contact angle returns more quickly to an untreated value.

Figure 67: Contact angle values of a 15 minute UV-O$_3$ treatment.

The standard deviation of these measurements is plotted in Figure 68. This graph shows the same linear trend as the 30-minute treatment after masking the outliers. However, Pearson's r coefficient is smaller than the coefficient in the 30-minute treatment. This means that the variation in contact angles is more significant than the 30-minute treatment. Therefore the fifteen-minute treatment can be seen as unreliable.
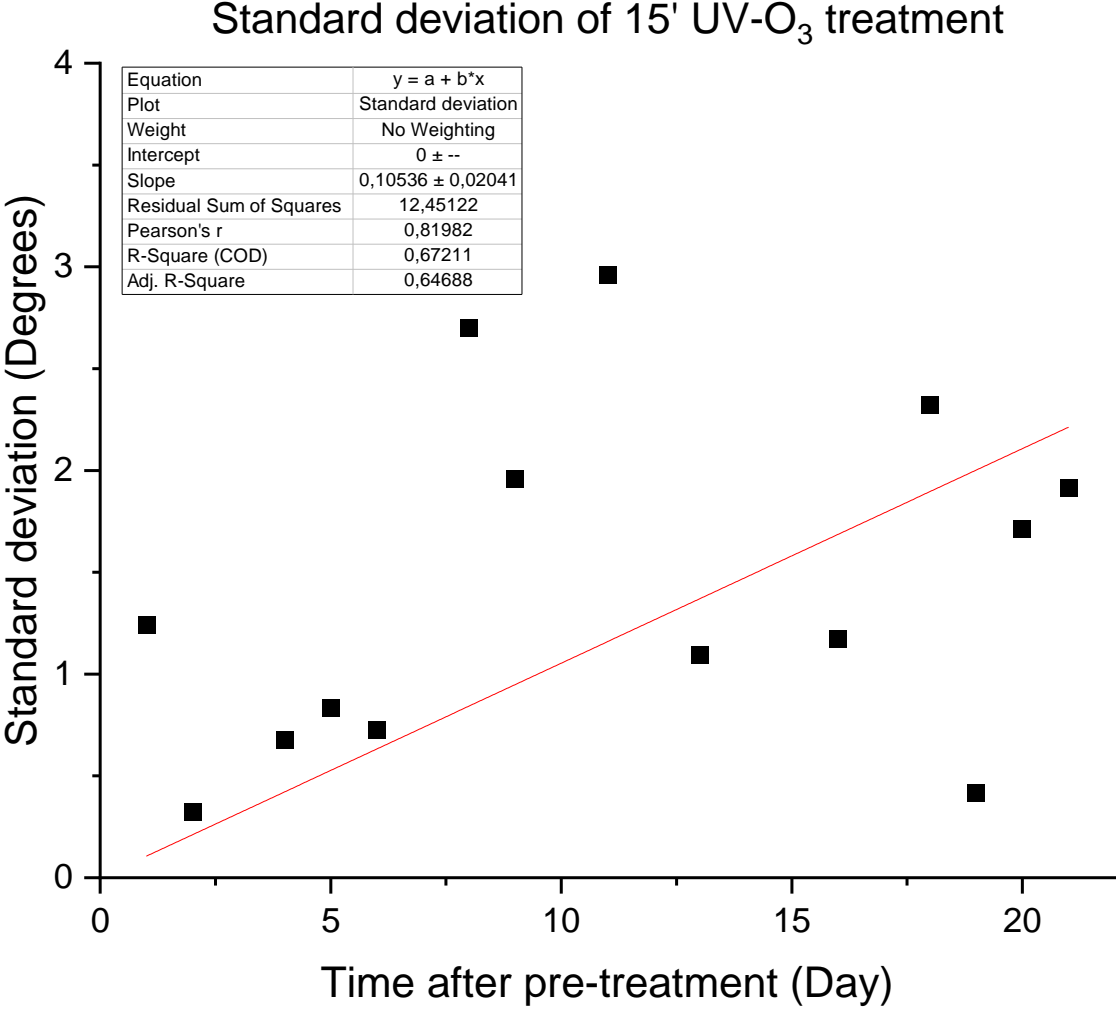
Figure 68: Standard deviation of contact angles in function of the day.

3.4.1.3 Pre-treatment of 60 minutes

A duration of 60-minutes is also possible. The contact angle of 21 samples is measured and plotted in Figure 69. Remarkably, the differences between the weekly batches are not noticeable. The contact angle of day one is lower than the previous periods. The contact angle seems to stabilise around ten to twelve degrees after ten days. Even after 21 days, the contact angle has not returned to an untreated value.

The same root function is also fitted on these values. This curve fits closer to the data points than the previous graphs. The reason for this is that 60-minutes is a relatively long period. The mercury lamp has enough time to heat, and therefore, there is a smaller variation between the days.
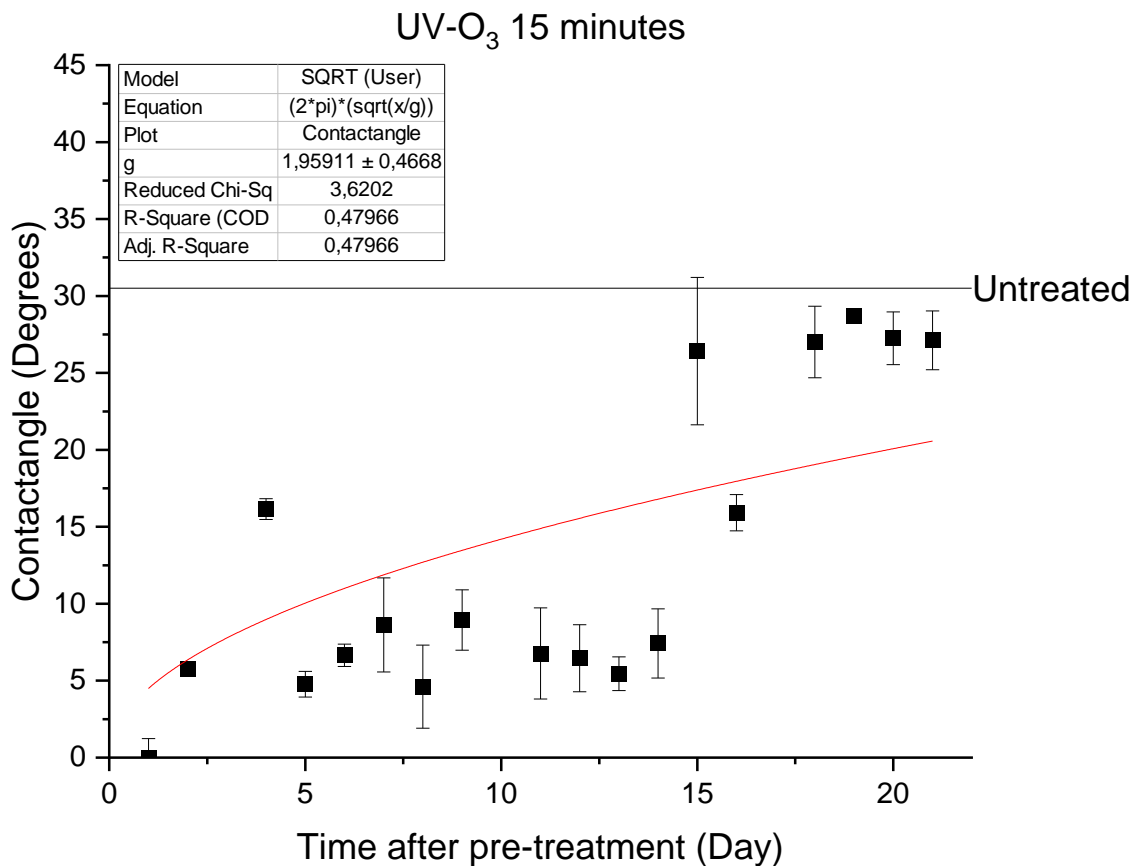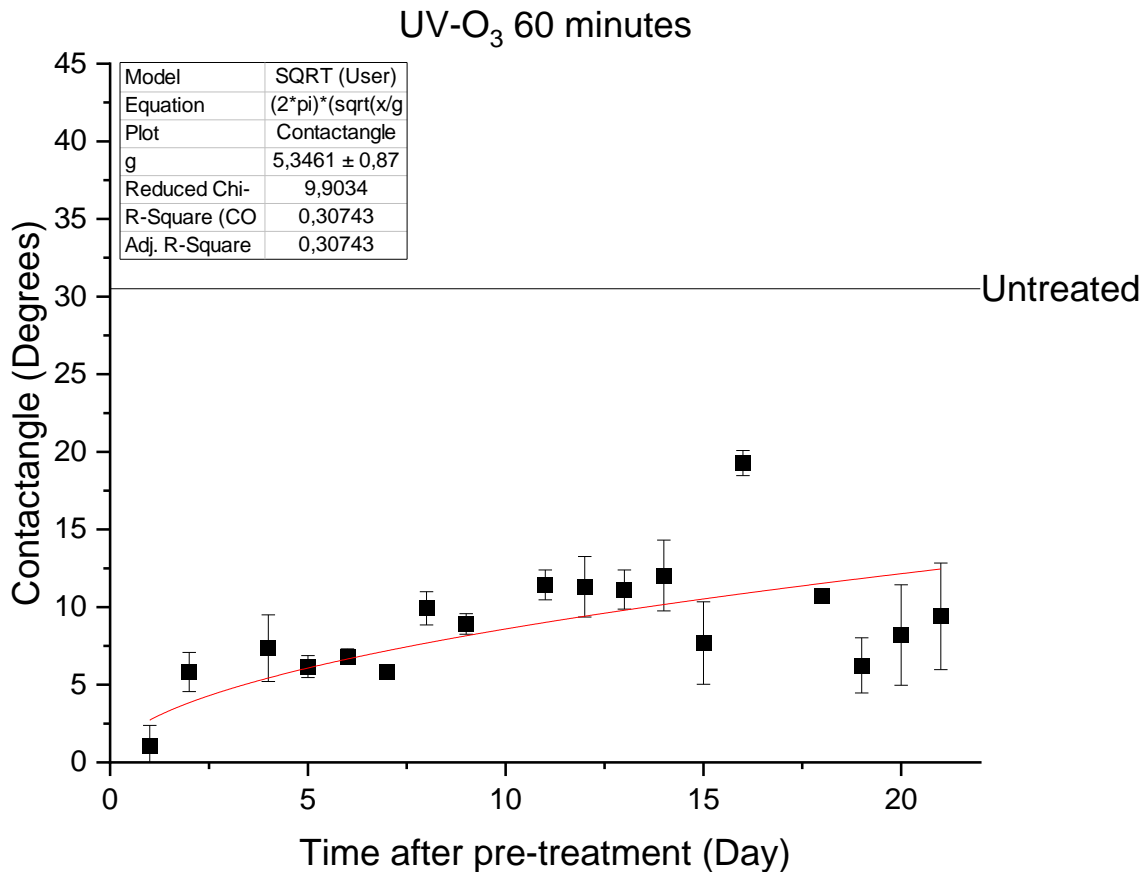

Figure 69: Contact angle values of a 60 minute UV-O$_3$ treatment.

The standard deviation of these measurements can also be plotted. Figure 70 shows a linear trend after two or three outliers are masked. The variation of the contact angles increases day by day. Pearson's r coefficient has a value of 0,92, which means that the data points are close to the fitted curve. A conclusion can be made that a treatment time of 60-minutes is more reliable because of the lower standard deviation.

Standard deviation of 60' UV-O$_3$ treatment

| Equation	y = a + b*x
Plot	Standard deviation
Weight	No Weighting
Intercept	0 ± --
Slope	0,14094 ± 0,0152
Residual Sum of Squares	8,08973
Pearson's r	0,9227
R-Square (COD)	0,85138
Adj. R-Square	0,84147
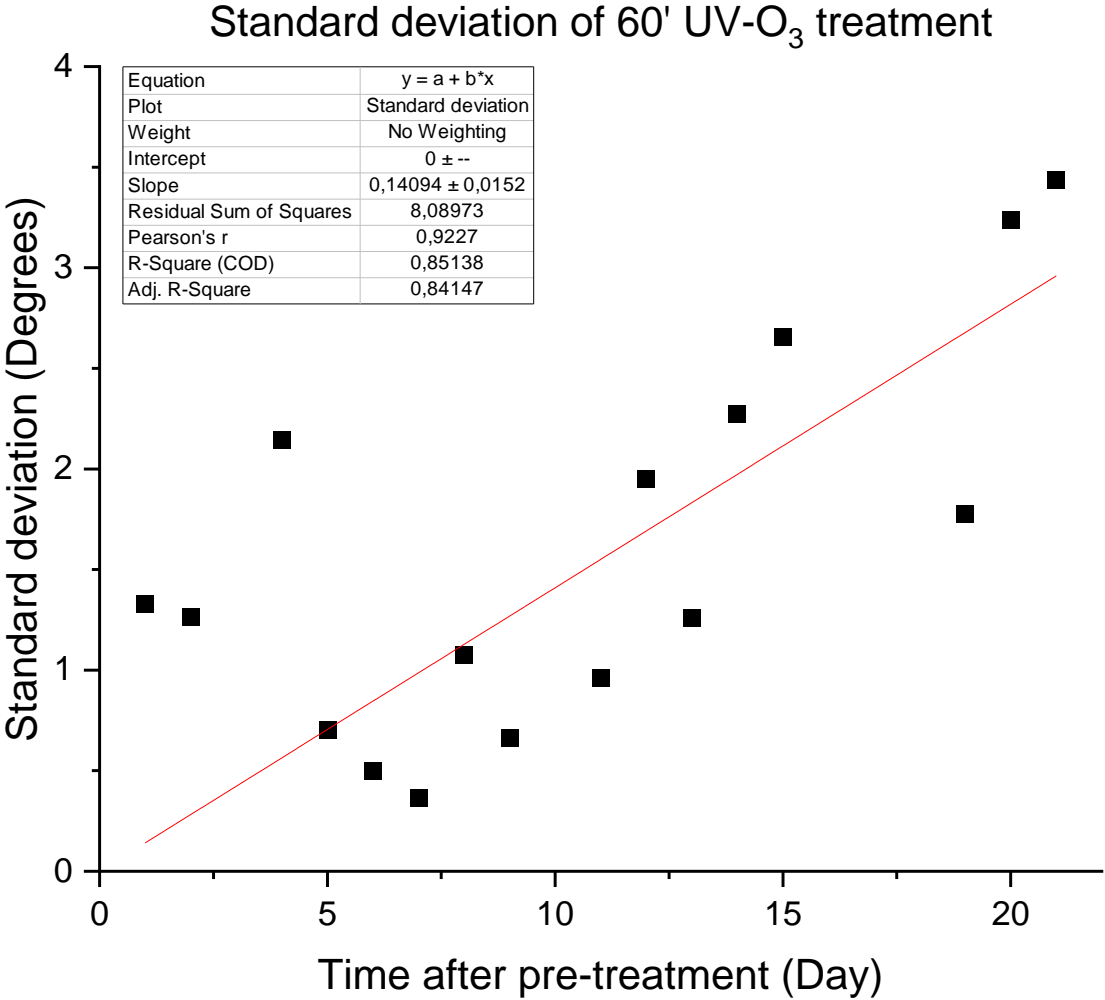
Figure 70: Standard deviation of contact angles in function of the day.

3.4.1.4   Pre-treatment of 120 minutes

The final duration period is 120 minutes. Figure 71 shows the contact angle values and evolution of the surface conditions. With this time, the differences between batches are even more minor. What is significant is that the contact angle stays around five degrees for the first few days. After ten days, the contact angle increases to ten degrees and more slightly. Even after 21 days, the contact angle has not reached fifteen degrees.

The same root function is fitted in Figure 71. The data points lay even closer to the fitted curve than the 60 minutes. A possible explanation is that 120 minutes is a very long period, the lamp has time to heat up, and every sample has the same surface conditions. This relates to the slight variation throughout the days.

Model	SQRT (User)
Equation	(2*pi)*(sqrt(x/g
Plot	Contactangle
g	7,10162 ± 1,2
Reduced Chi-	8,65302
R-Square (C	0,32092
Adj. R-Square	0,32092
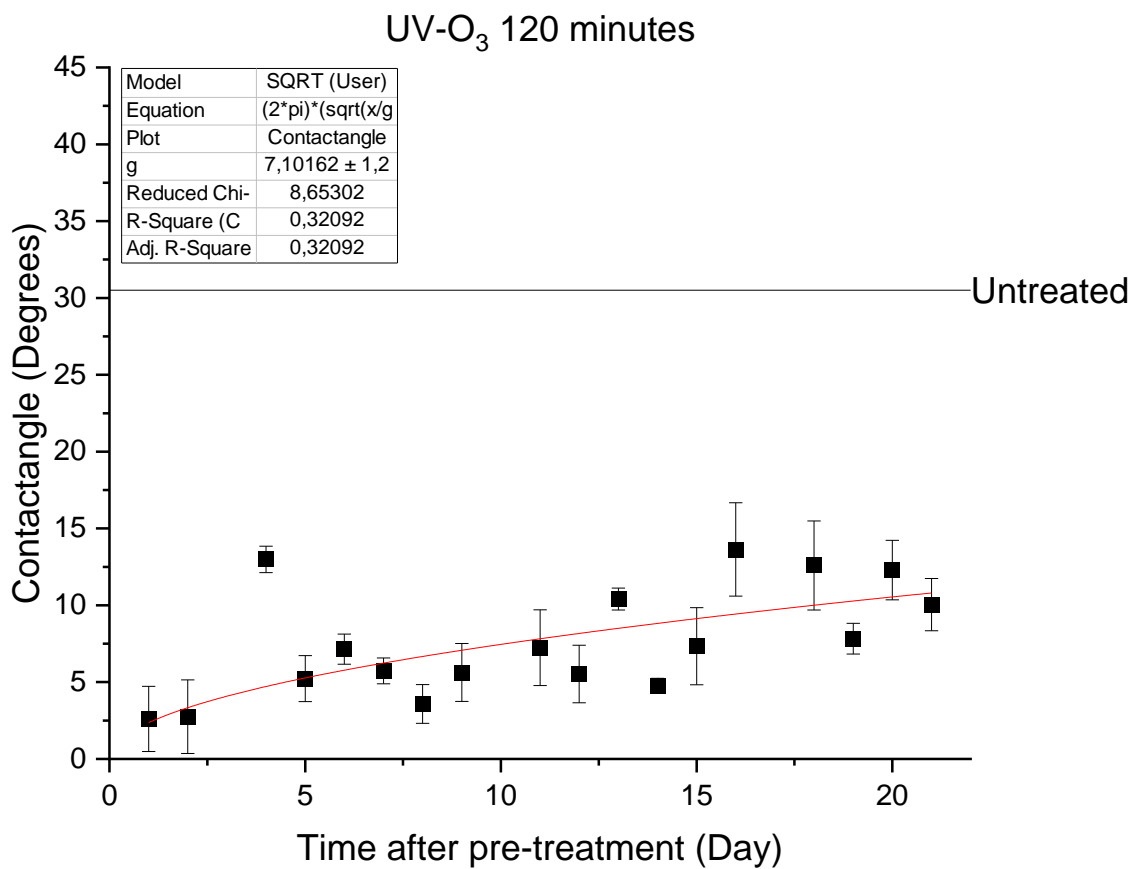
Figure 71: Contact angle values of a 120 minute treatment.

The standard deviation is also plotted in Figure 72. This standard deviation of 120 minutes period shows a linear trend. This linear trend is relatively flat. This flat line means that the variation remains the same throughout the days, with a slight increase in contact angle variation towards 21 days.
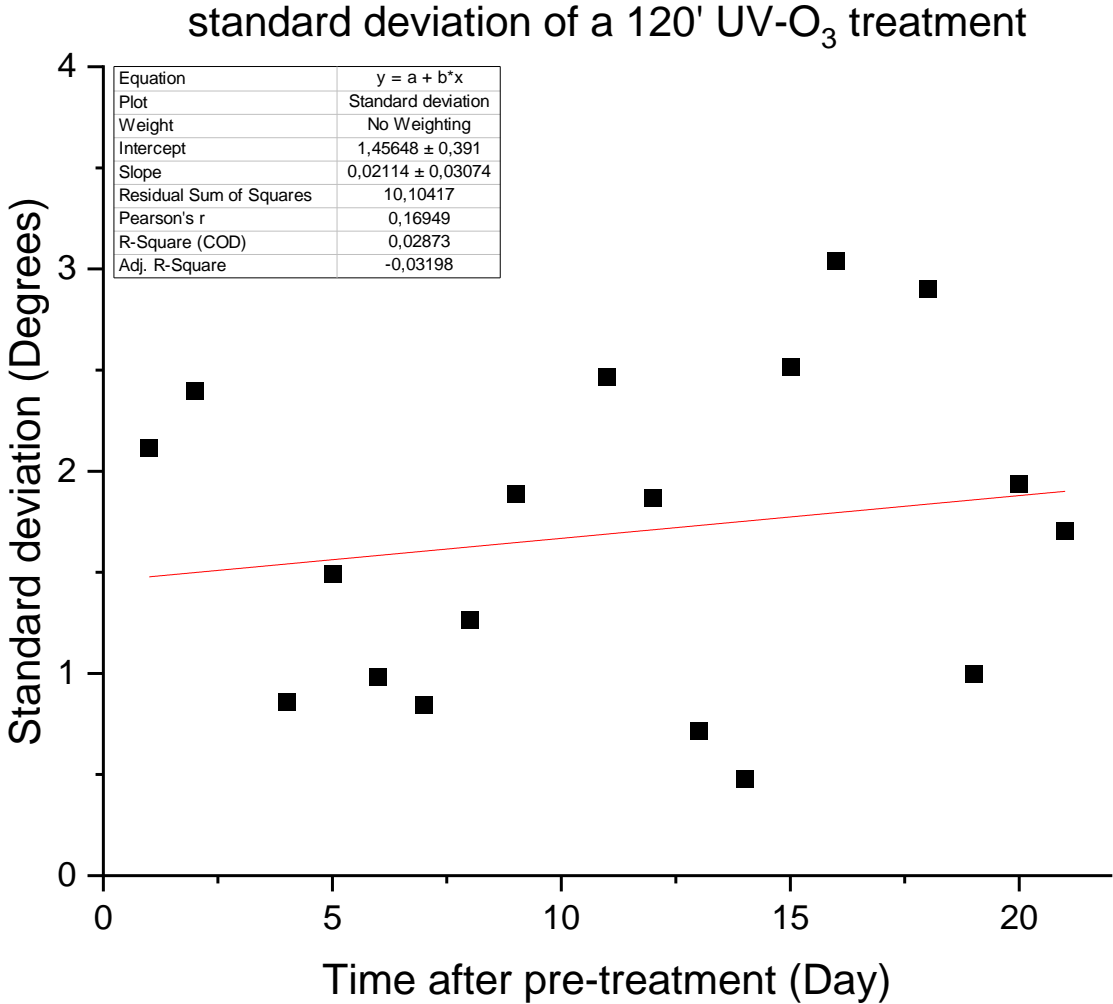
Figure 72: Standard deviation of contact angles in function of the day.

3.4.1.5 Comparison of the different periods

A noticeable difference can be seen when these four treatment periods are plotted on the same graph in Figure 73. The longer the duration of the UV-ozone treatment, the longer the contact angle remains at a lower value. However, the difference between 60 minutes and 120 minutes is relatively small. Therefore, a treatment time of 60 minutes is long enough to change the surface conditions.

A 30 minute pre-treatment period results in almost the same contact angle value as the more extended periods. Therefore, the 30 minute period complies if the sample is deposited with diamond nanoparticle seeds on the same day. A fifteen-minute period has a slightly larger contact angle on the first day. This difference with the 30 minutes is not noticeable, but there is a more significant variation in contact angle on the first day after the pre-treatment. It can be concluded that a fifteen-minute period is not reliable and therefore should not be used to alter the surface conditions of a fused silica glass sample.
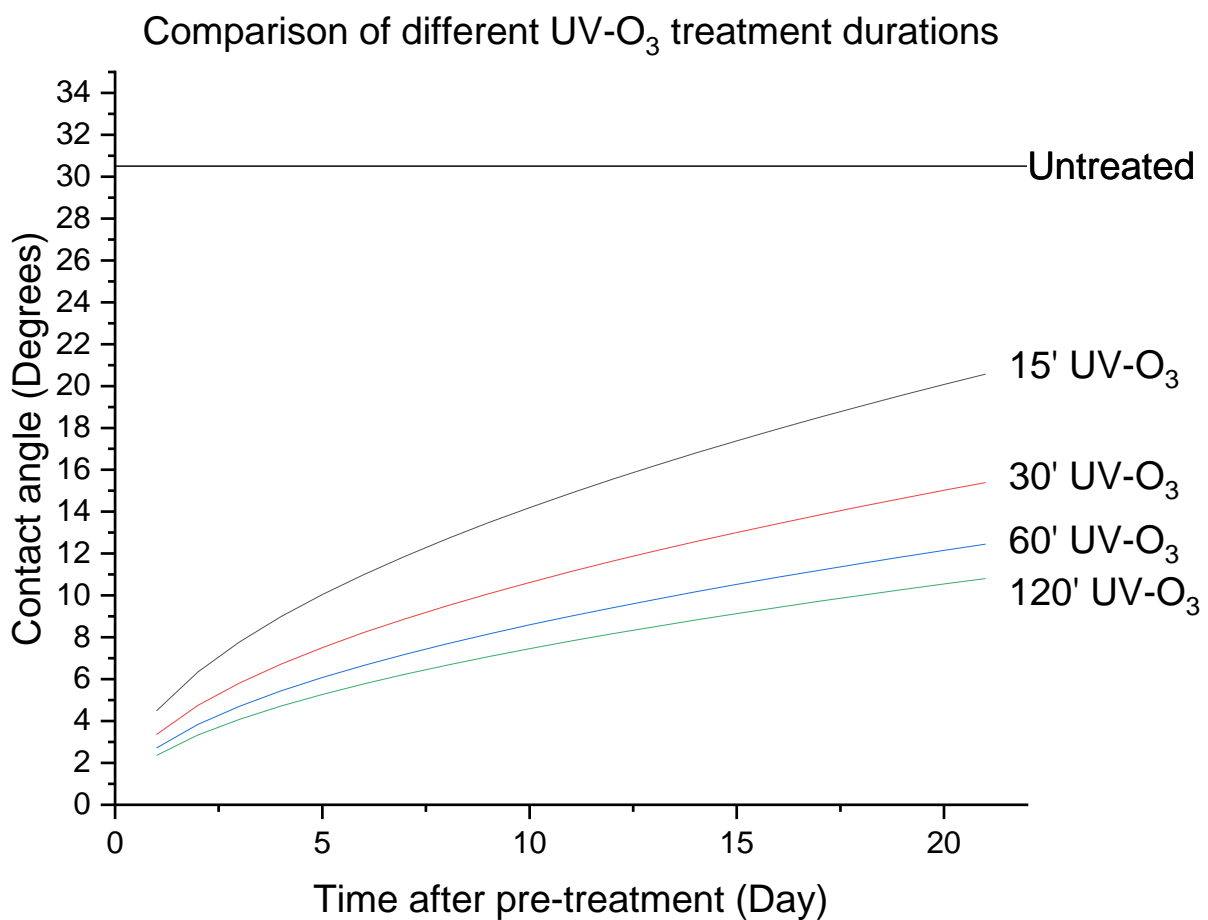
Figure 73: Comparison between different UV-O₃ durations.

3.4.1.6   Characterisation of ultrasonic spraycoating samples

The UV-O$_3$ treatment deteriorates over time. Therefore, it is important to determine an ideal window for the samples to be coated. In Figure 74 below, three samples are compared with each other using the optical microscope. Sample (a), the earliest one, shows different coloured spots which look like pinholes, but this is a difference in the layer height. Because the layer height is different here, the light interference is different, and therefore there seems to be a colour difference. With picture (b), the sample is still coated homogenous. However, in the last picture (c), the flow behaviour becomes more apparent and becomes quite visible with the optical microscope. So it can be concluded that from day six, the treatment is not effective enough anymore to get a homogeneous layer with the spray coating.
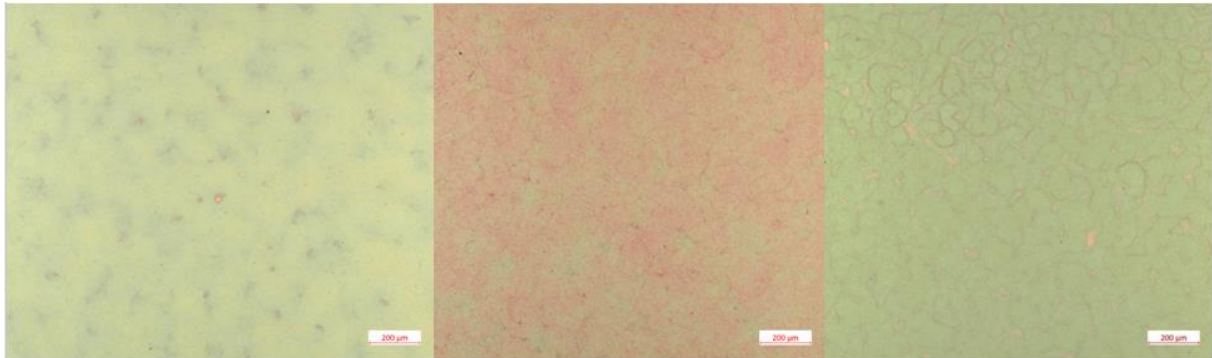
Figure 74: USSC Samples pre-treatment: UV-O$_3$. day 5 (a), day 6 (b), day 7 (c).

To ensure that the sample is not only optically closed and but also at the nanoscale, the SEM was used to check whether this is the case. Figure 75 below shows a SEM image of a sprayed sample with a three-day old UV-O$_3$ treatment. In this image, there are no pinholes or inconsistencies visible in the layer.
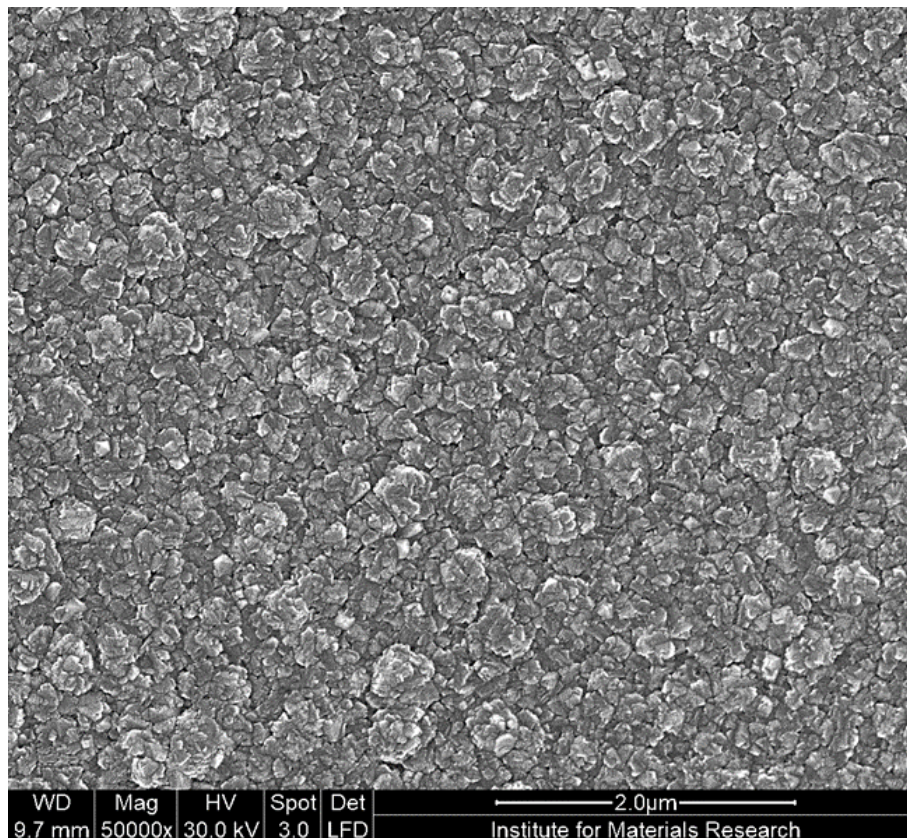
Figure 75: USSC Samples pre-treatment: UV-O$_3$. MA54: day 3.

The roughness of each spray-coated sample was also measured and plotted in Figure 76. This value stays even with little to no variance throughout the entire testing period.
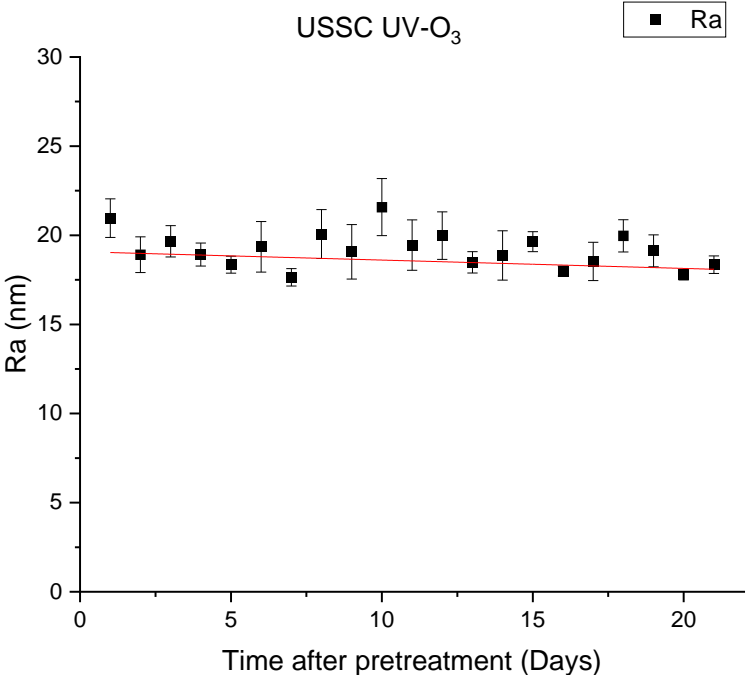
Figure 76: Ra roughness USSC samples UV-O₃.

The waviness was also checked for each sample. There was a lot of variance in the measurements, but the average stayed relatively the same throughout the 21 days as shown in Figure 77. The linear fit shows a downward trend due to the first two values having a higher waviness than the other.
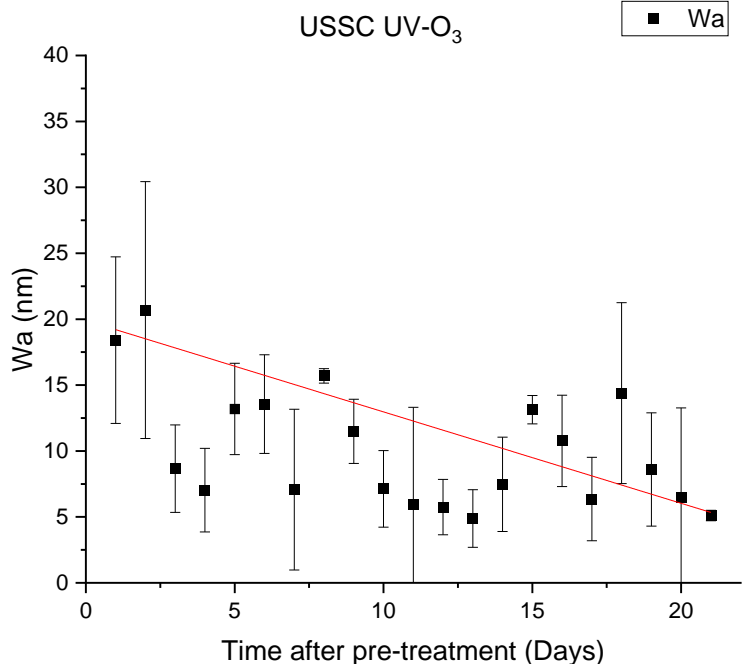
Figure 77: Wa roughness USSC samples UV-O₃

Withal the previous results, it can be concluded that for the best spray-coated sample and UV-O₃ pre-treatment, the ideal time window is before the treatment is six days old. This period is chosen because the sample looks better optically and has better coverage, as seen on the optical microscope. However, the average waviness seems to decrease when the time after the pre-treatment increases, but this difference is negligible.

3.4.1.7   Characterisation of inkjet samples

Two different conclusions must be drawn for the inkjet, one for the patterns and one for the surfaces. Because the effectiveness decreases over time, the ideal point may not be immediately after the treatment but rather when some of the effectiveness has worn off. Because of how the inkjet works with its drop depositing, it is possible that if the droplets flow too much, they can flow into the previous one and create heavy flow behaviour. In Figure 78 below, it is visible that after Figure 78 (a), the edge still shows quite some irregularities, while Figure 78 (b) has a clean edge with good coverage. Although the surface of the Figure 78 (a) sample is not that bad, the edges are not as clean, which still indicates some flow behaviour, whereas this is not the case for Figure 78 (b). If the pre-treatment was too long ago, the properties of printing surfaces are too poor, and the surfaces are unclear and not fully covered as visible in Figure 78 (c).

Figure 78: Inkjet samples UV-O₃ surfaces: day 4 after treatment (a), day 6 after treatment (b), day 18 after treatment (c).

Although this is also important, it is not so much the coverage that is looked at for the patterns, but rather how sharp the edges are and how the figure is visible. The droplets flow too much to get a distinctive pattern when the treatment is still very fresh. In figure 98 (a), the pattern shows a lot of flow behaviour with no clear lines. While figure 98 (b), the pattern is obvious, with the lines straight and crisp edges. If the wait is too long, the droplets begin to clump together, as seen in Figure 79 (c), and the patterns become blurry due to the flow behaviour.
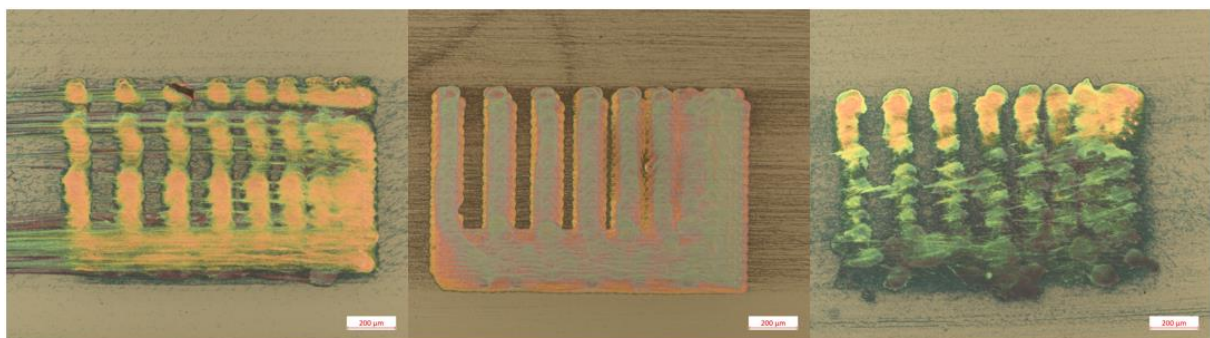
Figure 79: Inkjet samples UV-O₃ patterns: day 4 after treatment (a), day 6 after treatment (b), day 16 after treatment (c).

The roughness of the ink jetted samples were measured using the dektak profilometer. Although there is a slight upward trend as seen in Figure 80 below, the values remain very similar after the treatment, so it can be concluded that the roughness is not influenced by the time between the printing and the pre-treatment.
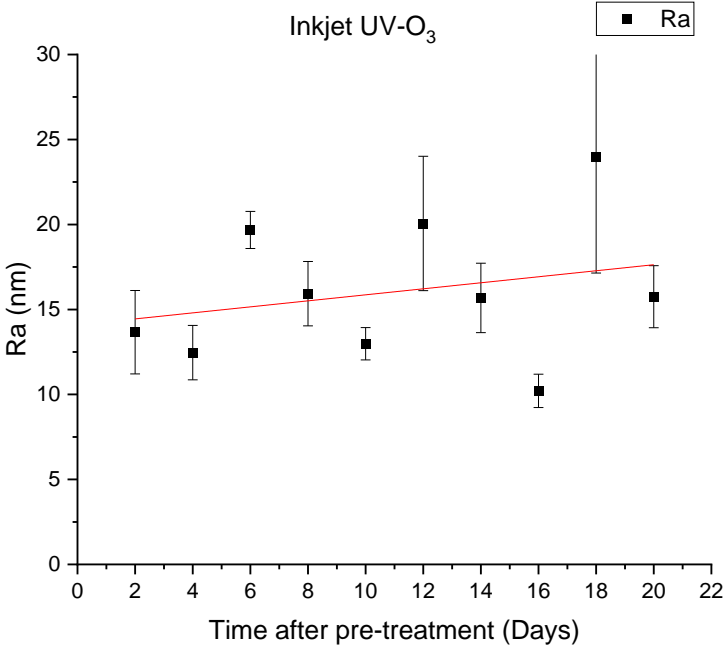
Figure 80: Ra roughness of inkjet samples with UV-O₃ treatment.

The waviness, Wa, was also measured, and here, the same conclusion can be drawn that the waviness is not influenced by the time between the printing and the pre-treatment.
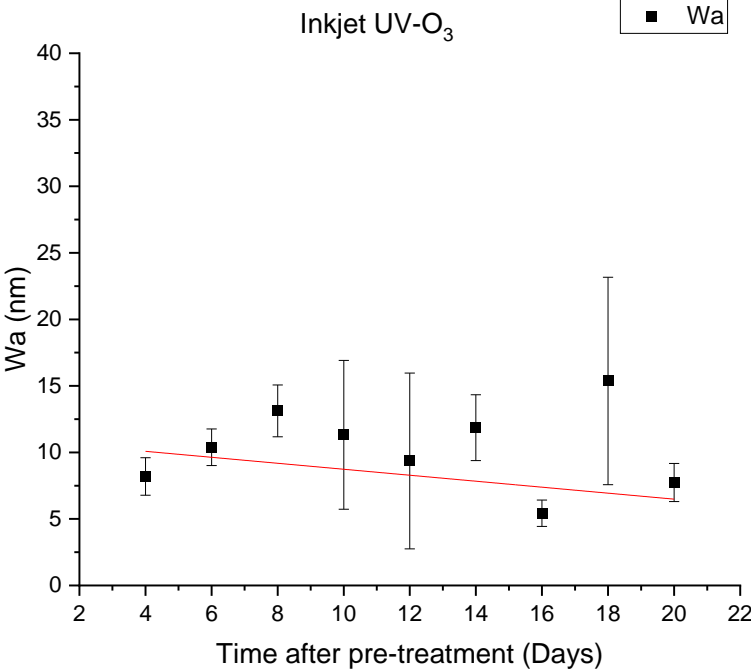
Figure 81: Wa value of inkjet samples with UV-O₃ treatment.

The conclusion from these results is that for patterns, a multiple-day period is available for printing, starting after day 4 and ending before day 16, with the ideal outcome being found at day 6. The conclusion is roughly the same for the printed surface, but the period is a little bit longer. Namely, surfaces can be printed up until day 18. As for the roughness, it is irrelevant when the sample is printed because the value stays relatively the same during the period.

3.4.2   O₂-Plasma

Oxygen-plasma is again a pre-treatment process that increases the surface free energy of the substrate's surface. The stage of the O₂-Plasma is also not big enough for 63 samples. Therefore, the experiment was performed in three different batches. These samples are used to measure the contact angle, print a pattern with the inkjet printer and apply a surface coating with the ultrasonic spray coater. The results of the contact angle measurements can be found in Figure 82.

The samples were put in a vacuum chamber. The plasma power was configured at 200 W with a duration of 2 minutes. The vacuum pressure was not the same for every batch. A slight variation in contact angle is expected.
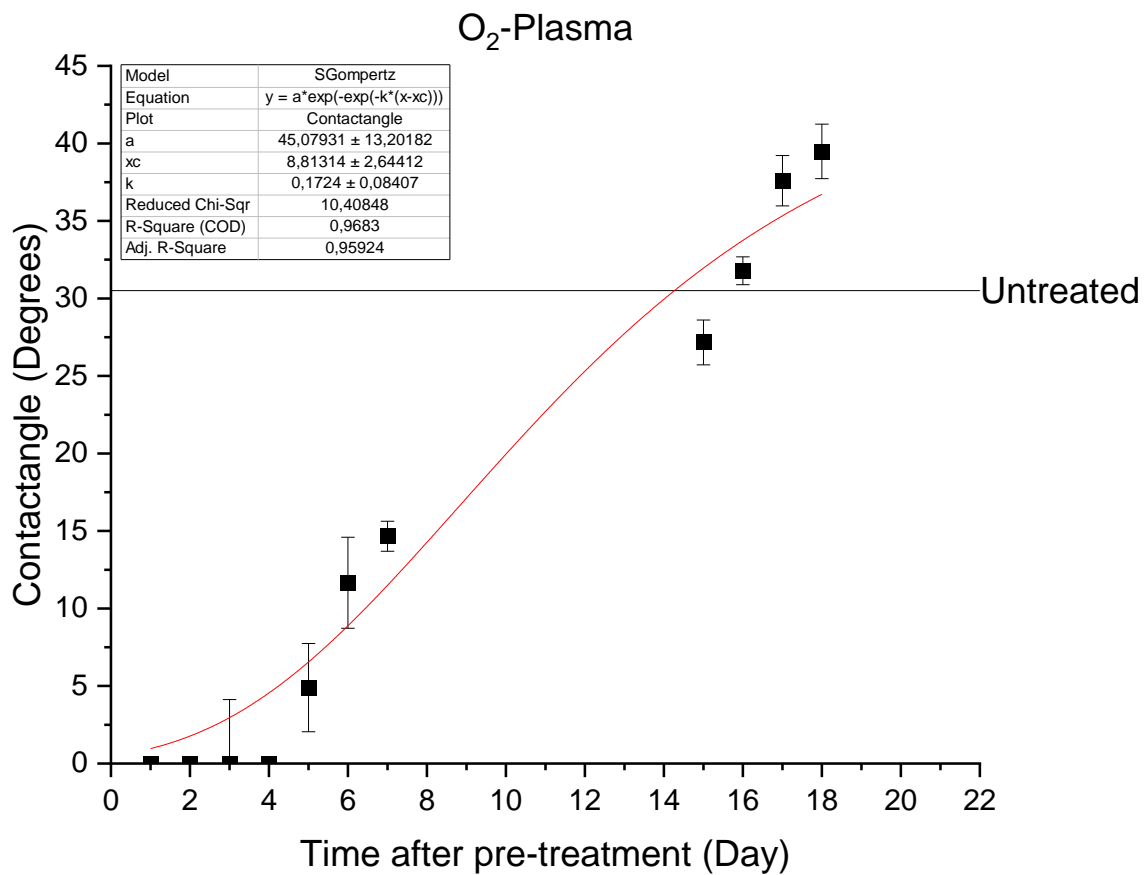
Figure 82: Contact angle values of a O₂-Plasma treatment.

The contact angle is unmeasurable for the first three days because the droplet expands immediately after touching the surface. After these three days, the value increases rapidly to 40 degrees. What stands out is that 40 degrees is higher than the untreated value of the glass. However, the expectation is that the contact angle value returns to an untreated value if the oxygen is elaborated. This is not the case due to the aggressive plasma etching. The surface roughness increases, and this decreases the surface wettability. Therefore, the value is higher than an untreated sample.

A Gompertz curve is fitted to these data points. This curve is a mathematical model for a time series. It can describe growth as being slow at the start and end of a given time period.

The standard deviation is plotted in Figure 83. The fitted linear pattern has a small slope, this means that the variation in contact angle increases when the time after pre-treatment increases. The general variation between these data points is also relatively small with only two degrees. This is a lower value then the UV-O$_3$ treatment.

Standard deviation of a O$_2$-plasma treatment

Equation	y = a + b*x
Plot	Standard deviation
Weight	No Weighting
Intercept	1,08964 ± 0,5155
Slope	0,02815 ± 0,04146
Residual Sum of Squares	8,67634
Pearson's r	0,20057
R-Square (COD)	0,04023
Adj. R-Square	-0,04702
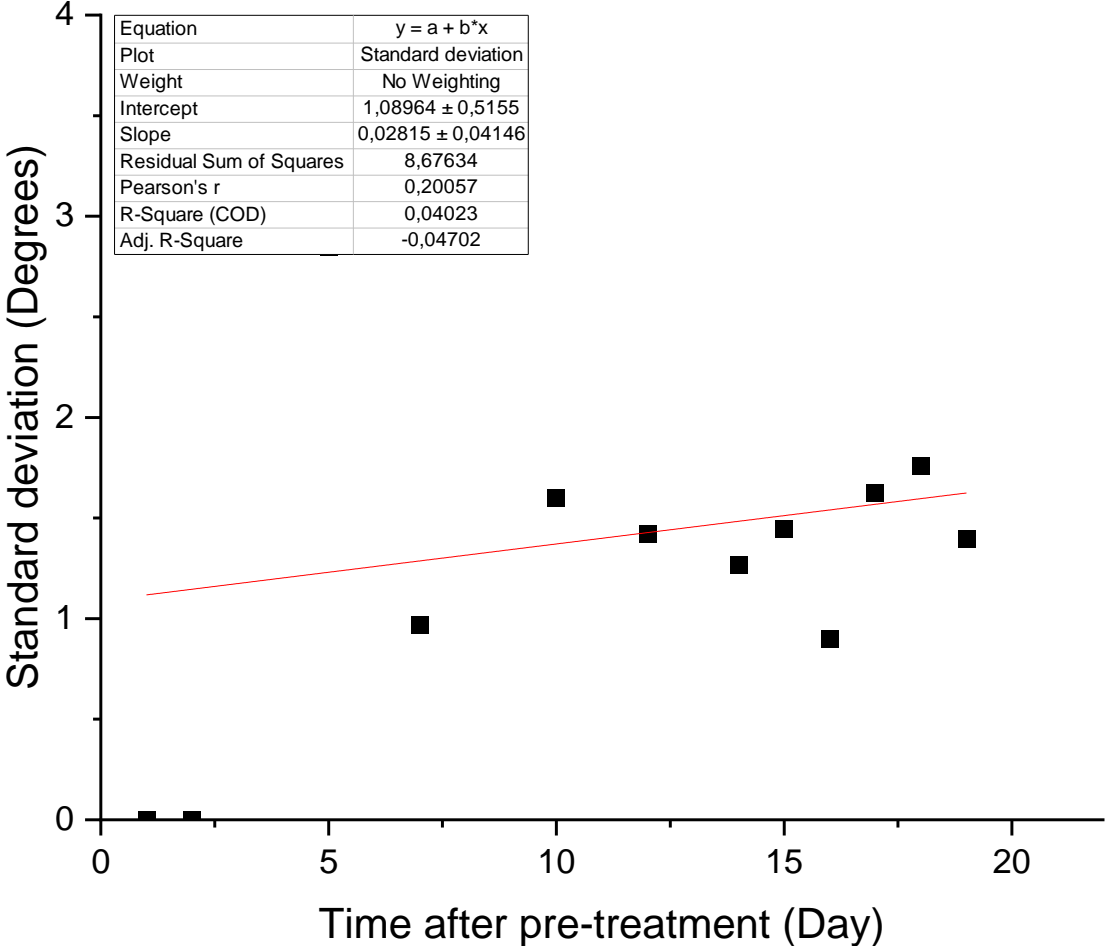
Figure 83: Standard deviation of a O$_2$-plasma treatment.

3.4.2.1 Characterisation of ultrasonic spraycoating samples

The evolution in surface free energy can also be visualised by daily spraycoating a sample. An optical microscope or SEM can see the difference is samples with a different contact angle. Figure 84 shows these visual differences. A sample that is spraycoated five days after the pre-treatment can be seen in Figure 84 a). This coating is relatively uniform and shows almost no coffee rings. From day six and onwards, the substrate shows coffee rings and a non-homogeneous coverage.
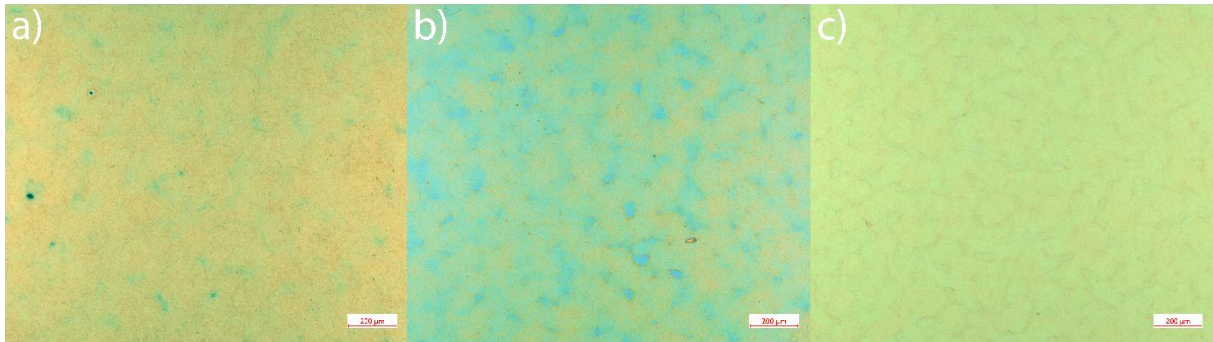
Figure 84: Comparison of deposited samples with USSC and a O₂-plasma treatment. 5 days after pre-treatment (a), 6 days after pre-treatment (b), 7 days after pre-treatment (c).

A scanning electron microscope also characterises the sample to ensure that the coating is fully closed without pinholes. Figure 85 shows this SEM picture of a coating deposited by an ultrasonic spray coater. This sample shows a coating without pinholes where the diamond nanoparticle seeds have grown against each other.
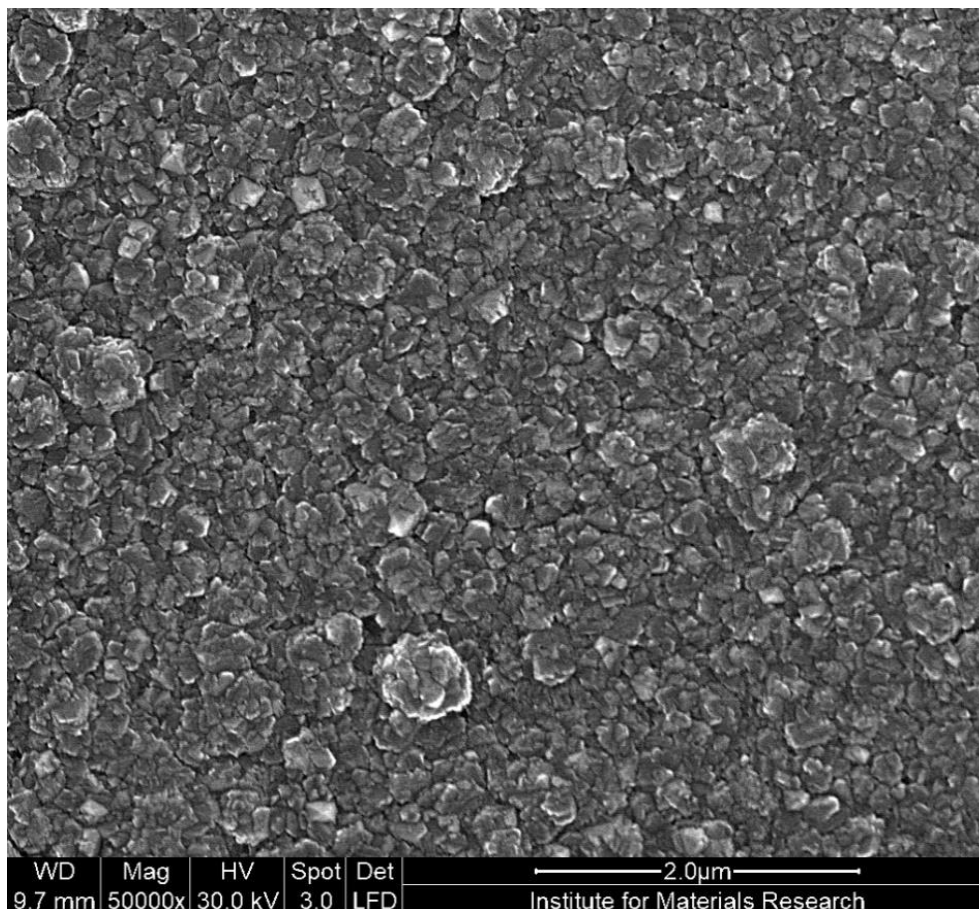
Figure 85: Closed coating deposited by a USSC after an O₂-plasma treatment.

The average surface roughness can be found in Figure 86. The roughness seems to have the same value over the 21 days. Measurements performed with the AFM could give a more in dept view in the variance of the values, but due to lack of time this was not possible. The same goes for the waviness in Figure 87, and the fitted trendline is almost horizontal. The pre-treatment seems only to influence the morphological characterisation.
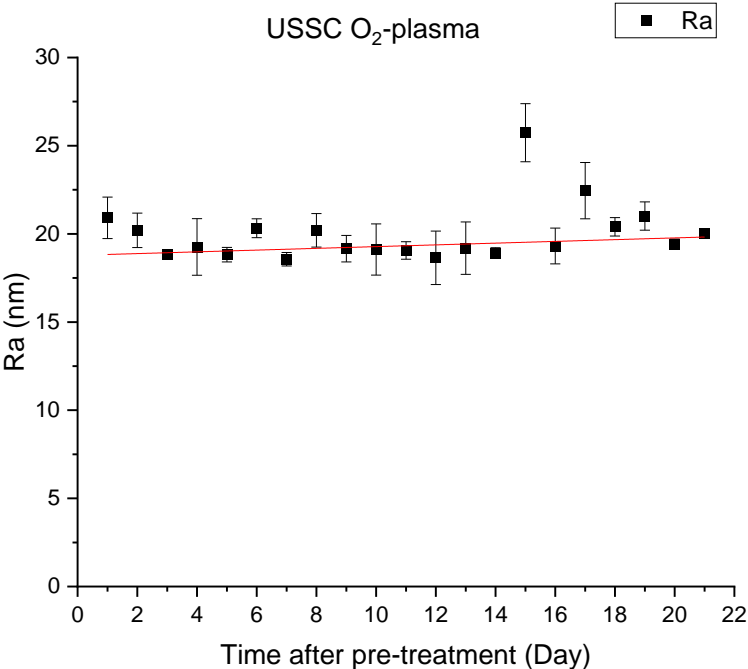
Figure 86: Average surface roughness of O_2-plasma treated and diamond deposited samples.
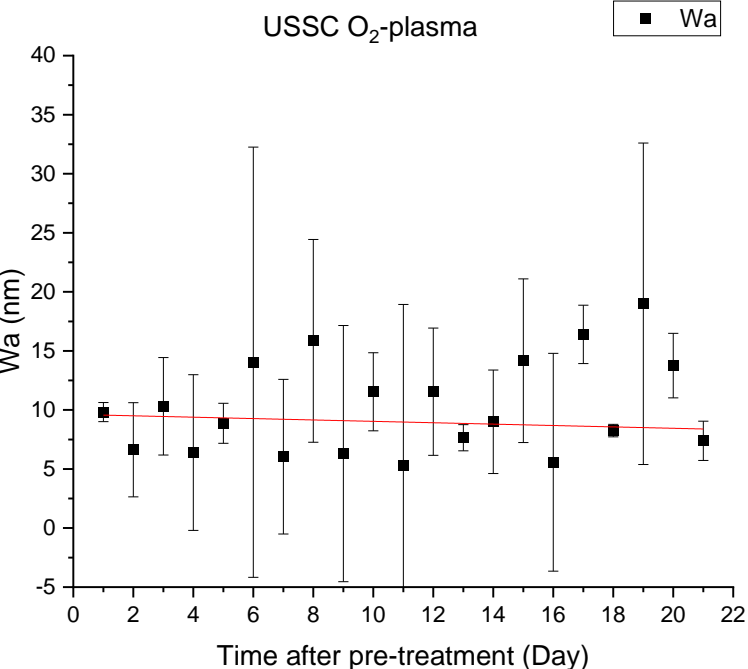
Figure 87: Waviness of O_2-plasma and diamond nanoseed deposited samples.

So a conclusion can be made that samples have to be spray coated within five days after an oxygen plasma treatment.

3.4.2.2 Characterisation of inkjet samples

Substrates can also be deposited with diamond nanoseeds by an inkjet printer. Various periods can be allocated for different kinds of inkjet printing, like surfaces, patterns or small dots. The printed surfaces can be seen in Figure 88. Figure 88 a) shows a surface printed eight days after the oxygen plasma treatment. This sample shows a heavy flow behaviour in the middle of the surface and no straight line near the edge of the printed surface.

A straight line can be seen on the edge of the surface in Figure 88 b) if a sample is printed ten days after the surface treatment. However, the surface itself still shows a sign of flow behaviour. The contact angle of the droplets deposited by the cartridge has a low angle and will flow into each other. Figure 88 c) shows a sample printed 18 days after the oxygen plasma treatment. The edges of the sample are very straight, and the flow behaviour is limited. Therefore, surfaces can be printed from ten days on after the oxygen plasma treatment.

Figure 88: Comparison of ink jetted surfaces. O₂-plasma treatment after 8 days (a), O₂-plasma treatment after 10 days (b), O₂-plasma treatment after 16 days (c).

Patterns can also be printed, as shown in Figure 89. Figure 89 a) has no straight lines in the pattern. The contact angle of the ejected droplets are too shallow and will flow into each other. The sample also shows a form of scratches throughout the pattern. This is a fault where the cause has not been found yet.

Figure 89 b) shows smoother lines than a). This sample is printed six days after the pre-treatment. The spacing with a size of 20 µm seems to flow into each other. From 40 µm, the two lines will stay apart from each other. The 20 µm spacing in Figure 89 c) also flows into each other, but the lines that accentuate the outline of the pattern are much smoother than b).
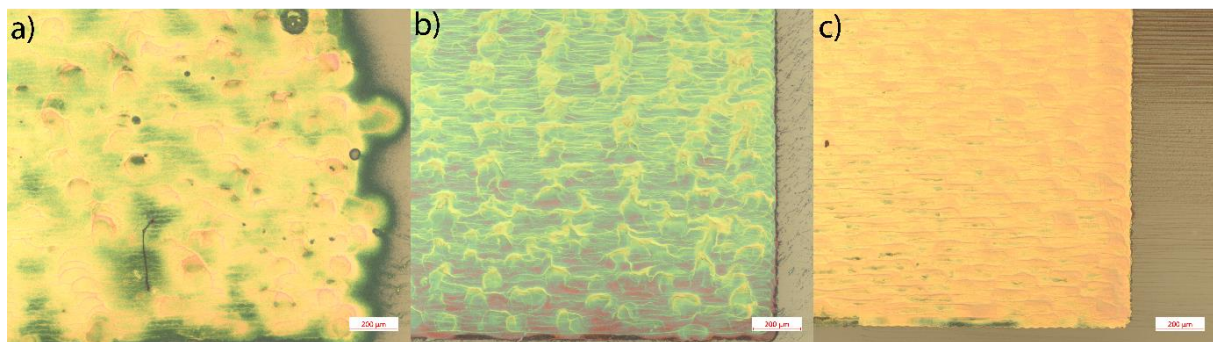

Figure 89: comparison of inkjetted patterns. O₂-plasma treatment after four days (a), O₂-plasma treatment after six days (b), O₂-plasma treatment after 16 days (c).

A conclusion can be made that it is possible to print patterns with a spacing of 40 µm six days after the oxygen plasma surface treatment. However, the pattern is not as clean as the pattern that is printed sixteen days after the treatment period.

The influence of the time after the pre-treatment process on the average surface roughness is not noticeable. This is shown in Figure 90. In this graph, no specific trend can be recognised.
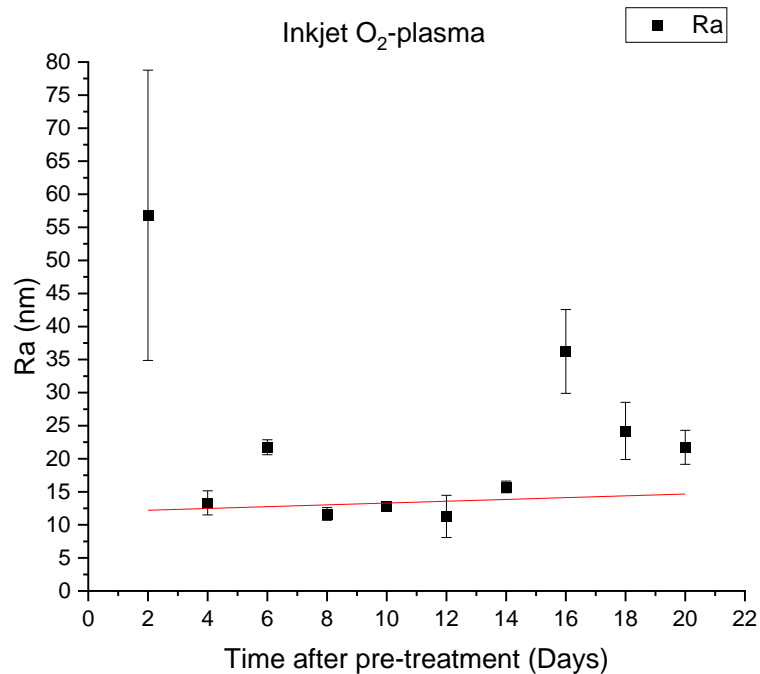
Figure 90: Average surface roughness of ink jetted surfaces after a O₂-plasma pre-treatment.

The waviness of the printed surfaces seems to increase slightly when the time after pre-treatment is also increased. This is shown in Figure 91. This is because the contact angle of the droplet increases which gives a less homogenous surface and this in turn leads to a higher waviness.
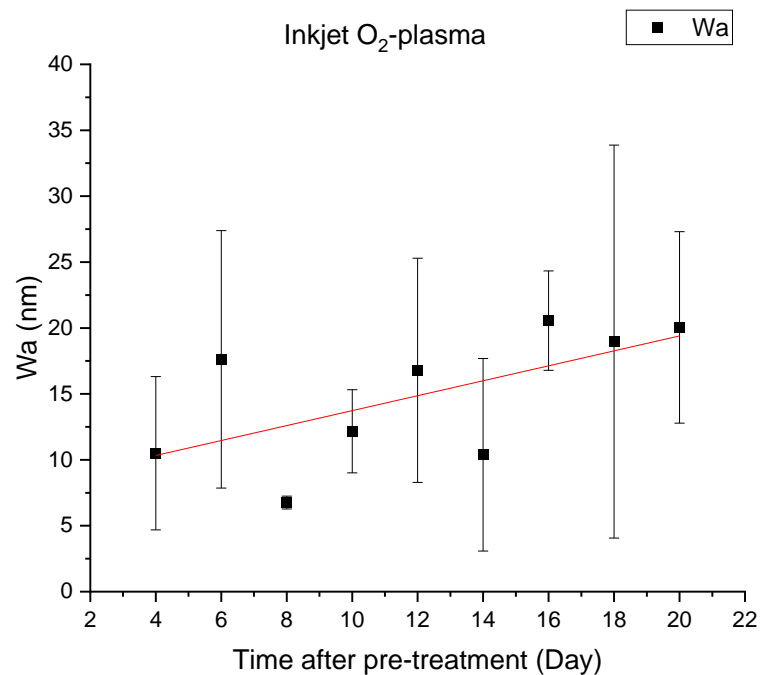
Figure 91: Waviness of printed surfaces after a O₂-plasma treatment.

3.4.3 CF₄-plasma

The last pre-treatment was the CF$_4$-plasma. With this treatment, the goal was to get a substrate with a hydrophobic behaviour because the goal was to print as tiny patterns as possible with the inkjet printer. Due to the nature of this pre-treatment method, it is only useful to print patterns with an inkjet printer and not use the ultrasonic spraycoater.

The problem here was that a hydrophilic behaviour was created on the first try. The settings of this first try were 100 W for 1,5 minutes. Then the power was increased to try and make a hydrophobic surface to 300 W for 3 minutes. After this was also unsuccessful, the thought was that metal particles sputtered on the glass because a metal stage was used. So the test was carried out again but with a carbon stage on 300 W for 3 minutes. This gave better results (contact angle of 43,7 degrees). Still, in an attempt to get an even better result, the stage was covered with microscopic slides so that none of the carbon was exposed to prevent the sputtering of carbon particles, as shown in Figure 92.
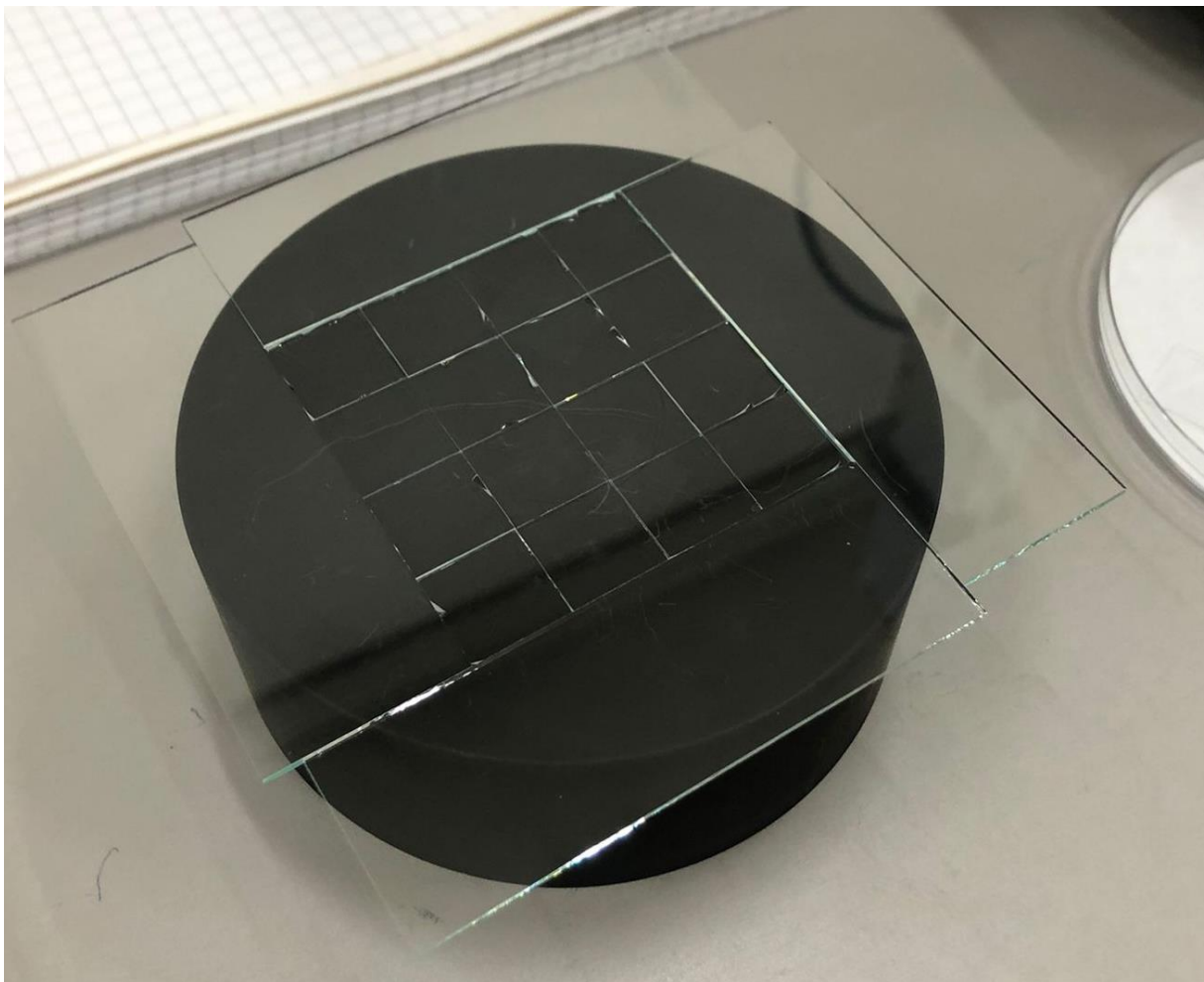
Figure 92: Glass substrates on a carbon stage covered with microscopic slides.

The problem with this setup was that there was no anode, so that no plasma could be created. Therefore the last, and most successful attempt was with the carbon stage and 300 W for 3 minutes with the glass substrates being laid with some space in between, as shown in Figure 93.
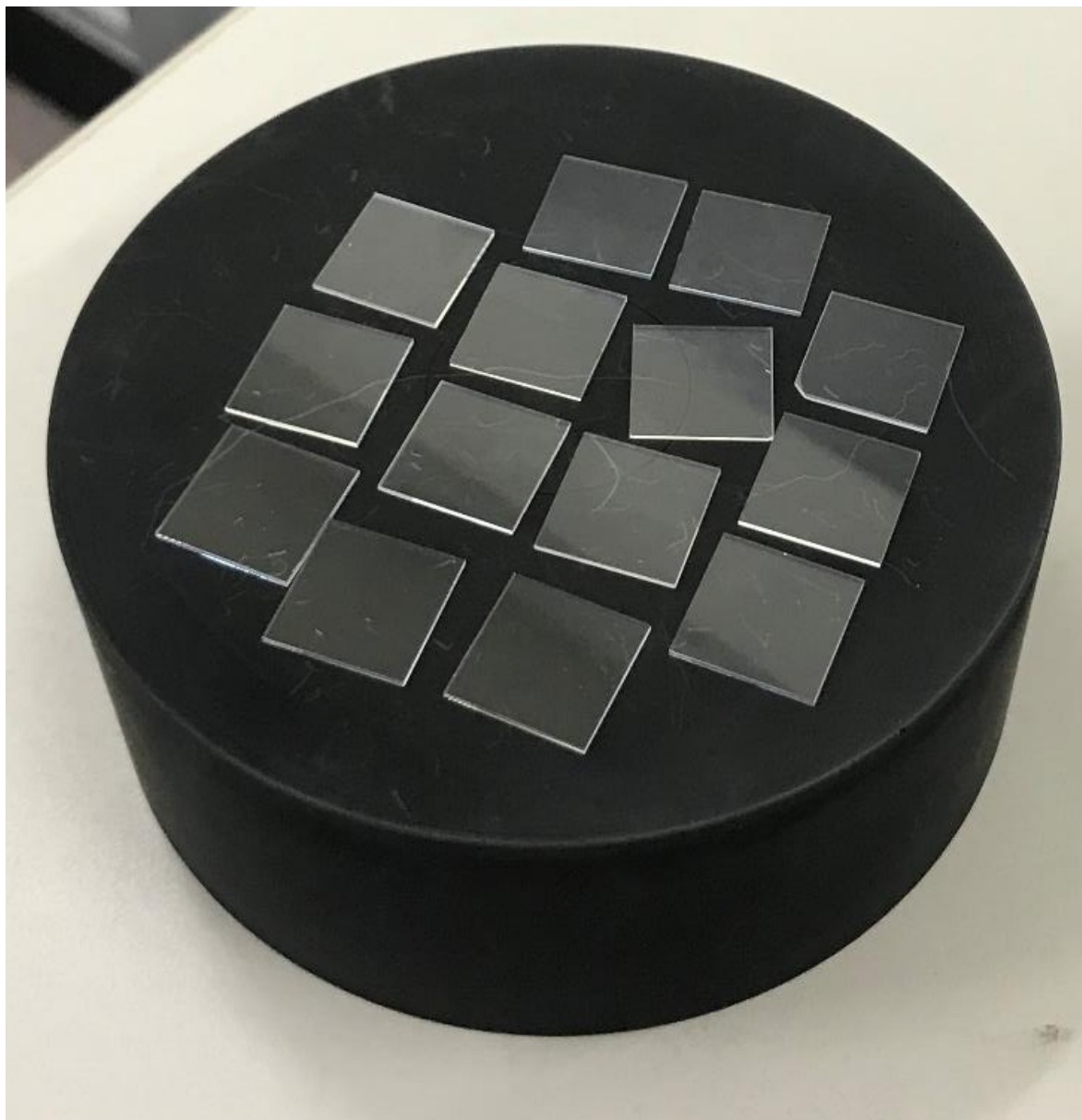
Figure 93: Glass substrates on a carbon stage.

The first batch of these samples was measured on a 24-hour interval, but no contact angle was detectable after the first day. The second batch was measured with 2-hour intervals, and this showed that the treatment worked but was very reactive and thus decreased very significantly in a short time due to the fluoride bonds disappearing. The result of this experiment is visible in Figure 94. On this figure, it is visible that there is an exponential progression of the contact angle. The first value is 30 degrees, which is a high contact angle, and after 2 hours, the value is already decreased, which shows a high decrease in effectiveness. After some time, the droplets start to flow out more and more and eventually, it flows out entirely.

CF$_4$-Plasma

Model	ExpDec1
Equation	y = A1*exp(-x/t1) + y0
Plot	Contactangle
y0	-1,52934 ± 3,36967
A1	51,91801 ± 3,5184
t1	470,76577 ± 73,1422
Reduced Chi-Sqr	5,77815
R-Square (COD)	0,98614
Adj. R-Square	0,97921
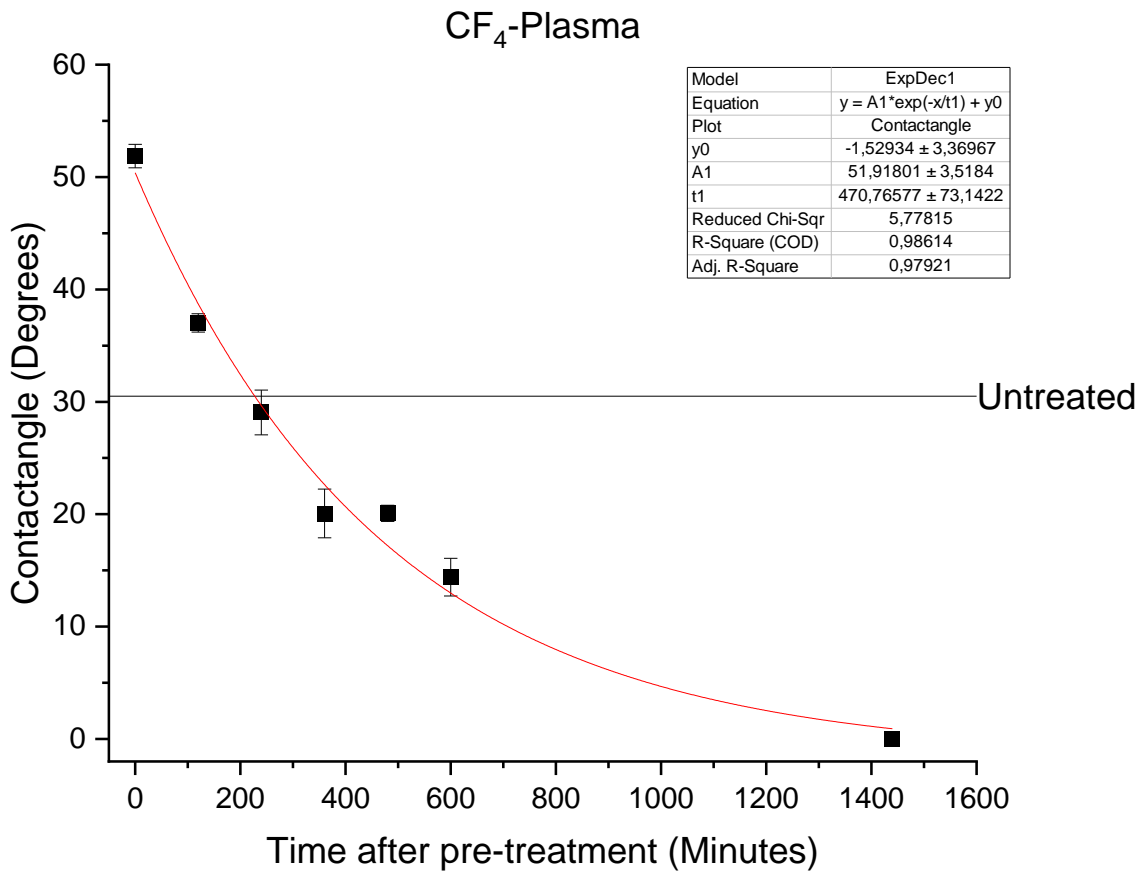
Figure 94: Contact angle values of a CF$_4$-plasma treatment.

From this data, it can be concluded that the CF$_4$-plasma treatment effectively creates a hydrophobic surface on fused silica, but its effectiveness decreases very rapidly.

3.4.3.1 Characterisation of inkjet samples

Because the effectiveness of CF$_4$-plasma treatment decreases so rapidly, it is not surprising that the best results come immediately after treatment. In Figure 95 visible below, the decline of effectiveness is visible with the samples going from good to worst.
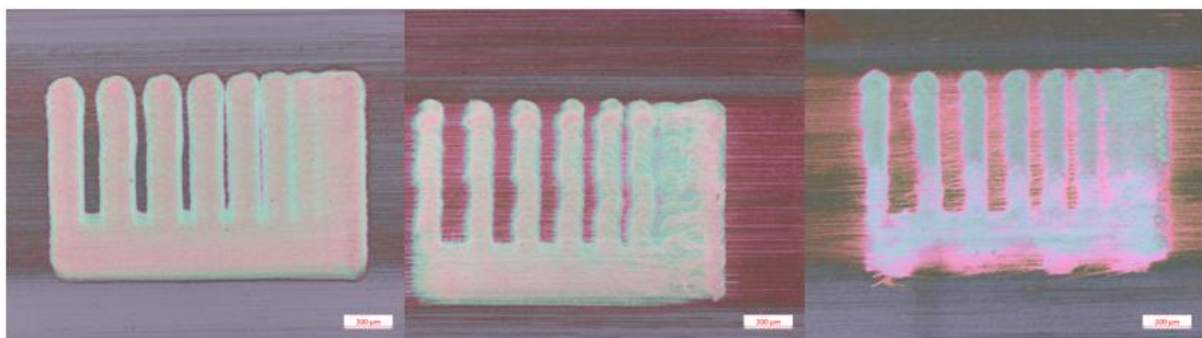
Figure 95: Inkjet samples with CF$_4$-plasma treatment: directly after treatment (a), 2 hours after treatment (b), 4 hours after treatment (c).

3.4.4 Measuring the diameter of inkjet printed dots

A part of the printed pattern with the inkjet was the dots. These dots' meaning was to measure the diameter and see if the contact angle increases and the diameter decreases. It was not possible to plot every day the dots were printed because the printing went wrong sometimes. In Table 20 below are the days and sample names listed which gave back good results. The values of these diameters are the means of 16 dots on the sample. An example of the illustration from which these values come is shown in Figure 96. These diameters were calculated using a Matlab script.

Table 20: Diameter of the dots

Sample	Diameter (µm)
MA20	53,174
MA37	46,5833
MA43	57,2174
MA62	62,0589
MA64	53,3592
MA86	41,3309
MA105	61,0061
MA109	54,6621
MA82	48,6499
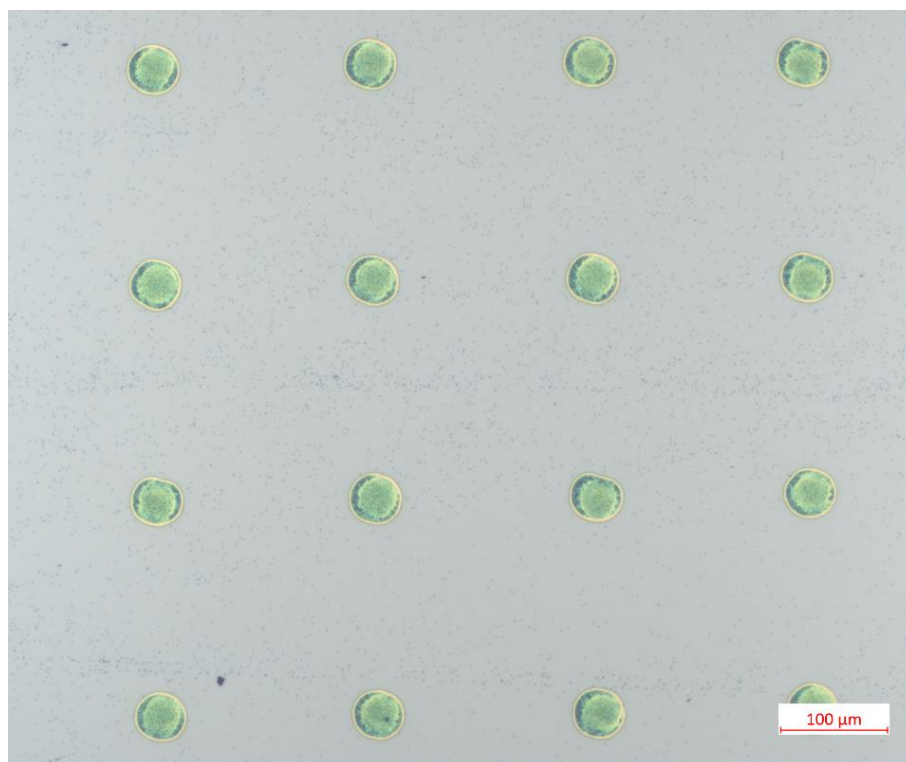
Figure 96: Dots of sample MA82 with 10x magnification with the OM.

The values from which the dots are measured are then split into the two different pre-treatments, UV-O_3 and O_2-plasma and arranged chronologically. Figure 97 (a) shows the results of the UV-O_3 treatment, which has a bit of variance in the results, but a downwards trend can be seen in the graph. The downward trend is more evident with the O_2-plasma results shown in Figure 97 (b).
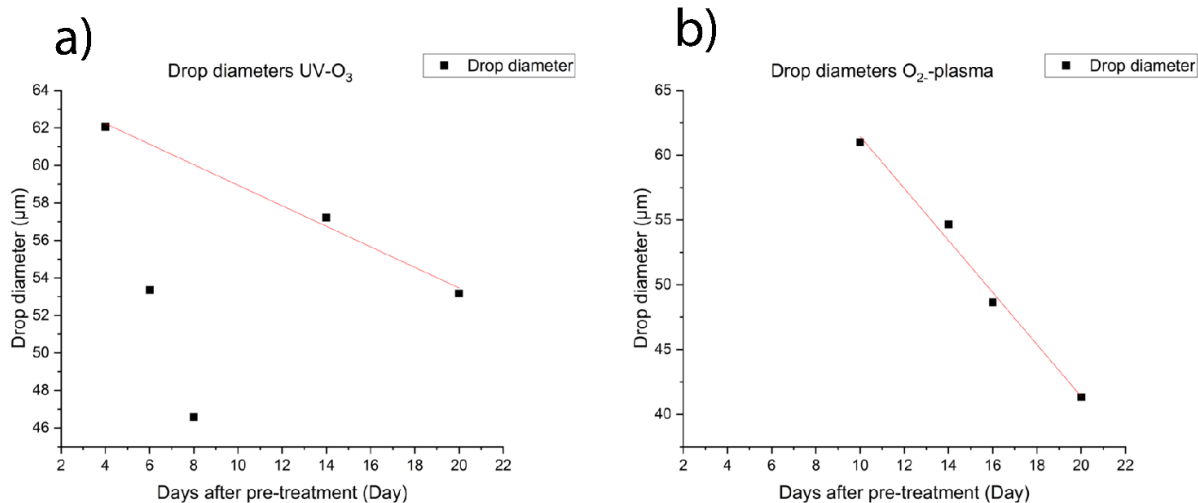
Figure 97: Evolution in drop diameter. UV-O$_3$ treatment (a), O$_2$-plasma treatment (b).

The conclusion for the two treatments is similar. In the expected line of thought, when the pre-treatment effectiveness decreases, and thus the contact angle increases, the diameter of the deposited drops will decrease. The droplet experiment with the CF$_4$ treatment failed and due to the lack of time it was not possible to recreate this experiment.

3.4.5   Conclusion of the different pre-treatment methods

A conclusion can be made for each of the pre-treatment methods and each deposition method. The period of five days after the pre-treatment of UV-O$_3$ or O$_2$-plasma is ideal for ultrasonic spraycoating applications. This period is concluded on the fact that the surface free energy of the substrate is too low to achieve a uniform coating after five days. This period is visualised in the red region one of Figure 98.

Two different conclusions can be made for inkjet printing due to the different pre-treatment methods and the intended design that needs to be printed. If a homogenous printed surface is wanted, a period of four to eighteen days after the UV-O$_3$ pre-treatment is preferred. This is because the contact angle of the jetted droplets will be too low before day four and the flow behaviour will be too much. However, a period of ten to sixteen days is preferred for the O$_2$-plasma treatment. A possible explanation for the two different periods is that the distribution of the diamond nanoparticle seeds is too much or the contact angle is too low due to the aggressive O2-plasma treatment. Therefore, the time after the pre-treatment is increased to have a higher contact angle and more uniform spreading of the droplets.

If a fine pattern is wanted, four to sixteen days is ideal after the UV-O$_3$ treatment, whereas an ideal day is six days after the treatment. For the O$_2$-plasma treatment, six days after the treatment gives adequate results, but the result increases if the time after the O$_2$-plasma pre-treatment is increased.

These regions are visualised in the graph in Figure 98. The green region number two is inkjet printing with a UV-O$_3$ pre-treatment. The blue region is for inkjet printing with an O$_2$-plasma pre-treatment. The CF$_4$-plasma treatment is not visible on the graph, this is because the time axis of the two graphs are different. The different size for the regions is due to the regions being plotted based on the days. The height of these regions is then increased to the treatment that is based on.
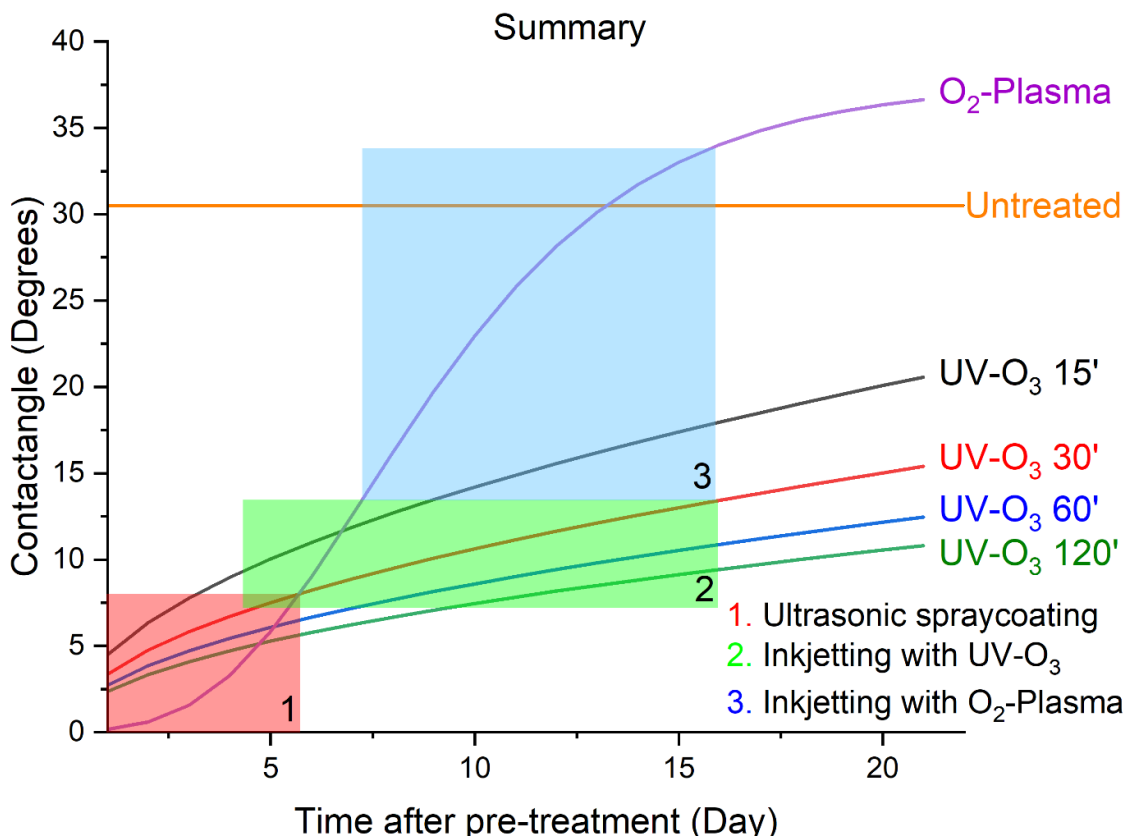

Figure 98: Conclusion of the different pre-treatment methods and time periods.

Even more delicate prints are possible with a CF_4-plasma pre-treatment. However, this experiment indicates that the influence of the CF_4 gas deteriorates relatively quick. Therefore, the deposition process with an inkjet printer needs to happen immediately after the pre-treatment process to ensure a good result.

The average surface roughness of samples is plotted in function of the pre-treatment time in Figure 99. These fused silica substrates are treated with all different pre-treatment methods and measured with an AFM. What stands out is that the plasma treatment methods have a much higher average roughness than the UV-O_3 treatment method. This is due to the fact that the plasma ball etches the surface deeper than the UV-O_3 treatment. The CF_4-plasma treatment had a duration of three minutes. This duration is twice as long as the O_2-plasma treatment. Therefore, the surface roughness of the CF_4-plasma substrate is higher than the O_2-plasma substrate.

The duration of the UV-O_3 pre-treatment method seems to influence the surface roughness of the substrate. The duration period of 15 minutes has a surface roughness of 0,438 nm, and this roughness increases to 1,043 nm if the duration is increased to 120 minutes. This measurement concludes that the UV-O_3 treatment has a significantly less course etching effect on the substrate.

The surface roughness of the UV-O_3 treated substrate is lower than that of the untreated substrate. This could be due to a measurement error or a cause for which no explanation has yet been found.
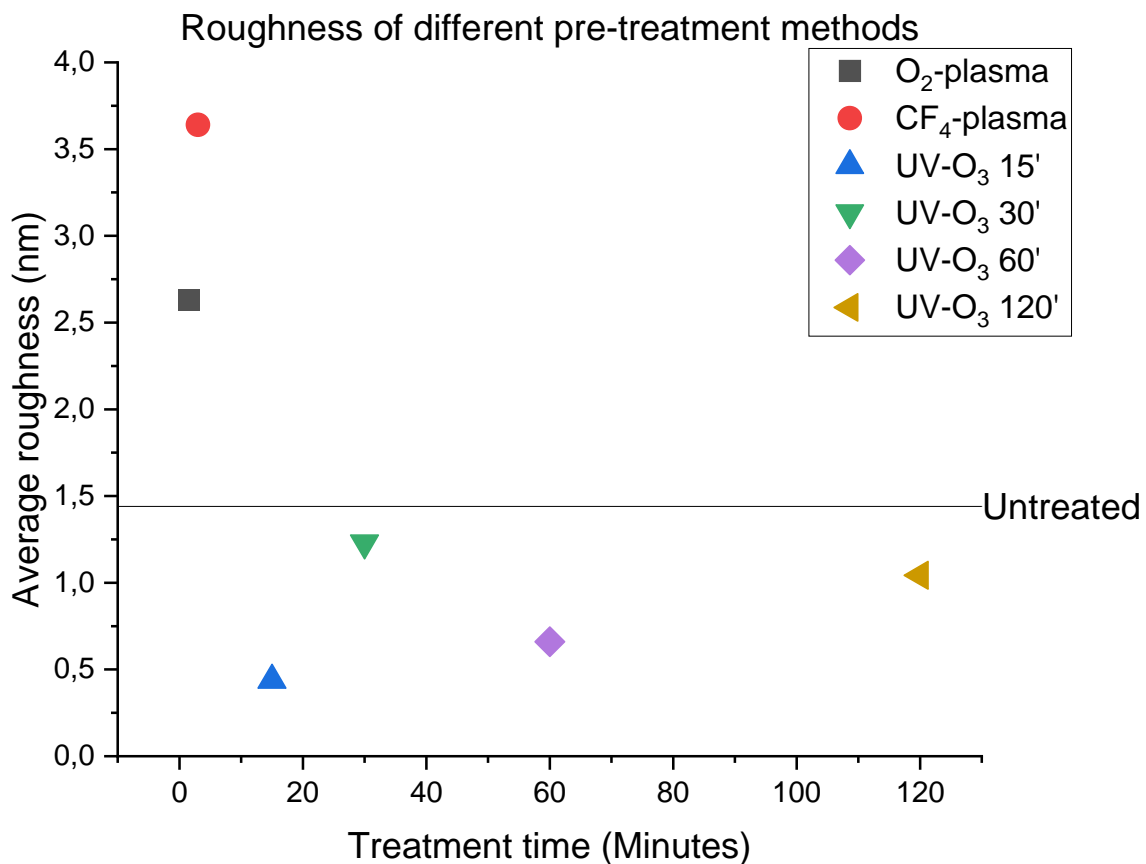
Figure 99: Surface roughness of different pre-treated substrates measured by AFM.

The best results achieved for printing small patterns can be found in Figure 100. The smallest imo-imomec logo that is printable with the resolution of the inkjet printer is 3,13 mm wide and is shown in Figure 100 a). Figure 100 b) shows a part of the imo-imomec logo, here it is possible to print a perfect readable logo with a line thickness of 229,1 µm.
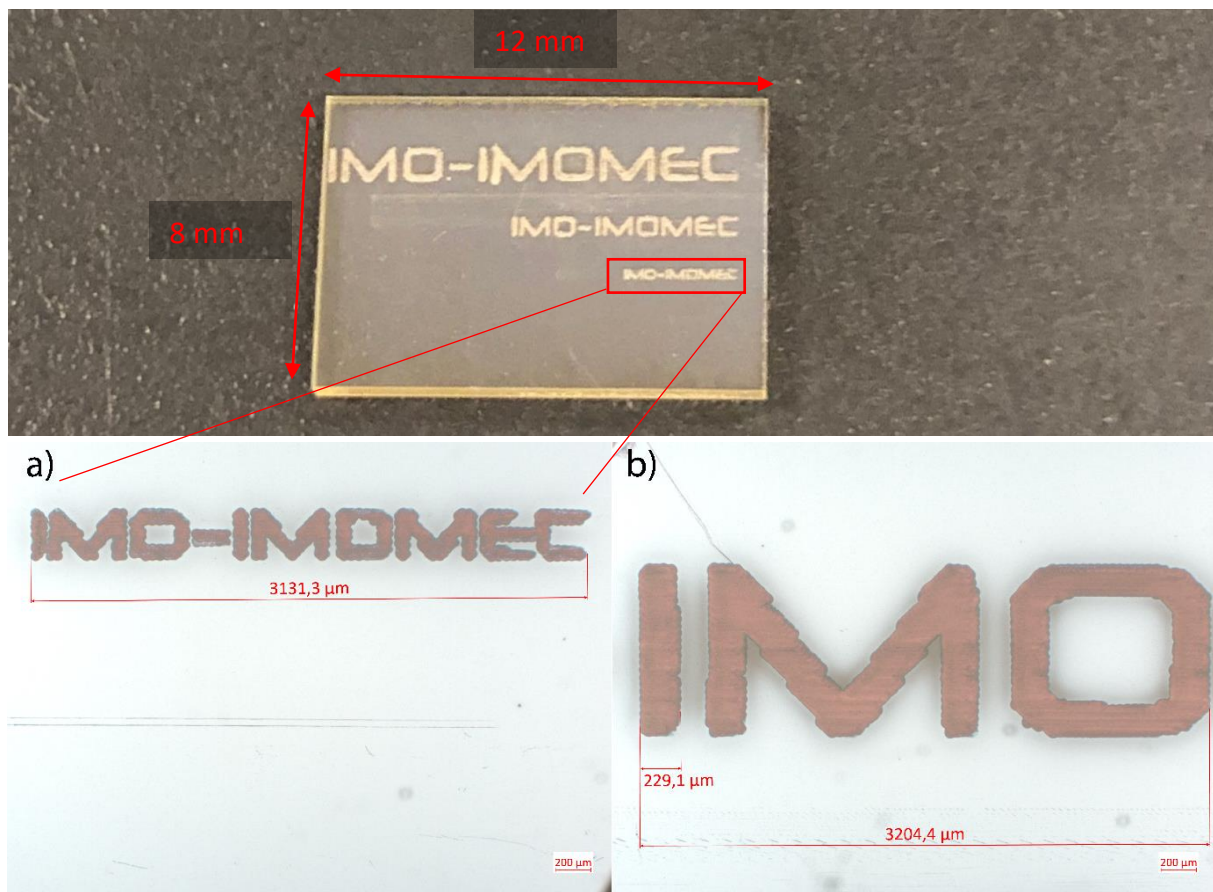
Figure 100: Best results for printing small patterns. Smallest achievable logo (a), perfect readable logo (b).

In Figure 101 below, the smallest achieved line spacing is shown. The designed distance of the pattern between the vertical lines is 60 µm, here an actual distance of 22 µm, distance A, is achieved. However, the distance B is 57,9 µm. This is closer to the designed distance of 60 µm. The difference can be explained due to the flow of the drop. The droplet is deposited on the drawn line, so half of the droplet flows to one side, which explains the difference.
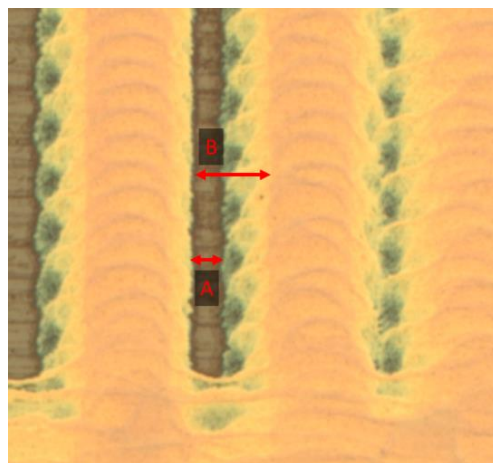
Figure 101: Spacing dimension results.

In Figure 102, a sample is shown that is deposited by diamond nanoparticle seeds three days after a UV-O_3 treatment. This sample has a uniform coverage with a minimum of coffee rings on it.
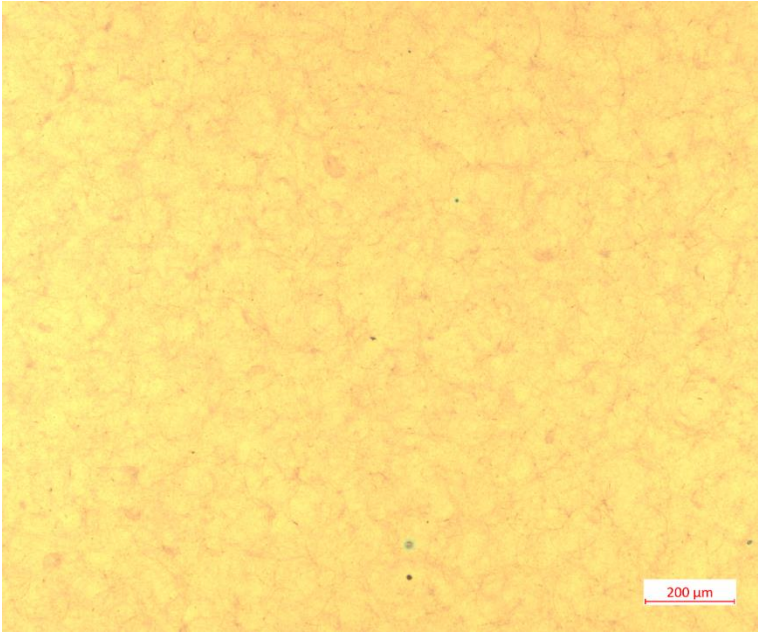
Figure 102: Best result for spraycoating surfaces.

Sand trickling tests from the ULTRAHARD project [62] on ultrasonic spraycoated samples show an average haze of 6 %. This result is achieved with substrates with an average surface roughness of 20 nm. The average surface roughness of the inkjet samples has a value of 12 nm. The expectation is that the haze will be less than 6 % because the light diffraction will be less significant due to the lower roughness of the inkjet samples. Figure 103 shows the haze of different deposition methods.
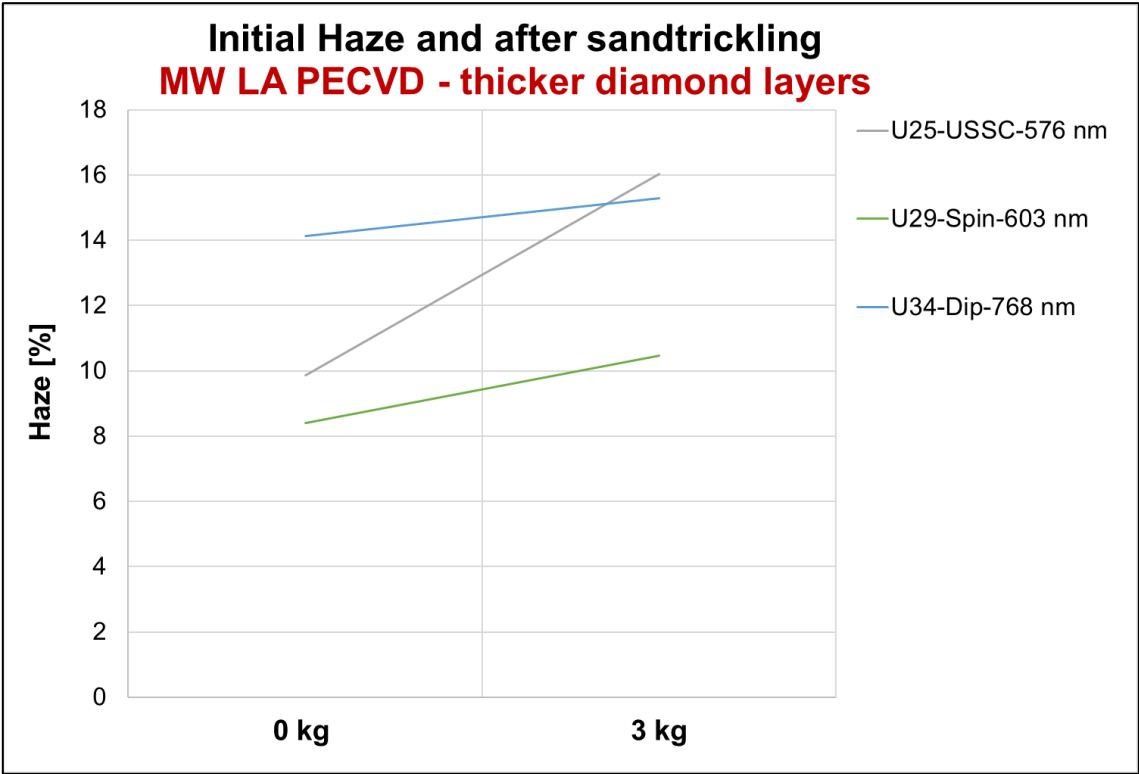
Figure 103: Haze measured before and after sand trickling test of different deposition methods [62].

4   Conclusion

This master's thesis indicates that is it possible to print fine patterns with an inkjet printer or cover surfaces with diamond nanoparticles by an ultrasonic spray coater. It is possible to print patterns with a line thickness of 93 µm, spacings between patterns from 60 µm and up, print surfaces that are almost homogeneous covered with a layer thickness of 230 nm. These coatings printed by the inkjet printer have an average surface roughness of 15 nm. There is no reference to compare these values since there is not a lot previous work on printing diamond coatings with an inkjet printer [63].

With the optimised parameters of the ultrasonic spray coater, it is possible to achieve a uniform coating with the same layer thickness of 230 nm. This coating has no pinholes and very little to no coffee rings. It is possible to achieve this coating with an average surface roughness of 20-25 nm. This surface roughness is around four times higher than a spin-coated substrate. The objective was to create a spraycoated surface with a surface roughness of around 20 nm. The conclusion is that this objective is achieved.

The next subject this master's thesis investigated was the evolution of the contact angle in function of time of different pre-treatment methods. These results are plotted in a graph, an ideal time-interval is determined for each pre-treatment method for each deposition technique. These achieved results have little to no flow behaviour and also little to no coffee rings.

A UV-O$_3$ treatment is a better pre-treatment method because the repeatability of the surface free energy is more reliable than an O$_2$-plasma treatment for both deposition techniques. However, the surface's micro-etching performed by the plasma treatments helps increase the contact angle of the droplet on the substrate. This increased contact angle results in the possibility to achieve finer prints with the inkjet printer.

The delivered work in this thesis helps researchers understand the evolution of different pre-treatment methods and maps out the perfect time interval for depositing diamond nanoparticle seeds on glass substrates.

This research can be supplemented with a further study in ink composition for the inkjet printer and further optimizing the inkjet parameters for even better and faster results. It is possible to print even finer prints with optimised parameters and get smaller spacings between patterns.

Another option is to investigate the evolution of the pre-treatment methods on different kinds of glass substrates and compare these to the results of the fused glass substrates.

With further optimizing the parameters of both the inkjet printer and ultrasonic spray coater, it is possible to see even more applications of diamond coatings on glass such as induction cooktops, windows of sand-blasting booths or even on the countertops of checkout scanners in stores. Printing diamond patterns will play a more significant role in the future for heat management in microchips.

References

[1]   P. Pobedinskas, G. Degutis, W. Dexters, J. D'Haen, M. K. van Bael, and K. Haenen, "Nanodiamond seeding on plasma-treated tantalum thin films and the role of surface contamination," *Applied Surface Science*, vol. 538, p. 148016, Feb. 2021, doi: 10.1016/j.apsusc.2020.148016.

[2]   Linseis, "Contact angle- measuring surface tension," 2021. https://www.linseis.com/en/properties/contact-angle/ (accessed Dec. 13, 2021).

[3]   J. E. Field, "The mechanical and strength properties of diamond," *Reports on Progress in Physics*, vol. 75, no. 12, p. 126505, Dec. 2012, doi: 10.1088/0034-4885/75/12/126505.

[4]   J. J. Gracio, Q. H. Fan, and J. C. Madaleno, "Diamond growth by chemical vapour deposition," vol. 43, no. 37, p. 374017, Sep. 2010, doi: 10.1088/0022-3727/43/37/374017.

[5]   diamond-materials.com, "Thermal conductivity of CVD diamonds," Nov. 20, 2021. https://www.diamond-materials.com/en/cvd-diamond/thermal/#:~:text=One%20of%20many%20remarkable%20properties,for%20diamond's%20high%20thermal%20conductivity. (accessed Nov. 20, 2021).

[6]   J. Carvill, "3 - Thermodynamics and heat transfer," in *Mechanical Engineer's Data Handbook*, J. Carvill, Ed. Oxford: Butterworth-Heinemann, 1993, pp. 102–145. doi: https://doi.org/10.1016/B978-0-08-051135-1.50008-X.

[7]   R. S. Balmer *et al.*, "Chemical vapour deposition synthetic diamond: materials, technology and applications," *Journal of Physics: Condensed Matter*, vol. 21, no. 36, pp. 1–24, Sep. 2009, doi: 10.1088/0953-8984/21/36/364221.

[8]   Plasmachem.com, "Single digit nanodiamonds," 2021. http://www.plasmachem.com/shop/en/single-digit-nanodiamonds/60-pl-sdnd-5p-1g.html (accessed Oct. 04, 2021).

[9]   Engineering Toolbox, "Water - Thermophysical properties," 2003. https://www.engineeringtoolbox.com/water-thermal-properties-d_162.html (accessed Oct. 12, 2021).

[10]   Engineering toolbox, "Acetone - Thermophysiscal Properties," Feb. 11, 2019. https://www.engineeringtoolbox.com/acetone-2-propanone-dimethyl-ketone-properties-d_2036.html (accessed Oct. 05, 2021).

[11]   Oerlikon Balzers, "Diamond coatings Oerlikon Balzers," Nov. 14, 2021. https://www.oerlikon.com/balzers/global/en/portfolio/balzers-surface-solutions/pvd-and-pacvd-based-coating-solutions/baldia-highest-wear-resistance-and-tightest-tolerances-when-machining-highly-abrasive-special-materials/ (accessed Nov. 24, 2021).

[12]   scnatu.com, "diamond coating on cutting tools," Nov. 24, 2021.

[13]   T. Guillemet, P.-M. Geffroy, J.-M. Heintz, N. Chandra, Y. Lu, and J.-F. Silvain, "An innovative process to fabricate copper/diamond composite films for thermal management applications," *Composites Part A: Applied Science and Manufacturing*, vol. 43, no. 10, pp. 1746–1753, 2012, doi: https://doi.org/10.1016/j.compositesa.2012.04.015.

[14] W. Brown and A. Malshe, "Diamond Heat Spreaders and Thermal Management," in *Diamond Films Handbook*, CRC Press, 2002. doi: 10.1201/9780203910603.ch11.

[15] R. Bogdanowicz *et al.*, "Improved surface coverage of an optical fibre with nanocrystalline diamond by the application of dip-coating seeding," *Diamond and Related Materials*, vol. 55, pp. 52–63, 2015, doi: https://doi.org/10.1016/j.diamond.2015.03.007.

[16] Lance Ulanoff, "New diamond-coated screen tech could be stronger than Gorilla Glass," Aug. 01, 2016. https://mashable.com/article/diamond-glass (accessed Nov. 25, 2021).

[17] Diamond materials, "Thermal Properties of CVD Diamond," 2018. https://www.diamond-materials.com/en/cvd-diamond/thermal/? (accessed Jan. 10, 2022).

[18] U. Wiklund, J. Gunnars, and S. Hogmark, "Influence of residual stresses on fracture and delamination of thin hard coatings," *Wear*, vol. 232, no. 2, pp. 262–269, 1999, doi: https://doi.org/10.1016/S0043-1648(99)00155-6.

[19] H. Hu and R. G. Larson, "Marangoni Effect Reverses Coffee-Ring Depositions," *The Journal of Physical Chemistry B*, vol. 110, no. 14, pp. 7090–7094, Apr. 2006, doi: 10.1021/jp0609232.

[20] H. Hu and R. G. Larson, "Marangoni Effect Reverses Coffee-Ring Depositions," *The Journal of Physical Chemistry B*, vol. 110, no. 14, pp. 7090–7094, Apr. 2006, doi: 10.1021/jp0609232.

[21] Krüss, "Surface free energy (SFE), surface energy," Jan. 2021, Accessed: Nov. 24, 2021. [Online]. Available: https://www.kruss-scientific.com/en/know-how/glossary/surface-free-energy#:~:text=Surface%20free%20energy%20(SFE)%20is,type%20of%20solid%2Dliquid%20contact.

[22] vwr.be, "Ultrasone reinigingsbaden." https://be.vwr.com/store/product/nl/10694225/ultrasone-reinigingsbaden-usc (accessed Oct. 04, 2021).

[23] Three Bond Technical News, "Ultraviolet-Ozone Surface Treatment," pp. 2–6, Mar. 1987, Accessed: Oct. 04, 2021. [Online]. Available: https://www.threebond.co.jp/en/technical/technicalnews/pdf/tech17.pdf

[24] K. Umeda *et al.*, "Impact of UV/O$_3$ treatment on solution-processed amorphous InGaZnO$_4$ thin-film transistors," *Journal of Applied Physics*, vol. 113, no. 18, p. 184509, May 2013, doi: 10.1063/1.4804667.

[25] Samcointl.com, "The Basics of UV-Ozone Cleaning of Surfaces," 2021. https://www.samcointl.com/basics-uv-ozone-cleaning-surfaces/ (accessed Oct. 04, 2021).

[26] R. Kohli, "Chapter 2 - UV-Ozone Cleaning for Removal of Surface Contaminants," in *Developments in Surface Contamination and Cleaning*, R. Kohli and K. L. Mittal, Eds. Oxford: William Andrew Publishing, 2015, pp. 71–104. doi: https://doi.org/10.1016/B978-0-323-29961-9.00002-8.

[27] Wesley Taylor, "Technical Synopsis of Plasma Surface Treatments," Gainesville, FL, 2009. Accessed: Oct. 13, 2021. [Online]. Available: https://www.iopp.org/files/public/TaylorWesleyUFlorida.pdf

[28] A. Marshall, "Low pressure plasma cleaning," Apr. 23, 2020. https://www.inseto.co.uk/explanation-of-low-pressure-plasma-cleaning-ikb-014/ (accessed Oct. 27, 2021).

[29] J. Šimončicová, S. Kryštofová, V. Medvecká, K. Ďurišová, and B. Kaliňáková, "Technical applications of plasma treatments: current state and perspectives," *Applied Microbiology and Biotechnology*, vol. 103, no. 13, Jul. 2019, doi: 10.1007/s00253-019-09877-x.

[30] thierry-corp.com, "Corona Discharge enhancing adhesion capabilities," 2021. https://www.thierry-corp.com/plasma-knowledgebase/corona-discharge#:~:text=A%20corona%20discharge%20is%20the,voltage%20to%20small%20electro de%20tip (accessed Oct. 04, 2021).

[31] L. E. Scriven, "Physics and Applications of DIP Coating and Spin Coating," *MRS Proceedings*, vol. 121, p. 717, Feb. 1988, doi: 10.1557/PROC-121-717.

[32] S. Bose, S. S. Keller, T. S. Alstrøm, A. Boisen, and K. Almdal, "Process Optimization of Ultrasonic Spray Coating of Polymer Films," *Langmuir*, vol. 29, no. 23, pp. 6911–6919, Jun. 2013, doi: 10.1021/la4010246.

[33] S. Slegers, M. Linzas, J. Drijkoningen, J. D'Haen, N. K. Reddy, and W. Deferme, "Surface Roughness Reduction of Additive Manufactured Products by Applying a Functional Coating Using Ultrasonic Spray Coating," *Coatings*, vol. 7, no. 12, 2017, doi: 10.3390/coatings7120208.

[34] P. Verding, W. Deferme, and W. Steffen, "Velocity and size measurement of droplets from an ultrasonic spray coater using photon correlation spectroscopy and turbidimetry," *Appl. Opt.*, vol. 59, no. 25, pp. 7496–7503, Sep. 2020, doi: 10.1364/AO.402579.

[35] Tim Philips, "Introduction to industrial inkjet printing," Aug. 08, 2010. https://imieurope.com/inkjet-blog/2016/2/8/industrial-inkjet-printing (accessed Oct. 12, 2021).

[36] Fujifilm, "Dimatix Materials Printer," 2021. https://www.fujifilm.com/us/en/business/inkjet-solutions/inkjet-technology-integration/dmp-2850 (accessed Oct. 12, 2021).

[37] M. A. Shah, D.-G. Lee, B.-Y. Lee, and S. Hur, "Classifications and Applications of Inkjet Printing Technology: A Review," *IEEE Access*, vol. 9, pp. 140079–140102, 2021, doi: 10.1109/ACCESS.2021.3119219.

[38] T. Vuorinen, J. Niittynen, T. Kankkunen, T. M. Kraft, and M. Mäntysalo, "Inkjet-Printed Graphene/PEDOT:PSS Temperature Sensors on a Skin-Conformable Polyurethane Substrate," *Scientific Reports*, vol. 6, no. 1, p. 35289, 2016, doi: 10.1038/srep35289.

[39] R. Haubner, "Low-pressure diamond: from the unbelievable to technical products," *ChemTexts*, vol. 7, no. 2, p. 10, 2021, doi: 10.1007/s40828-021-00136-z.

[40] K. Tsugawa, M. Ishihara, J. Kim, M. Hasegawa, and Y. Koga, "Large Area and Low Temperature Nanodiamond Coating by Microwave Plasma Chemical Vapor Deposition," *New diamond and frontier carbon technology: an international journal on new diamond, frontier carbon and related materials*, vol. 16, pp. 337–346, Jun. 2007.

[41] vaxasoftware.com, "Gibbs free enery of materials," Aug. 27, 2007. http://www.vaxasoftware.com/doc_eduen/qui/dtermoq.pdf (accessed Nov. 17, 2021).

[42] A. Gicquel, K. Hassouni, F. Silva, and J. Achard, "CVD diamond films: from growth to applications," *Current Applied Physics*, vol. 1, no. 6, pp. 479–496, 2001, doi: https://doi.org/10.1016/S1567-1739(01)00061-X.

[43]   X. Chen, B. Zheng, and H. Liu, "Optical and digital microscopic imaging techniques and applications in pathology," *Analytical cellular pathology (Amsterdam)*, vol. 34, no. 1–2, pp. 5–18, 2011, doi: 10.3233/ACP-2011-0006.

[44]   Microbehunter, "What are the differences between brightfield, darkfield and phase contrast?," *https://www.microbehunter.com/what-are-the-differences-between-brightfield-darkfield-and-phase-contrast/*, Feb. 09, 2013. https://www.microbehunter.com/what-are-the-differences-between-brightfield-darkfield-and-phase-contrast/ (accessed Oct. 20, 2021).

[45]   S. , K. Salading and E. , S. Miller, "Light Microscopy," Sep. 13, 2006. http://www.biologyreference.com/La-Ma/Light-Microscopy.html (accessed Oct. 20, 2021).

[46]   Zeiss, "ZEISS Axio Observer for Life Science Research," Nov. 14, 2016. https://www.zeiss.com/microscopy/int/products/light-microscopes/axio-observer-for-biology.html (accessed Oct. 20, 2021).

[47]   "VHA Diagnostic Electron Microscopy Program," Sep. 01, 2017. https://www.va.gov/DIAGNOSTICEM/What_Is_Electron_Microscopy_and_How_Does_It_Work.asp#:~:text=The%20electron%20microscope%20uses%20a,visible%20light%20to%20magnify%20images.&text=This%20stream%20is%20confined%20and,thin%2C%20focused%2C%20monochromatic%20be (accessed Oct. 20, 2021).

[48]   Purdue University, "Scanning electron microscope," Oct. 05, 2017. https://www.purdue.edu/ehps/rem/laboratory/equipment%20safety/Research%20Equipment/sem.html#:~:text=The%20SEM%20is%20an%20instrument,microscope%20by%20an%20electron%20gun.&text=Once%20the%20beam%20hits%20the,are%20ejected%20from%20the%20sample. (accessed Oct. 20, 2021).

[49]   R.R.L. De Oliveira, D.A.C. Albuquerque, T.G.S. Cruz, F.M. Yamaji, and F.L. Leite, "Measurement of the Nanoscale Roughness by Atomic Force Microscopy," São Carlos, 2012.

[50]   Oxford Instruments, "AFM Principle - How Does an Atomic Force Microscope Work?," Sep. 18, 2020. https://afm.oxinst.com/outreach/how-does-an-afm-microscope-work (accessed Oct. 24, 2021).

[51]   Harrison Electropolishing, "Ra & RMS: Calculating the surface roughness," May 27, 2012. http://www.harrisonep.com/electropolishing-ra.html#:~:text=1%2C%20Ra%20is%20the%20arithmetic,a%20surfaces%20peaks%20and%20valleys. (accessed Oct. 27, 2021).

[52]   A. W. Stähli, "The technique of Lapping." Sep. 28, 2020. Accessed: Oct. 28, 2021. [Online]. Available: https://www.stahliusa.com/stahli-publication/the-technique-of-lapping/surface-finish-quality/

[53]   KEYENCE, "Root mean square deviation (Rq, Pq, Wq)," Nov. 17, 2016. https://www.keyence.com/ss/products/microscope/roughness/line/root-mean-square-deviation.jsp#:~:text=Root%20mean%20square%20deviation%20indicates,waviness%20for%20the%20waviness%20profile. (accessed Oct. 27, 2021).

[54]   Upmold, "Surface finish Ra and Rz Roughness Specification," Sep. 20, 2017. https://upmold.com/surface-finish-ra-rz/#:~:text=RZ%20is%20the%20average%20value,Surface%20roughness%20terminology%20and%20parameters (accessed Oct. 27, 2021).

[55]   Olympus, "Surface Roughness Measurement—Parameters," May 15, 2020. https://www.olympus-ims.com/en/metrology/surface-roughness-measurement-portal/parameters/#!cms[focus]=007 (accessed Oct. 29, 2021).

[56]   M. Golabczak, "Estimation of Carbon Coatings Manufactured on Magnesium Alloys," in *Special Issues on Magnesium Alloys*, InTech, 2011. doi: 10.5772/18024.

[57]   A. Piegari and F. Flory, *Optical thin films and Coatings*, Second. Deans, Matthew, 2018.

[58]   E. Klimm, T. Kaltenbach, D. Philipp, M. Masche, K.-A. Weiss, and M. Koehl, "Soiling and abrasion testing of surfaces for solar energy systems adapted to extreme climatic conditions." Sep. 2015.

[59]   ASTM International, "Standard Test Methods for Rating Adhesion by Tape Test." West Conshohocken, PA, 2009. doi: 10.1520/D3359-09.

[60]   S. Azizian and M. Hemmati, "Surface Tension of Binary Mixtures of Ethanol + Ethylene Glycol from 20 to 50 °C," *Journal of Chemical & Engineering Data*, vol. 48, no. 3, pp. 662–663, Mar. 2003, doi: 10.1021/je025639s.

[61]   N. Derom and B. Janssen, "Optimalisatie van procesparameters voor krasbestendige en anti-reflecterende coatings via ultrasoon spraycoaten van nanokristallijne diamanten deklagen," Diepenbeek, 2021.

[62]   P. Verding, "ULTRAHARD meeting ." Diepenbeek, Dec. 16, 2021.

[63]   Y.-C. Chen, Y. Tzeng, A.-J. Cheng, R. Dean, M. Park, and B. M. Wilamowski, "Inkjet printing of nanodiamond suspensions in ethylene glycol for CVD growth of patterned diamond structures and practical applications," *Diamond and Related Materials*, vol. 18, no. 2, pp. 146–150, 2009, doi: https://doi.org/10.1016/j.diamond.2008.10.004.